



UNIVERSITÀ DEGLI STUDI DI NAPOLI FEDERICO II  
POLO DELLE SCIENZE E DELLE TECNOLOGIE  
FACOLTÀ DI INGEGNERIA



DIPARTIMENTO DI INGEGNERIA ELETTRICA

**Performance Evaluation and Troubleshooting  
of Radiofrequency Digital Transmitters**

Michele Vadursi

TESI DI DOTTORATO DI RICERCA IN INGEGNERIA ELETTRICA

XVIII CICLO

(Coordinatore: Prof. Giovanni Miano)

TUTOR

PROF. MASSIMO D'APUZZO

CO-TUTOR

PROF. LEOPOLDO ANGRISANI

(UNIVERSITÀ DI NAPOLI FEDERICO II - DIEL) (UNIVERSITÀ DI NAPOLI FEDERICO II - DIS)



## **ABSTRACT**

The research activity accounted for in this Ph.D. thesis belongs to the general field of electrical and electronic measurements. The attention is focused, in particular, on performance evaluation and troubleshooting of radiofrequency digital communication transmitters, a fundamental issue in applied research and industrial production of modern communication systems. Several measurements included in testing and troubleshooting procedures utilized by major manufacturers, or included in international standards, are taken into consideration. The original contribution consists in the development of original measurement methods, based on digital signal processing, which result more reliable, and/or repeatable, and/or efficient than the publicized ones. The proposed methods are based on digital signal processing, and operate in time, frequency, time-frequency and modulation domains.

Besides being based on rigorous methodological approaches, the proposed methods take advantage of a wide experimental activity. All the proposed methods are extensively tested, by applying them to simulated, emulated and real communication signals. Measurement results are analyzed and compared to those achievable through the application of existing methods and/or instrumentation available on the market.



## **ACKNOWLEDGEMENTS**

Many are the persons I would like to thank for their support and concrete help in the development of this work.

Two of them, Prof. Massimo D'Apuzzo and Prof. Leopoldo Angrisani, have their names written at the bottom of the front page as my tutors, though they deserve to be put at the very top. I express my personal gratitude to them, whose continuous inspiration and scientific support have been driving factors to accomplish this goal.

A sincere thank goes to Prof. Giovanni Miano, who has coordinated the Ph.D. course with competence and devotion.

It has been my pleasure, and luck, to work in the unique workgroup of Electrical and Electronic Measurements of the University of Naples Federico II. It is a very special scientific and research group, of which I am proud to be part. My personal appreciation goes to each and every member of the group, from leading professors to technicians and young researchers, with whom I have had the occasion of exchanging ideas and cooperating.

I would like to direct a very special thank to Prof. Antonio Langella, the dean of our group, whose incomparable expertise, firm guidance, fruitful help and personal dedication are of immeasurable value.

I am also personally grateful to Prof. Nello Polese for his valuable teachings and precious encouragement, Prof. Aldo Baccigalupi for his human support and helpful suggestions, and Prof. Felice Cennamo for his motivation and his kindness.

A warm thank to my dear colleagues and friends Mauro D'Arco, Nicola Pasquino, Rosario Schiano Lo Moriello, Annalisa Liccardo, and Alessandro Masi, with whom I have cooperated, exchanged ideas, and had a lot of fun, too!

It is also my sincere desire to acknowledge Antonio Grillo, Umberto Cesaro and Alessandro Teotino for their help and availability.

Last but not least, I must give immense thanks to my parents and my sister for the unconditional support they have provided me through my entire life, and to my beloved Angela, the greatest joy in my life, who illuminates my existence and makes every day a special day with her love.

## CONTENTS

Introduction .....	1
CHAPTER I Transmitter Testing and Troubleshooting.....	5
I.1 - Digital transmitters .....	5
I.2 - Transmitter testing .....	7
I.2.1 - In-band measurements .....	8
I.2.2 - Out-of-band measurements.....	11
I.3 - Transmitter troubleshooting.....	11
I.3.1 - Compression .....	12
I.3.2 - I/Q impairments .....	12
I.3.3 - Incorrect symbol rate .....	15
I.3.4 - Wrong filter coefficients and incorrect windowing.....	15
I.3.5 - IF filter non-idealities .....	16
I.3.6 - Local oscillator instability .....	16
I.3.7 - Interfering tones.....	16
I.3.8 - DAC impairments .....	17
I.3.9 - Burst shaping impairments .....	17
CHAPTER II Performance Evaluation .....	19

II.1 - Introduction.....	19
II.2 - Power measurement.....	19
II.2.1 - Introduction.....	19
II.2.2 - Theory underlying the proposed method.....	20
II.2.3 - Proposed method.....	23
II.2.4 - Performance assessment.....	27
II.2.5 - Conclusion.....	32
II.3 - CCDF curve measurement.....	32
II.3.1 - Introduction.....	32
II.3.2 - Proposed Approaches.....	34
II.3.3 - Performance assessment.....	36
II.4 - Transmitter transient measurement.....	40
II.4.1 - Introduction.....	40
II.4.2 - Proposed method.....	41
II.4.3 - Performance assessment.....	43
II.4.4 - Tests on real transmitters.....	48
II.4.5 - Conclusion.....	50
CHAPTER III I/Q Impairments Detection and Evaluation.....	53
III.1 - Introduction.....	53
III.2 - A measurement method based on clustering.....	53
III.2.1 - Introduction.....	53
III.2.2 - Impairments affecting I/Q modulators.....	55
III.2.3 - Proposed method.....	56
III.2.4 - Performance assessment.....	59
III.2.5 - Conclusion.....	62
III.3 - A measurement method based on error vector analysis.....	63
III.3.1 - Introduction.....	63
III.3.2 - Theoretical background.....	64
III.3.3 - Proposed method.....	66
III.3.4 - Performance assessment.....	71
III.3.5 - Conclusion.....	75
III.4 - I/Q impairment detection and evaluation on OFDM transmitters.....	76
III.4.1 - Introduction.....	76

III.4.2 - Problem statement.....	77
III.4.3 - Proposed method.....	80
III.4.4 - Performance assessment.....	83
III.4.5 - Conclusion.....	85
CHAPTER IV Conclusion .....	87
References .....	89
List of Figures.....	97
List of Tables.....	101



## **INTRODUCTION**

Digital communications have been experiencing a significant development since the last decade of last century, both in terms of users and provided services. The increasing demand for ubiquitous wireless communication and the willingness to enhance the video and audio broadcasting offer are probably the main reasons for such a rapid and extended growth. A milestone in this process is represented by GSM (Global System for Mobile communications) [1], whose *ex ante* standardization has been one of the key factors for its worldwide great and unprecedented success. Following the example of GSM, several new continental and world standards for wireless digital communication systems have been developed in the last years. They range from mobile communication (UMTS [2], CDMA2000, PHS, etc.) to both local and wide area connectivity (Bluetooth [3], 802.11 [4],[5],[6],[7], and WiMax [8], respectively), up to digital video and audio broadcasting (DAB [9], DVB [10], [11], [12]).

A direct consequence of such a sustained development is that R&D (Research and Development) engineers and manufactures have been, and still are, involved in designing and developing components and systems characterized by higher and higher performance in terms of achievable transmission rate and spectral effectiveness. Moreover, to encourage customers and therefore support the success of the new systems, satisfying or at least acceptable quality of service (QoS) degrees must be pursued. At the same time, requirements imposed by both national and international standards and regulations have to be met. The need for reliable and

repeatable testing solutions consequently arises. Moreover, in order to reduce time-to-market, which is a fundamental issue in a more and more competitive commercial scenario, R&D engineers and manufacturers also need to test their designs and troubleshoot their products in a very short time. Not only must testing and troubleshooting procedures be reliable and repeatable enough to conveniently verify QoS and regulations requirements, but they should also be efficient enough to help reduce the time-to-market and speed up production, installation and maintenance stages.

The research activity accounted for in this Ph.D. thesis has focused on performance evaluation and troubleshooting of radiofrequency digital transmitters, a fundamental issue in applied research and industrial production of modern communication systems. Several measurements included in testing and troubleshooting procedures utilized by major manufacturers, or included in international standards, have been taken into consideration. The goal has been the development of original measurement methods, based on digital signal processing, which could result more reliable, and/or repeatable, and/or efficient than the publicized ones. Regarding reliability, efforts have been dedicated to design methods providing smaller difference between expected and measured quantities of interest. Concerning repeatability, a smaller dispersion of the results of successive measurements carried out in a very short time, under the same operating conditions, and following the same measurement procedure, has been sought. As for efficiency, one or more of the following goals (not necessarily independent of one another) have been pursued: (i) reduced measurement time, (ii) reduced cost of measurement equipment, (iii) increased measurement automation, (iv) less *a priori* information on the system under test, and (v) increased flexibility, intended as the capability of adapting with minor modifications to newer standards and systems.

All the proposed methods have been extensively tested, by applying them to simulated, emulated and real communication signals. Measurement results have been analyzed and compared to those achievable through the application of existing methods and/or instrumentation available on the market.

The Ph.D. thesis is organized as follows. In Chapter I, the model of a typical radiofrequency digital transmitter is introduced, and its main functional blocks are described; moreover, the most significant measurements involved in transmitters testing and troubleshooting are reported. Chapter II deals with performance evaluation, and specifically presents some original proposals for power measurement, CCDF curves evaluation and

transient measurements; the results of the wide experimental activity intended to assess the performance of the proposed measurement methods, also with respect to pre-existing solutions, are also given. In Chapter III, troubleshooting issues are addressed, with special regard to detection and evaluation of I/Q impairments affecting the modulator, which is the core of a digital transmitter; in particular, three different methods are proposed, which are suitable for different operating conditions and modulation systems. Although characterized by different pros and cons, the three methods exhibit very good performance in terms of reliability and repeatability, each of them representing a valid and useful choice for a specific case. On the whole, they cover all practical cases of generic I/Q modulators, including OFDM (Orthogonal Frequency Division Multiplexing) systems. Along with details of the proposed methods, the chapter accounts for the results achieved in the great number of experiments. Finally, conclusions are drawn in Chapter IV.



# CHAPTER I

## TRANSMITTER TESTING AND TROUBLESHOOTING

### **I.1 - Digital transmitters**

The simplified block diagram of a radiofrequency digital transmitter, based on I/Q modulation, is shown in Fig.I.1. The waveform depicted at the input of the transmitter is to be intended as digital, that is either representing the quantized discrete-time version of an analog signal (e.g. voice) coming out of an analog-to-digital converter, or consisting of digital data. Input data usually undergoes source coding and channel coding. Source coding generally involves compression, which aims at removing redundancy, thus allowing a more efficient spectral utilization [13],[14],[15],[16]. Channel coding consists in introducing controlled redundancy that can be exploited by the receiver to face problems due to noise and interference encountered by the transmitted signal through the channel; in a word, channel coding provides protection from errors [17],[18]. Burst errors can sometimes occur, for instance, in the class of channels characterized by multipath and fading. To face burst errors, interleaving of coded data is usually adopted. The symbol encoder maps groups of input serial bit stream into the I and Q waveforms, that is into symbols of the I/Q plane peculiar to the specific communication system. Examples of symbol mapping performed by the symbol encoder are reported, for instance, in Section 4.5 of [10], and Section 9 of [11]. The symbol

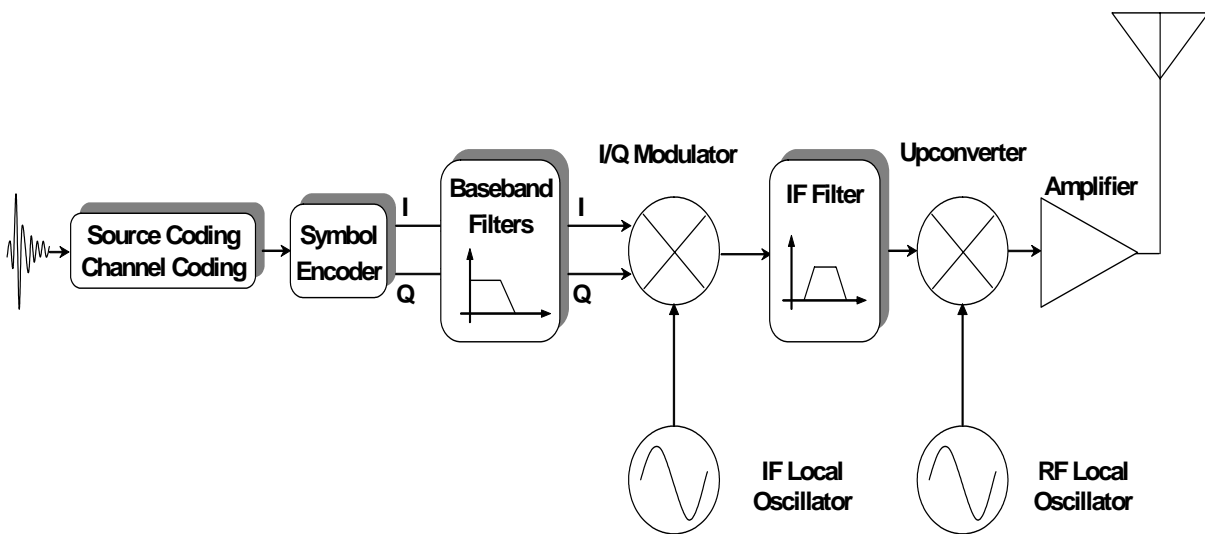


**Fig.I.1 – Block diagram of a radiofrequency digital transmitter.**

encoder also accounts for symbol clock, which defines frequency and symbol timing. I and Q baseband signals are then filtered to limit their spectrum, and baseband filters are chosen according to specific optimization strategies, which can involve the receiver, as well. The correct filters must be chosen so as to minimize ISI (Inter-Symbol Interference); Nyquist filters are a relevant example [19],[20],[21],[22]. Filtered baseband components are then fed into the I/Q modulator, where they modulate two orthogonal carriers, usually at intermediate frequency (IF). The signal at the output of the I/Q modulator is a combination of the two modulated orthogonal carriers. The signal is eventually IF filtered, upconverted to radiofrequency (RF) and finally amplified for radio transmission.

The location of the DAC (Digital-to-Analog Converter) is not a trivial question. Where does the digital section end? Symbol encoder and baseband filters are usually implemented digitally. Current trend is to implement digitally also the modulation section, and place the DAC before the IF filter, instead of utilizing two DACs on the I and Q branches before the IF modulator input. The simplified block diagram depicted in Fig.I.1 is quite general, although several variations are possible in practice, depending on the particular design choices related to multiplexing and modulation scheme.

## I.2 - Transmitter testing

Different tests are carried out at different stages of the design of a digital communication transmitter. Individual components the transmitter is made of are, at first, tested individually, in order to verify their conformance to requirements and specifications. After assembling the transmitter, strict conformance tests are carried out, in order to verify system requirements along with design robustness, and grant interoperability of products made by different manufacturers. Conformance tests are usually performed at antenna port, through an ideal receiver. Possible causes of degradation must consequently be inferred from measurement results at the antenna port.

Measurements on the transmitted signal are carried out in different domains: *time* domain, *frequency* domain, and *modulation* domain. Time domain analysis is required, for instance, on transmitters implementing TDMA (Time Division Multiple Access) techniques, in order to measure burst shaping and timing; it is also performed on the RF signal envelope at the output of spectrum analyzers operating in zero span mode, and on demodulated I and Q components. Crucial information on spectral occupancy, out-of-band emissions, and possible interference, are provided by the analysis in the frequency domain, which is carried out through analog or FFT (Fast Fourier Transform)-based spectrum analyzers. Modulation domain analysis can be carried out by comparing the demodulated signal to an ideal reference; as it will be shown in the following, a number of possible impairments and non-idealities that are responsible for signal distortion in the modulation domain can be inferred by modulation domain measurements.

Finally, a potentially powerful tool in transmitter testing is constituted by time-frequency representations (TFRs) [23], [24], [25], [26], [27], [28]. TFRs, which are implemented through digital signal processing algorithms, account for the evolution of signal spectral content versus time, and can provide some advantages in terms of measurement efficiency and costs. Their use is at the basis of some of the measurement solutions presented in the following sections of the thesis.

Measurements on digital communication transmitters are classified into in-band and out-of-band measurements. In-band measurements are carried out within the frequency band occupied by the particular communication system, and are further divided into in-channel and out-of-channel measurements. In such classification, the *channel* is to be intended as the

frequency channel the transmitter is operating in, and it does not necessarily coincides with the common meaning of *channel* in a communication system, which can refer also to a particular timeslot or code. In the next two sections, a brief description of most common measurements in digital communication transmitter testing are described, following the classification given in [29].

### *1.2.1 - In-band measurements*

#### *A. In-channel measurements*

##### *Channel bandwidth*

It is good practice, first, to perform a channel bandwidth measurement. In most cases of interest, depending on the baseband filter specifications, the 3 dB bandwidth approximates the symbol rate; its measurement can therefore reveal major errors in transmitter design.

##### *Carrier frequency*

Carrier frequency measurements are of great importance. Not only can frequency errors result in possible interference, but they can also be responsible for possible problems in the carrier recovery process at receiver side.

##### *Channel power*

Channel power is the average power of the signal in the *channel*, according to the acceptance given in Section I.2. It is usually measured as the integral of power spectrum density over the frequency band of interest, although the measurement method depends on the particular communication standard [30],[31],[32].

##### *Occupied bandwidth*

Occupied bandwidth is defined as the frequency interval, centered at the tune frequency of the monitored channel, over which the integral of the power spectral density equals  $x\%$  of the average power, where  $x\%$  is usually chosen equal to either 95% or 99%.

##### *Peak to average ratio*

Peak-to-average power ratio (PAR) is the ratio of the peak envelope power to the average envelope power of a signal during a given period of time.

##### *CCDF curves*

PAR only takes into account the signal mean and the peak value and is strongly dependent on the duration of the signal. More generally, characterizing a signal by providing

information on just one power level (e.g. the peak) can be not sufficient. This is particularly true for modern digital telecommunication systems, which adopt more and more complex modulation schemes. CCDF (Complementary Cumulative Distribution Function) curves provide a statistical description of power levels of an RF signal [33]. A CCDF curve is, in fact, a plot of relative power level, expressed in decibel (dB), versus probability. Specifically,  $CCDF(x)$  represents the probability that the signal envelope power is at least  $x$  dB above the average power. Fig.I.2 shows the CCDF curve of a digitally synthesized CDMA (Code Division Multiple Access) signal consisting of a single data channel.

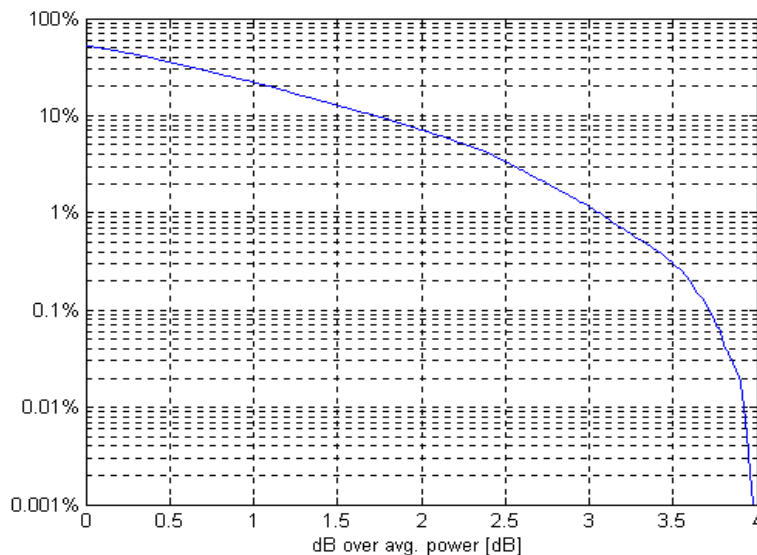


**Fig.I.2 – CCDF curve of a CDMA signal.**

#### *Timing measurements*

Timing measurements are common on TDMA systems. As transmitters in TDMA systems generate bursty signals, turn on and turn off phases can introduce interference with adjacent frequency channels. A set of measurements are usually carried out, including burst width, rise time, fall time, peak power, and duty cycle, in order to characterize the bursts.

#### *Modulation quality measurements*

Modulation quality measurements involve the demodulation of the transmitted signal through an ideal receiver, and the comparison of the demodulated signal to an ideal one. The measurements to carry out depend on the particular modulation scheme, and standard. The

most common are EVM (Error Vector Magnitude) [32],[34], phase and frequency error [31], coefficient rho ( $\rho$ ), and code-domain power [30].

Error vector (EV) is defined as the vector difference between the actual and ideal symbol position on the I/Q plane (Fig.I.3). Its magnitude, EVM, is a key modulation quality metric in most modern communication systems [35], since most impairments and non-idealities of the transmitter affect its value. Besides providing quantitative information on modulation quality, a thorough analysis of EVM can help detecting *which* are the most significant impairments and non-idealities of the transmitter under test; this feature is discussed later in this chapter, as it turns out to be useful in troubleshooting.

With regard to communication systems like GSM, which characterized by constant-envelope modulation formats, modulation quality is determined by analyzing the I/Q phase and frequency errors. The phase error is determined by comparing the actual and reference phase trajectories, whereas the mean gradient of the phase error evolution versus time is the frequency error. Problems in the baseband section of the transmitter and distortion introduced by the output amplifier are possible causes of phase error. A stable frequency error is due to a difference between specified and actual carrier frequency, whereas short-term instability of the local oscillator is one of the possible causes of unstable frequency error.

Coefficient  $\rho$  is one of the modulation quality metrics used in CDMA systems. It is the ratio of correlated power to total power transmitted, when a single code channel is transmitted. The transmitted energy that does not correlate behaves as added noise, with

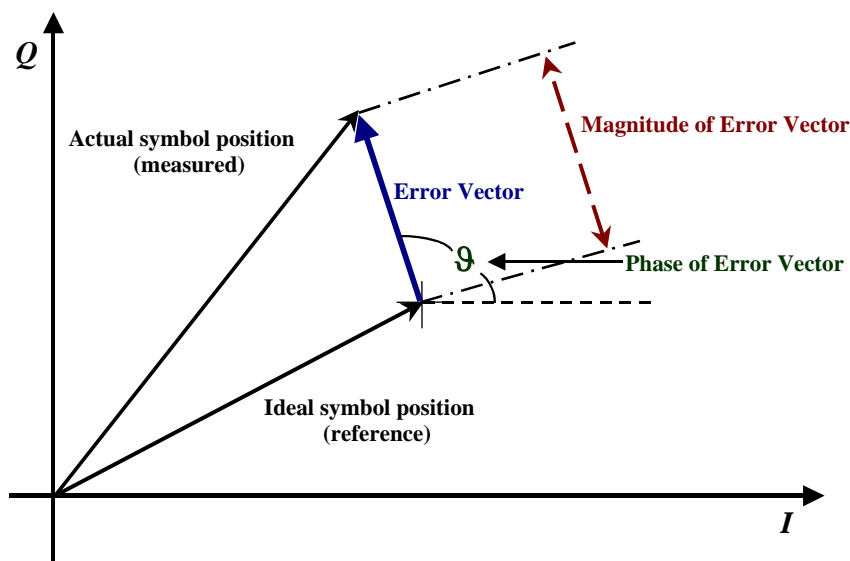


**Fig.I.3 – Error vector definition.**

consequent potential interference on other channels. Code-domain power measures the fraction of total power transmitted in each code channel of a CDMA system; it is evaluated through code-correlation algorithms.

*B. Out-of-channel measurements*

*Adjacent Channel Power Ratio*

Adjacent Channel Power Ratio (ACPR) is defined as the ratio of the average power in the adjacent channel to the channel power. It gives information about the interference of the signal under examination on adjacent channels. As ACPR depends on the statistics of the transmitted signal, care must be taken to perform ACPR measurements with sense. Specifically, test signals must be accurately chosen, because the results of ACPR measurements made on the same transmitter can significantly vary, depending on the statistics of the signal. As an example, higher values of PAR can be responsible for more interference; similarly, the number of data channels in CDMA systems have direct impact on the power statistics of the signal, and therefore on ACPR. It has to be said that adjacent channel power measurements are differently named and carried out according to different communication standards [30],[31],[32].

*Spurious*

It can happen that spurious emissions, due to combination of signals in the transmitter, fall within the band of the communication system. Standards usually define power levels spurious that in-band emissions must not reach in order to avoid interference with other frequency channel of the system.

*I.2.2 - Out-of-band measurements*

*Spurious and harmonics*

Spurious emissions outside the system frequency band are due to transmitter non-linearities. They can be responsible for interference with other communication systems.

**I.3 - Transmitter troubleshooting**

Conformance of a transmitter with the standard is verified through tests, which can be performed at the antenna port, as well as at other sections of the transmitter. Since impairments that can occur at different parts of the system are responsible for performance

not meeting standard's requirements, during test stages it is important to single out the sources of impairment. Nevertheless, this is not an easy task, mainly because larger and larger parts of modern communication systems are implemented digitally, and because some of the parts of the transmitter are not accessible. Major manufacturers adopt and suggest troubleshooting procedures designed to help recognize and troubleshoot possible problems from measurements performed at antenna port. Such procedures, designed to have a minimum impact on the time-to-market, rely on the ability to infer possible impairments from a look at the signal, or at the instrument display. In this section, some relevant examples of how possible problems affecting the transmitter can be singled out from the analysis of transmitted signal are given.

### *1.3.1 - Compression*

If instantaneous power level of the signal at the input of the power amplifier, which represents the final block in Fig.I.1, is too high, the amplifier can be driven into saturation, and signal compression can occur, with consequent non-linear distortion on the transmitted signal. Compression can be inferred, for instance, by comparing the CCDF curves of signals at the input and at the output of the amplifier. If compression occurs, the "output" CCDF denotes lower probability of reaching high power values. In case the input section of the amplifier cannot be accessed, comparison can be drawn between CCDF curves measured at the antenna port for lower amplitudes of the transmitted signal.

### *1.3.2 - I/Q impairments*

Fig.I.4 shows the I/Q section of a digital transmitter, whose input is represented by the I and Q discrete-time signals provided by the symbol encoder, and whose output feeds the IF filter. I/Q impairments can be caused by differences between the I and Q paths of the modulator. The most common are (i) gain imbalance, (ii) quadrature error, and (iii) voltage offsets. Difference between gains of the amplifiers on the I and Q separate paths can induce a distortion on the I/Q diagram similar to that shown in Fig.I.5, where gain on the Q path is clearly higher. The effect of gain imbalance is definitely more evident when IF section is implemented in an analog way. A phase shift between the two carriers modulated by signals on the I and Q paths not exactly equal to  $\pi/2$  rad is responsible for a quadrature error, whose effects on the I/Q diagram are depicted in Fig.I.6. Finally, DC offsets possibly introduced in

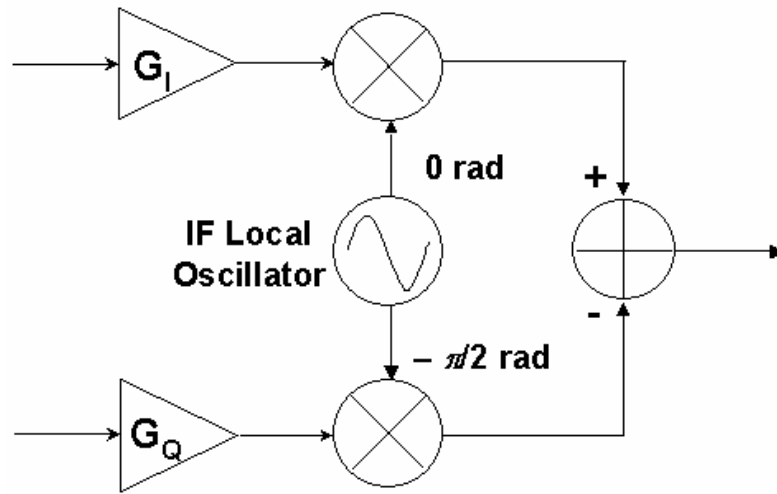


Fig.I.4 – I/Q section of a digital transmitter.

the I and Q paths, for instance added in the amplifier, determine a translation of the I/Q diagram (Fig.I.7). I/Q impairments cause an increase in the error probability, because they reduce the minimum distance of symbols from decision region boundaries; this is visible in Fig.I.5, Fig.I.6, and Fig.I.7, where red dots represent the nominal symbol positions, and blue crosses correspond to the actual symbol positions due to impairments. An analytical model for the effects of such impairments on the demodulated signal is presented in (III.2).

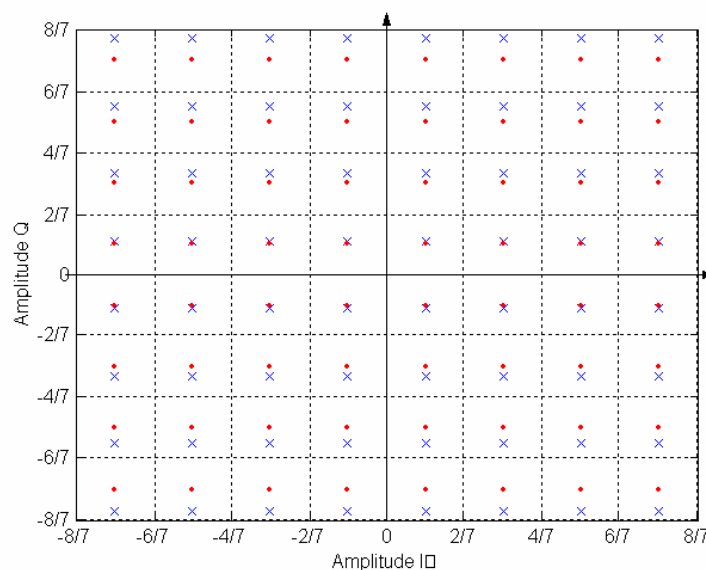
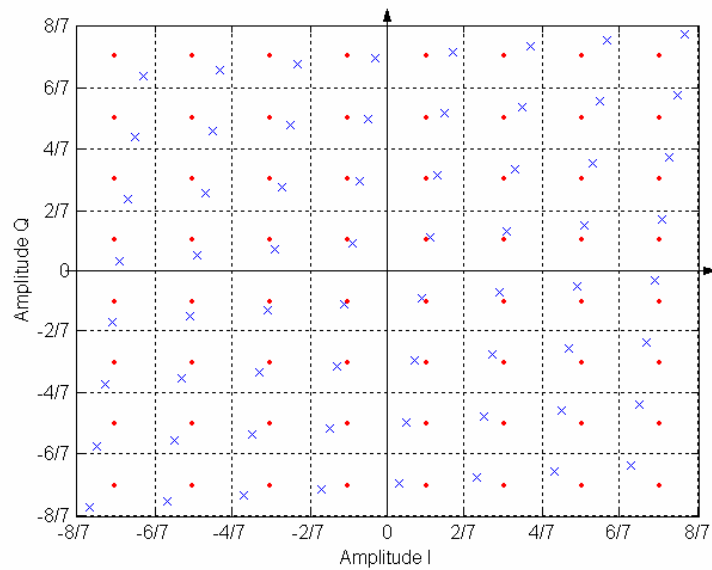
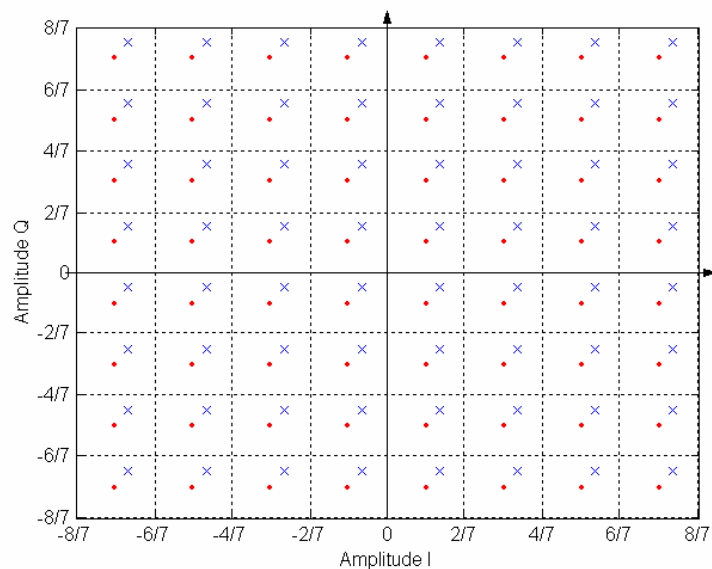


Fig.I.5 – Effect of the presence of gain imbalance for a 64-QAM signal constellation with unitary maximum I/Q component value.



**Fig.I.6 – Effect of the presence of quadrature error for a 64-QAM signal constellation with unitary maximum I/Q component value.**



**Fig.I.7 – Effect of the presence of positive offsets on the in-phase and quadrature components for a 64-QAM signal constellation with unitary maximum I/Q component value.**

The presence of I/Q impairments can be inferred by analyzing the EVM, although it is difficult to determine *which* impairment is present without a look at the I/Q diagram.

### 1.3.3 - Incorrect symbol rate

An incorrect symbol rate is a defect of the symbol encoder, which can affect the ability to correctly interpret symbols at receiver side. Its presence can be deduced from the evolution versus time of EVM, which exhibits a typical “V” shape, as shown in Fig.I.8.

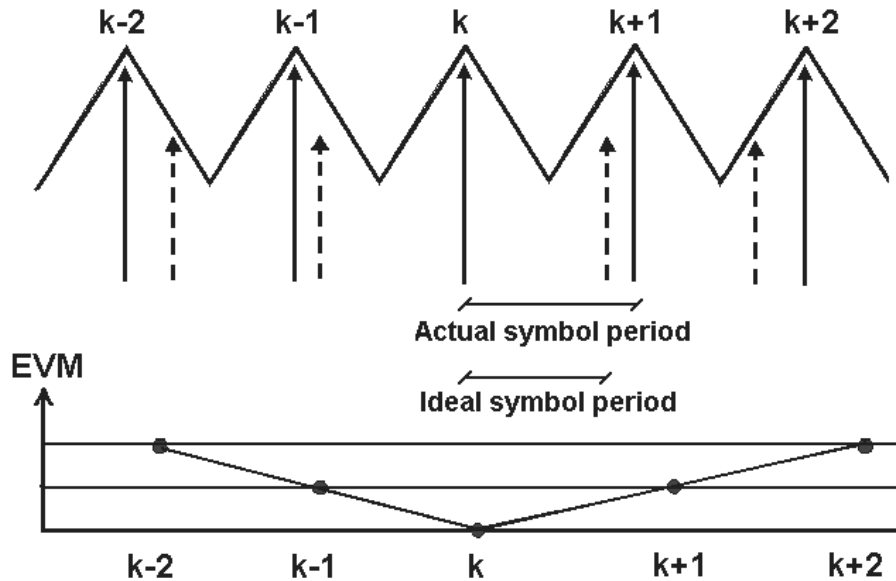
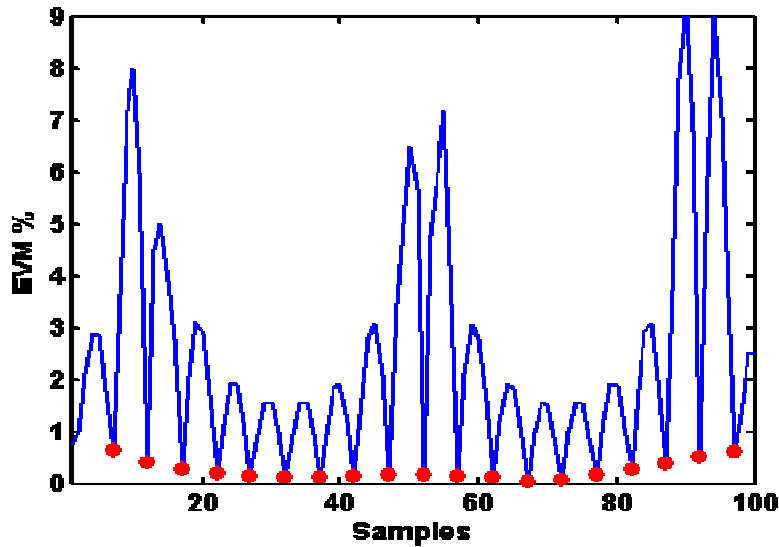


Fig.I.8 – Incorrect symbol rate and evolution versus time of EVM.

### 1.3.4 - Wrong filter coefficients and incorrect windowing

If baseband filtering is implemented incorrectly, amplitude overshoot in the signal or interference in the adjacent frequency channel may occur. In systems using Nyquist filters, possible problems are caused by an incorrect choice of roll off factor,  $\alpha$ . Furthermore, the approximation of the ideally IIR (Infinite Impulse Response) filter by means of a FIR (Finite Impulse Response) one can cause problems in case the truncation is too abrupt. An incorrect value of  $\alpha$ , as well as incorrect windowing, cause incorrect transitions between successive symbols, while the symbol points remain at their original location. The analysis of evolution versus time of EVM can therefore be of great help for detecting such problems, since a diagram similar to that depicted in Fig.I.9 is experienced.



**Fig.I.9 – Evolution versus time of EVM in the presence of wrong filter coefficients and/or incorrect windowing.**

### *1.3.5 - IF filter non-idealities*

The IF filter is deputed to eliminate out-of-channel interference after the I/Q modulation. Its amplitude should ideally be flat in the band of interest, and its group delay should be constant across the same bandwidth. A typical impairment that can affect IF filters is ripple in the frequency response, which causes a degradation of the I/Q diagram accounted for by EVM.

### *1.3.6 - Local oscillator instability*

Instability of local oscillators (LO) may induce interference with other channels. Both I/Q diagram and phase error evolution versus time give evidence of LO instability.

### *1.3.7 - Interfering tones*

An interfering tone can disturb the transmitted signal if it falls within the signal's bandwidth, while it can cause interference with other channels or systems if it is outside of the signal bandwidth. While the frequency-domain analysis of the transmitted signal frequency can clearly give evidence of the latter case, it could be of no utility in the former, since the tone could be masked inside the spectrum. On the contrary, the I/Q diagram can reveal circles around nominal positions of the symbols, if the tone amplitude is not too small. Circles due to

a tone of small amplitude may, in fact, be confused with noise. A good method to measure amplitude and frequency of interfering tones is to perform a spectral analysis of the EV. As shown in Fig.I.10, the tone stands out of the magnitude spectrum of the EV.

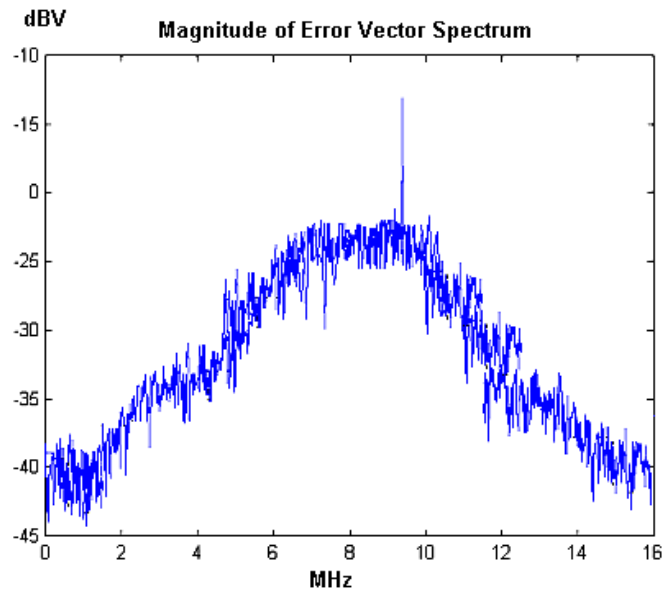


**Fig.I.10 –Magnitude spectrum of EV in the presence of an interfering tone inside signal bandwidth.**

### *1.3.8 - DAC impairments*

Although a DAC should ideally output a series of delta impulses, impulses of a certain width are observed in practice. A  $\sin(x)/x$  function in the frequency domain must therefore be compensated for a correct functioning of the system; otherwise a distortion in the spectrum of transmitted signal occurs.

### *1.3.9 - Burst shaping impairments*

In TDMA systems, a burst modulator is present in the block diagram of the transmitter, before the final amplification stage. If burst parameters are not in accordance with specifications, harmful interference can occur. Overshoot on power-up, frequency drift, amplitude droop, and erroneous burst width are only some of the potential problems that can be experienced. Time-domain measurements and TFR-based measurements can help troubleshooting this kind of impairments.



## **CHAPTER II**

### **PERFORMANCE EVALUATION**

#### **II.1 - Introduction**

The chapter presents some original measurement methods for performance evaluation of RF digital communication transmitters. Power measurement, CCDF curve estimation, and transient evaluation, which are some of the most significant measurements carried out to assess transmitter performance, are in particular dealt with. For each measurement, a state of art is discussed, the proposed method is described, details about the experimental setup are given, and experimental results are commented on in order to assess the performance of the method.

#### **II.2 - Power measurement**

##### *II.2.1 - Introduction*

Power measurement in digital wireless communication systems is not an easy task. This is particularly true in the presence of spread spectrum and/or wideband signals, due to their noise-like nature and high crest factor (peak to average power ratio). Repeatability problems, usually accompanied by low accuracy, are, in fact, often experienced in power measurements involving the integration of the power spectral density (PSD) of the RF signal over a specified

frequency range [30],[36],[37],[38],[39]; channel power, occupied bandwidth and adjacent channel power ratio measurements are relevant examples [2],[40],[41],[42],[43].

With the aim of overcoming the aforementioned problems, a method for power measurement in digital wireless communication systems has recently been published [44], which is based on non-parametric solutions for spectral estimation. The main limit of the method is its heavy computational burden, which can compromise its use in production and testing stages of digital wireless equipment. Reducing measurement time, while granting the same good repeatability as that provided by the use of non-parametric PSD estimators, is still an open issue. To this end, the utilization of a parametric spectral estimator, characterized by reduced convergence time, is investigated in this section. Specifically, a new method for power measurement is proposed, which first digitizes the RF signal under test, then estimates its true PSD according to Burg's parametric solution, and finally applies straightforward measurement algorithms to the PSD, in order to evaluate the quantities of interest.

Advantages of the new method are proved through a number of experimental tests, carried out on both laboratory WCDMA (Wideband Code Domain Multiple Access) signals peculiar to UMTS (Universal Mobile Telecommunication System) [2], synthesized by means of an arbitrary waveform generator, and real DVB-S (Digital Video Broadcasting - Satellite) [10] signals, received through a professional satellite station.

### *II.2.2 - Theory underlying the proposed method*

Some theoretical notes on parametrical PSD estimation are given in the following; further details can be found in [45].

Suppose that the discrete parametric stationary process  $\{X_t\}$  has a PSD that is completely determined by  $k$  parameters  $a_1, a_2, \dots, a_k$ , namely

$$S(f) = S(f; a_1, a_2, \dots, a_k) \quad . \quad (II.1)$$

Given a time series that can be regarded as a realization of this process, if the parameters of  $S(\cdot)$  can reasonably be estimated from this data by  $\hat{a}_1, \hat{a}_2, \dots, \hat{a}_k$ , then

$$\hat{S}(f) = S(f; \hat{a}_1, \hat{a}_2, \dots, \hat{a}_k) \quad (II.2)$$

is a reasonable estimate of  $S(f)$ .

An autoregressive model of order  $p$ ,  $AR(p)$ , is the most widely used functional form for PSD estimation. A stationary  $AR(p)$  process  $\{Y_t\}$  with zero mean satisfies the equation

$$Y_t = \phi_{1,p} Y_{t-1} + \phi_{2,p} Y_{t-2} + \dots + \phi_{p,p} Y_{t-p} + \varepsilon_t \quad (\text{II.3})$$

where  $\phi_{1,p}, \phi_{2,p}, \dots, \phi_{p,p}$  are  $p$  fixed coefficients, and  $\{\varepsilon_t\}$  is a white noise process with zero mean and variance  $\sigma_p^2$ . The process  $\{\varepsilon_t\}$  is often called the innovations process associated with the AR( $p$ ) process, and  $\sigma_p^2$  is called the innovations variance.

The PSD for a stationary AR( $p$ ) process is given by

$$S(f) = \frac{\sigma_p^2 T_s}{\left| 1 - \sum_{m=1}^p \phi_{m,p} e^{-j2\pi m f T_s} \right|^2}, \quad |f| \leq f_N \quad (\text{II.4})$$

where  $T_s=1/f_s$  is the sampling interval between values in the process, and  $f_N=1/(2T_s)$  is the Nyquist frequency.

The two main rationales for this particular class of parametric PSD functions can be so synthesized: first, it can be shown that any continuous PSD can be approximated arbitrarily well by an AR( $p$ ) PSD, if  $p$  is chosen large enough [46], and, second, there exist efficient algorithms for fitting AR( $p$ ) models to time series.

Consequently, assumed that  $p$  is known, to form an AR( $p$ ) PSD estimate it is necessary to properly estimate the  $p+1$  parameters  $\phi_{1,p}, \phi_{2,p}, \dots, \phi_{p,p}$ , and  $\sigma_p^2$ . The question is how to estimate them. If both sides of equation are multiplied by  $Y_{t-k}$ , the equation

$$Y_t Y_{t-k} = \sum_{m=1}^p \phi_{m,p} Y_{t-m} Y_{t-k} + \varepsilon_t Y_{t-k} \quad (\text{II.5})$$

is yielded. By taking expectations, we have

$$s_k = \sum_{m=1}^p \phi_{m,p} s_{k-m} + E[\varepsilon_t Y_{t-k}] \quad (\text{II.6})$$

where

$$s_k = E[Y_t Y_{t-k}] \quad (\text{II.7})$$

is the autocovariance sequence. The plausible fact that  $E[\varepsilon_t Y_{t-k}] = 0$ , for  $k > 0$ , implies that

$$E[\varepsilon_t Y_t] = E\left[\varepsilon_t \left(\sum_{m=1}^p \phi_{m,p} Y_{t-m} + \varepsilon_t\right)\right] = \sum_{m=1}^p \phi_{m,p} \cdot E[\varepsilon_t Y_{t-m}] + E[\varepsilon_t^2] = \sigma_p^2. \quad (\text{II.8})$$

Hence, by observing that  $s_j = s_{-j}$ , equation (II.6), evaluated for  $k = 0, 1, \dots, p$ , leads to the so-called augmented Yule-Walker equations:

$$\begin{bmatrix} s_0 & s_1 & \cdots & s_p \\ s_1 & s_0 & \cdots & s_{p-1} \\ \vdots & \vdots & \ddots & \vdots \\ s_p & s_{p-1} & \cdots & s_0 \end{bmatrix} \begin{bmatrix} 1 \\ -\phi_{1,p} \\ \vdots \\ -\phi_{p,p} \end{bmatrix} = \begin{bmatrix} \sigma_p^2 \\ 0 \\ \vdots \\ 0 \end{bmatrix} \quad (II.9)$$

In the presence of a time series that is a realization of a portion  $X_1, X_2, \dots, X_N$  of any discrete parameter stationary process with zero mean  $\{X_t\}$ , an AR( $p$ ) model could be fit by replacing  $s_k$  with

$$\hat{s}_k \equiv \frac{1}{N} \sum_{t=1}^{N-|k|} X_t X_{t+|k|} \quad (II.10)$$

and solving system (II.9) by inversion. The better the arbitrary stationary process  $\{X_t\}$  is approximated by an AR( $p$ ) stationary process, the more reasonable is this procedure. Concerning this, given the values of  $X_{t-1}, X_{t-2}, \dots, X_{t-k}$  of a stationary process  $\{X_t\}$  with zero mean, the best linear prediction of the value of  $X_t$ , i.e. the one that minimizes the mean square error [47], is

$$\bar{X}_t(k) \equiv \sum_{m=1}^k \phi_{m,k} X_{t-m} \quad (II.11)$$

also named the *forward predictor of  $X_t$  of length  $k$* .

To avoid matrix inversion, a time-consuming task, system (II.9) can be solved through Levinson-Durbin recursions [47], which take advantage of a nice property of parameters  $\phi_{1,p}, \phi_{2,p}, \dots, \phi_{p,p}$  and  $\sigma_p^2$ . Equation (II.11) induces, in fact, a recursive procedure, at the  $k$ -th stage of which, given the estimates  $\bar{\phi}_{1,k-1}, \bar{\phi}_{2,k-1}, \dots, \bar{\phi}_{k-1,k-1}, \bar{\sigma}_{k-1}^2$ , an estimate of the partial autocorrelation coefficient  $\phi_{k,k}$  is attained as

$$\bar{\phi}_{k,k} = \frac{\hat{s}_k - \sum_{m=1}^{k-1} \bar{\phi}_{m,k-1} \hat{s}_{k-m}}{\bar{\sigma}_{k-1}^2} \quad (II.12)$$

and the  $k$  parameters  $\phi_{1,k}, \phi_{2,k}, \dots, \phi_{k-1,k}, \sigma_k^2$  are then calculated according to:

$$\bar{\phi}_{m,k} = \bar{\phi}_{m,k-1} - \bar{\phi}_{k,k} \bar{\phi}_{k-m,k-1}, \quad 1 \leq m \leq k-1 \quad (\text{II.13})$$

$$\bar{\sigma}_k^2 = \bar{\sigma}_{k-1}^2 (1 - \bar{\phi}_{k,k}^2) \quad (\text{II.14})$$

It is worth noting that, even though Levinson-Durbin recursions grant a significant reduction of computational burden, the need to estimate the autocovariance sequence in order to solve system (II.9) there still exists. A key role in the recursive procedure is, in fact, played by the partial autocorrelation coefficient  $\phi_{k,k}$ , estimated according to (II.12).

### II.2.3 - Proposed method

From an operative point of view, the proposed method can be divided into three stages, each of which is described in the following.

#### A. RF signal downconversion and digitization

As it happens with vector signal analyzers (VSA) and performance spectrum analyzers (PSA), the input RF signal is first downconverted to a suitable IF, and then digitized by means of a data acquisition system (DAS), the bandwidth of which has to include all the significant spectral content of the downconverted signal.

#### B. Power spectral density estimation

Let  $X_1, X_2, \dots, X_N$  be the samples of the downconverted signal. A proper digital signal processing-based approach, based on Burg's solution, is applied to the acquired samples in order to derive an estimate of the PSD of the downconverted signal. In particular, the optimal AR model order,  $p$ , along with estimates  $\bar{\phi}_{1,p}, \dots, \bar{\phi}_{p,p}, \bar{\sigma}_p^2$  of the parameters  $\phi_{1,p}, \dots, \phi_{p,p}, \sigma_p^2$  that appear in (II.4), are assessed.

Burg still uses relations (II.13) and (II.14), but estimates the partial autocorrelation coefficient  $\phi_{k,k}$  on the basis of observed data, rather than estimated autocovariance sequence. Specifically, the approach followed to estimate  $\phi_{k,k}$  consists in minimizing a certain sum of prediction errors, namely

$$SS_k(\bar{\phi}_{k,k}) \equiv \sum_{t=k+1}^N \left[ \bar{e}_t^2(k) + \bar{e}_{t-k}^2(k) \right] \quad (\text{II.15})$$

where  $\bar{e}_t^2(k)$  and  $\bar{e}_{t-k}^2(k)$  are the so-called *observed order k forward and backward prediction errors*, whose expressions are, respectively,

$$\bar{e}_t(k) \equiv X_t - \sum_{m=1}^k \bar{\phi}_{m,k} X_{t-m}, \quad k+1 \leq t \leq N \quad (\text{II.16})$$

and

$$\bar{e}_{t-k}(k) \equiv X_{t-k} - \sum_{m=1}^k \bar{\phi}_{m,k} X_{t-k+m}, \quad k+1 \leq t \leq N. \quad (\text{II.17})$$

By substituting (II.13) into expressions (II.16) and (II.17) and rearranging, observed order  $k$  forward and backward prediction errors can be calculated in terms of order  $k-1$  errors, according to

$$\bar{e}_t(k) = \bar{e}_t(k-1) - \bar{\phi}_{k,k} \bar{e}_{t-k}(k-1), \quad k+1 \leq t \leq N \quad (\text{II.18})$$

and

$$\bar{e}_{t-k}(k) = \bar{e}_{t-k}(k-1) - \bar{\phi}_{k,k} \bar{e}_t(k-1), \quad k+1 \leq t \leq N. \quad (\text{II.19})$$

Function  $SS_k$  in (II.15) can then be equivalently written as a quadratic function of  $\bar{\phi}_{k,k}$ ,

$$SS_k(\bar{\phi}_{k,k}) \equiv A_k - 2\bar{\phi}_{k,k} B_k + A_k \bar{\phi}_{k,k}^2 \quad (\text{II.20})$$

whose coefficients are

$$A_k = \sum_{t=k+1}^N \left[ \bar{e}_t^2(k-1) + \bar{e}_{t-k}^2(k-1) \right] \quad (\text{II.21})$$

and

$$B_k = 2 \sum_{t=k+1}^N \bar{e}_t(k-1) \bar{e}_{t-k}(k-1) \quad (\text{II.22})$$

The value of  $\bar{\phi}_{k,k}$  that minimizes  $SS_k$  can be therefore simply calculated as

$$\bar{\phi}_{k,k} = \frac{B_k}{A_k} \quad (\text{II.23})$$

The flow chart in Fig.II.1 schematizes the algorithm implemented to assess the optimal AR order,  $p$ , and estimate the PSD. In particular, initialization of observed forward and

backward prediction errors and innovations variance is first required. Their initial values are chosen according, respectively, to

$$\bar{e}_t(0) = \bar{e}_t(0) = X_t \quad (\text{II.24})$$

and

$$\bar{\sigma}_0^2 = \frac{1}{N} \sum_{t=1}^N X_t^2 \quad (\text{II.25})$$

Successively, starting from  $k = 1$ , the routine evolves through the following steps:

1. Auxiliary terms  $A_k$  and  $B_k$  are calculated according to (II.21) and (II.22).
2. An estimate of  $\phi_{k,k}$  is gained as in (II.23).
3. A check on the estimated partial autocorrelation coefficient is performed. In particular, if

$$|\bar{\phi}_{k,k}| < \delta = \frac{2}{\sqrt{N}}, \text{ order } p \text{ is put equal to } k-1, \text{ and the routine halts, otherwise it goes to the}$$

next step.

4. Order  $k$  backward and forward prediction errors are evaluated according to (II.18) and (II.19).
5. Estimations of  $\phi_{m,k}$ ,  $m = 1, 2, \dots, k-1$  and  $\sigma_k^2$  are calculated according to (II.13) and (II.14).
6. Order  $k$  estimate of the PSD,  $\bar{S}^{(k)}(f)$ , is evaluated in accordance to (II.4):

$$\bar{S}^{(k)}(f) = \frac{\sigma_k^2 T_s}{\left| 1 - \sum_{m=1}^k \phi_{m,k} e^{-j2\pi m f T_s} \right|^2} \quad (\text{II.26})$$

7. Index  $k$  is incremented by 1, and the routine is re-executed from step 1.

When the routine halts, the AR model order  $p$  is set equal to  $k-1$ , and the current PSD estimate  $\bar{S}^{(k-1)}(f)$  becomes the final PSD estimate, which is given in input to the next stage of the proposed method.

The value of  $\delta$  in step 3 is chosen as the result of a number of tests on simulated and emulated signals. The rationale for the choice relies upon the consideration that for a Gaussian AR( $p$ ) process, the  $\bar{\phi}_{k,k}$  terms for  $k > p$  are, approximately, independently distributed with zero mean and a variance equal about to  $1/N$  [48].

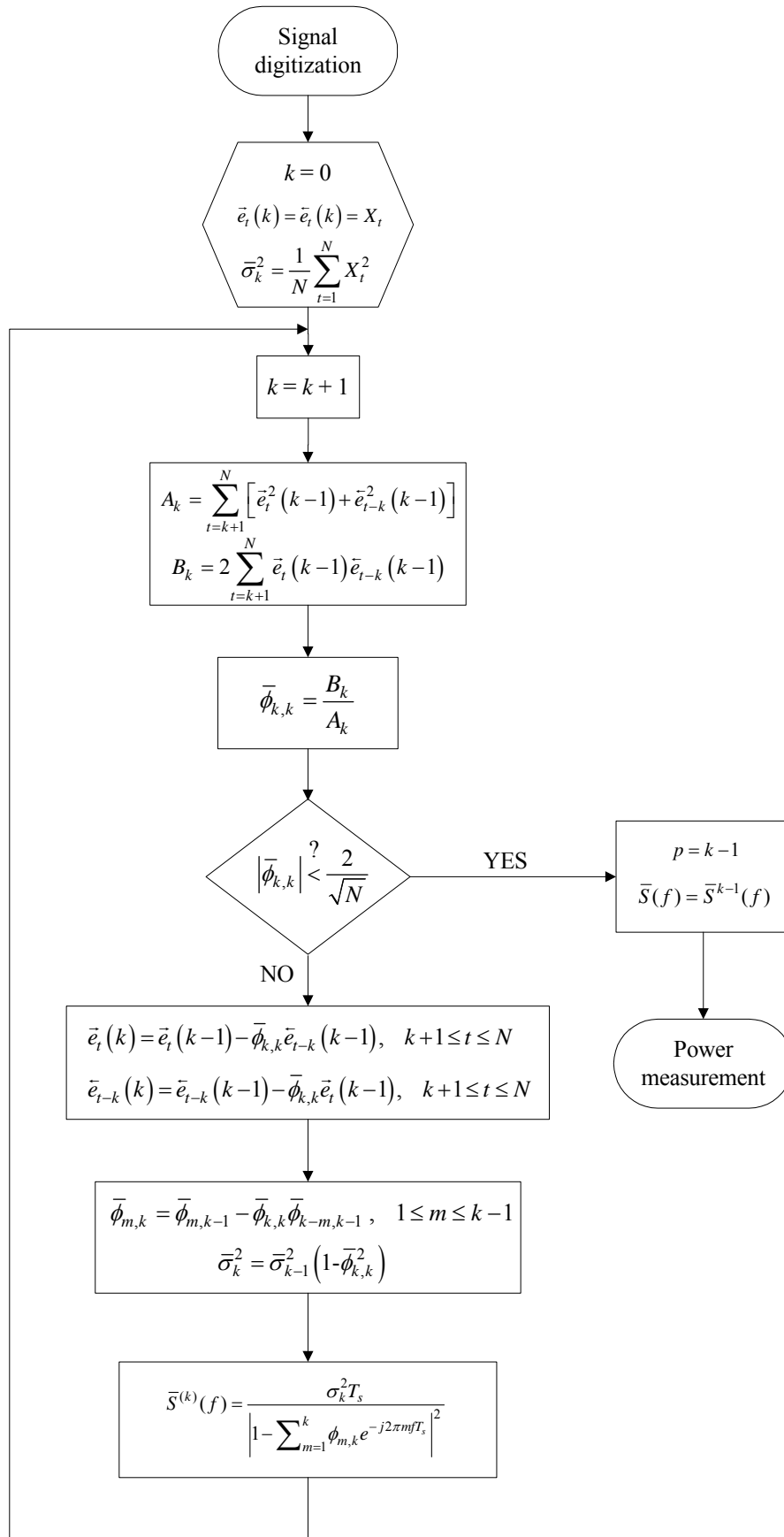


Fig.II.1 - Flow chart diagram of the PSD estimation routine.

### C. Power measurement

Once the PSD of the analyzed signal has been estimated, power measurement can be carried out by means of very straightforward algorithms. In particular, average power, channel power and occupied bandwidth measurements are taken into account. Average power is evaluated by integrating the estimated PSD over the whole frequency span analyzed. With regard to channel power, the frequency interval, centered at the tune frequency of the monitored channel and whose extent is as wide as the channel spacing of the specific system, is first established; then, the desired power is obtained by integrating the PSD over the aforementioned frequency interval. Concerning occupied bandwidth, it is defined as the frequency interval, centered at the tune frequency of the monitored channel, over which the integral of the estimated PSD equals 99% of the average power. Occupied bandwidth is calculated as the difference  $f_2 - f_1$  between the two frequency values,  $f_2$  and  $f_1$ , which make each of the two frequency intervals  $[f_2, f_s/2]$  and  $[0, f_1]$  contain 0.5% of the average power.

### II.2.4 - Performance assessment

The proposed method has been validated through an extended experimental activity. In particular, WCDMA and DVB-S signals have been taken into consideration; the former have been synthesized by means of a proper arbitrary waveform generator, whereas the latter have been received through a professional satellite station.

#### A. Measurement station

A suitable measurement station, shown in Fig.II.2, has been set up to assess the performance of the method. It consists of 1) a processing and control unit, namely a personal computer, 2) a digital storage oscilloscope (DSO) *LeCroy LC 584AL<sup>TM</sup>* [49] (8-bit resolution, 1 GHz bandwidth, 8 GS/s maximum sample rate), 3) a spectrum analyzer *Agilent Technologies HP8594E<sup>TM</sup>* [50] (9 kHz - 2.9 GHz input frequency range, channel power and occupied bandwidth measurement personalities), 4) a spectrum analyzer *Anritsu MS2687B<sup>TM</sup>* [51] (9 kHz – 30 GHz input frequency range, up to 20 MHz resolution bandwidth), acting as downconverter at 66 MHz intermediate frequency, 5) a vector signal analyzer, *Agilent Technologies E4406A<sup>TM</sup>* [52] (7 MHz – 4.0 GHz input frequency range), 6) a performance spectrum analyzer, *Agilent Technologies E4440A<sup>TM</sup>* [53] (3 Hz - 26.5 GHz input frequency range), 7) an RF power meter, *Agilent Technologies E4416A<sup>TM</sup>* [54] (100 kHz – 6.0 GHz input frequency range, 300 kHz, 1.5 MHz, and 5 MHz selectable bandwidth) and 8) the signal source, which is either a digital RF signal generator, *Agilent Technologies E4432B<sup>TM</sup>* [55]

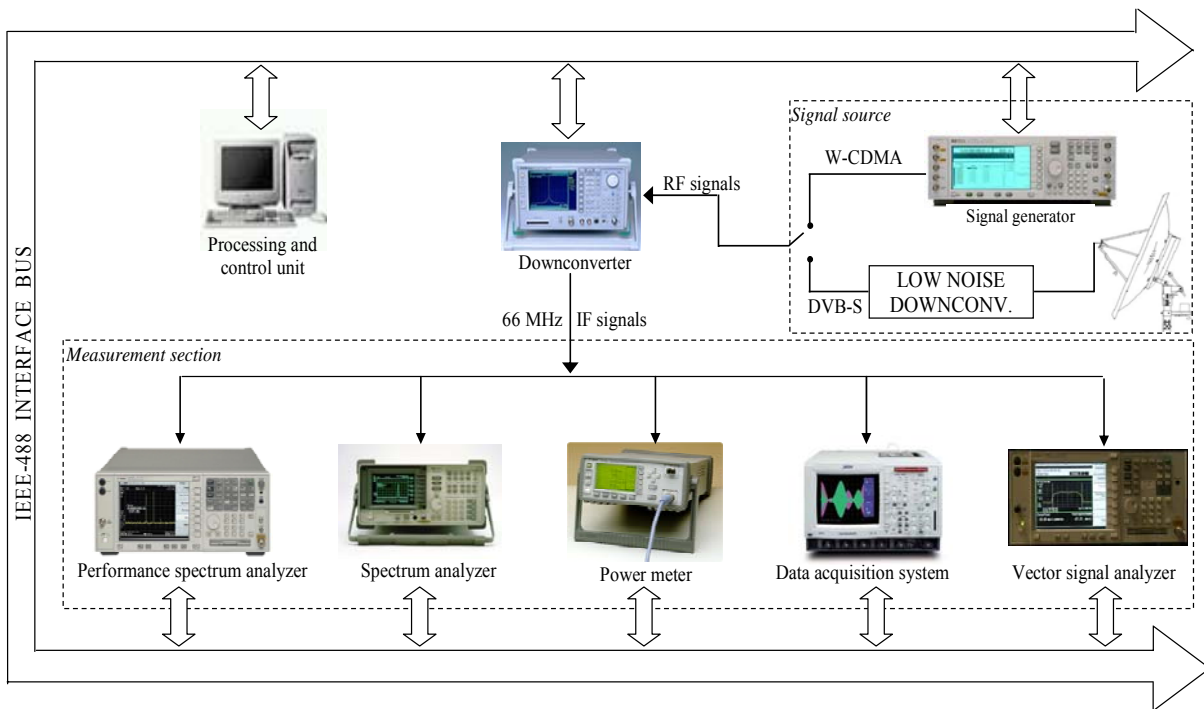


**Fig.II.2– Measurement station.**

(250 kHz – 3.0 GHz output frequency range, I/Q analog inputs) with arbitrary waveform generation (AWG) capability (14-bit vertical resolution, 1 Megasample memory depth, 40 MHz maximum sample clock), or the output of a low noise downconverter (52 dB gain, 0.7 dB noise figure), fed by the satellite signal received through a 1.790 m-diameter parabolic antenna. All the instruments, except the satellite station, are interconnected by means of an IEEE-488 standard interface bus.

### *B. Laboratory wideband signals*

WCDMA test signals have been generated by exploiting the AWG capability of the digital RF generator. Both uplink and downlink signals have been considered. The RF signal is given in input to the spectrum analyzer *Anritsu MS2687B<sup>TM</sup>*, which operates in zero-span mode to downconvert it to 66 MHz intermediate frequency. The downconverted signal is digitized by the DSO at 200 MS/s, and a record of 32,768 acquired samples is retrieved. Measurement algorithms are then applied to the acquired samples in order to evaluate average power, channel power, and occupied bandwidth.

### *C. Real wideband signals*

Experiments have been carried out also on real telecommunication signals. In particular, two different DVB-S signals, *RAI International 4* and *BBC Prime*, have been taken into account, which are emitted, respectively, by *Hot Bird 1* (transponder number 8), and *Hot Bird*

3 (transponder number 27) satellites [56]. *RAI International 4* signal is, in particular, characterized by a central frequency equal to 11.381 GHz, a symbol rate equal to 4.4 Msymbol/s, and a FEC (Forward Error Correction) of 7/8, whereas *BBC Prime* signal is characterized by a central frequency equal to 11.131 GHz, a symbol rate equal to 5.632 Msymbol/s, and a FEC of 3/4. The choice of such signals is imposed by the maximum resolution bandwidth of the spectrum analyzer *Anritsu MS2687B<sup>TM</sup>*.

After being received through the 1.790 m-diameter parabolic antenna, satellite signals are routed to the low noise downconverter, which performs a low noise amplification and a downconversion from *Ku* band (10.7 ÷ 12.75 GHz) to *L* band (950 ÷ 2150 MHz). The *L* band signal is then given in input to the spectrum analyzer *Anritsu MS2687B<sup>TM</sup>*, which operates in zero-span mode to downconvert it to 66 MHz intermediate frequency. The downconverted signal is digitized by the DSO at 200 MS/s, and a record of 32,768 acquired samples is retrieved. Measurement algorithms are then applied to the acquired samples in order to evaluate channel power.

#### D. Results

Table II.1 and Table II.2 depict the results of measurements performed on, respectively, uplink and downlink WCDMA signals; a typical PSD provided by the proposed method is shown in Fig.II.3. Table II.3 gives the results of channel power measurements performed on *RAI International 4* and *BBC Prime* DVB-S signals. All results are expressed in terms of average value  $\mu$  and experimental standard deviation  $\sigma$  over 50 consecutive measurements.

**Table II.1 - Comparison of measurement results obtained in the experiments on uplink WCDMA signals.**

	Average Power		Channel Power		Occupied Bandwidth	
	$\mu$ [dBm]	$\sigma$ [dBm]	$\mu$ [dBm]	$\sigma$ [dBm]	$\mu$ [MHz]	$\sigma$ [MHz]
<i>Proposed method</i>	-29.65	-52.24	-28.81	-49.54	4.069	0.0007
<i>Non-parametric method</i>	-29.49	-48.89	-28.90	-49.75	4.070	0.001
<i>Power Meter</i>	-29.22	-48.64				
<i>Spectrum Analyzer</i>			-30.10	-40.11	4.140	0.078
<i>VSA</i>			-28.93	-44.02		
<i>PSA</i>			-29.31	-45.32	4.074	0.0088

**Table II.2 - Comparison of measurement results obtained in the experiments on downlink WCDMA signals.**

	Average Power		Channel Power		Occupied Bandwidth	
	$\mu$ [dBm]	$\sigma$ [dBm]	$\mu$ [dBm]	$\sigma$ [dBm]	$\mu$ [MHz]	$\sigma$ [MHz]
<i>Proposed method</i>	-29.66	-52.18	-28.74	-51.46	4.135	0.0013
<i>Non-parametric method</i>	-29.54	-50.27	-28.89	-50.12	4.137	0.0015
<i>Power Meter</i>	-29.78	-49.28				
<i>Spectrum Analyzer</i>			-29.98	-40.57	4.280	0.11
VSA			-28.92	-43.29		
PSA			-29.29	-45.56	4.178	0.011

The results of the proposed method are compared to those provided both by the method based on non-parametric estimation [44] and other instruments included in the measurement station. Specifically, the power meter and VSA have executed, respectively, average and channel power measurements, whereas the spectrum analyzer and PSA have provided both occupied bandwidth and channel power values.

From the analysis of the results, the following considerations can be drawn.

- Concurrence of measurement results achieved through different methods and instruments is experienced.
- Repeatability of the proposed method is comparable to that of the method based on non-parametric estimation; experimental standard deviations are very similar to each other.
- Experimental standard deviation of the proposed method is significantly lower than

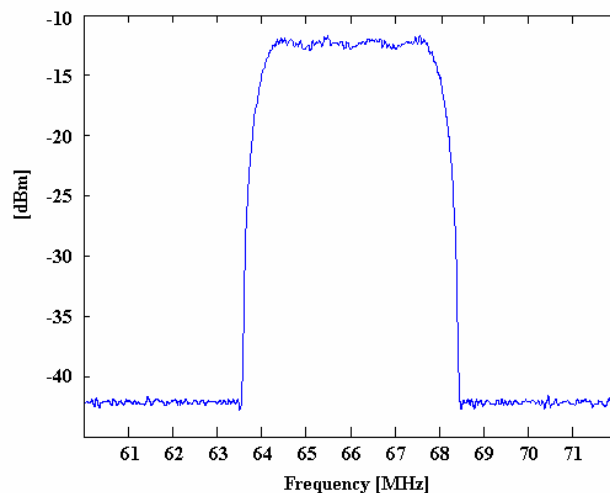


**Fig.II.3 – PSD of a WCDMA signal estimated through the proposed approach.**

that characterizing measurements carried out through the spectrum analyzer. It is even lower with respect to VSA and PSA, which are specifically addressed to this kind of signals.

- Regarding measurement time, the proposed method comes out to be much more convenient and effective. The application of the proposed method takes, in fact, from about 4% to 14% of the time needed to apply non parametric estimation, whatever the configuration adopted.
- With regard to real signals, the proposed method has proved effective and exhibited good performance even in very critical measurement conditions (Fig.II.4).

**Table II.3 - Comparison of channel power measurement results obtained in the experiments on DVB S signals.**

	<i>RAI International 4</i>		<i>BBC Prime</i>	
	$\mu$ [dBm]	$\sigma$ [dBm]	$\mu$ [dBm]	$\sigma$ [dBm]
<i>New method</i>	-62.30	-75.85	-55.67	-74.72
<i>Previous method</i>	-62.19	-76.37	-55.75	-73.96
<i>Spectrum Analyzer</i>	-62.53	-69.14	-54.80	-66.75
VSA	-63.44	-71.25	-55.84	-72.46
PSA	-62.91	-72.18	-55.98	-73.71

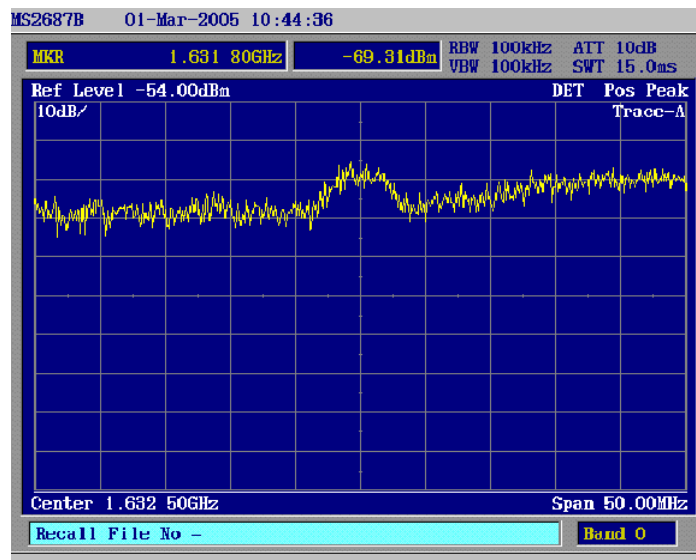


**Fig.II.4 - PSD of Rai International 4 signal attained through the spectrum analyzer Anritsu MS2687B<sup>TM</sup>; very critical measurement conditions are highlighted.**

### *II.2.5 - Conclusion*

A new method for power measurement in digital wireless communication systems has been presented. It is based on parametric spectral estimation, following Burg's solution. Besides overcoming repeatability problems, which often affect such measurement, the method copes with the long convergence time that is the main limitation of an alternative method, based on non-parametric spectral estimation, and presented in [44].

The performance of the method has been assessed by means of a number of experiments, carried out on both laboratory and real wideband telecommunication signals, through a suitable measurement station. Experimental results have shown that repeatability problems experienced with specialized instrumentation are mitigated by the method. Moreover, a comparison of the achieved performance to that granted by the previous method has highlighted comparable experimental standard deviations along with reduced measurement time.

## **II.3 - CCDF curve measurement**

### *II.3.1 - Introduction*

CCDF curves provide a statistical description of power levels of an RF signal. A CCDF curve is, in fact, a plot of relative power level, expressed in dB, versus probability. Specifically,  $CCDF(x)$  represents the probability that the signal envelope power is at least  $x$  dB above the average power; the envelope power is defined as:

$$P(t) = I^2(t) + Q^2(t) \quad (II.27)$$

where  $I$  and  $Q$  are the baseband in-phase and quadrature components of the RF signal. As it is suggested by the definition, a CCDF curve is a strictly decreasing function and its value in the origin of the  $x$ -axis represents the percentage of time the signal spends above its average power level.

CCDF curves are very important for designing, testing and troubleshooting telecommunication components and apparatuses [33],[57]. With regard to design, they give a valid help in preventing signal compression due to the non-linearity of some components such as power amplifiers. The information provided by CCDF curves, in fact, allows designing the amplifier on the basis of the particular signal expected in input; e.g. a Quadrature Phase Shift Keying (QPSK)-modulated input signal will impose different design requirements than a

64-QAM (Quadrature Amplitude Modulation) one. Vice versa, given the amplifier gain versus input power, the CCDF curve can be useful to determine the optimal input signal level. Concerning testing and troubleshooting, CCDF curves are an excellent tool for quantifying compression effects; if a signal is linearly amplified, in fact, its CCDF does not vary, while compression due to non-linearity would result in a decrease of the CCDF.

For the sake of clarity, Fig.II.5 shows the envelope power of a WCDMA signal. Its CCDF curve is given in Fig.II.6: the percentage of time the signal spends above each power level specified by the  $x$ -axis estimates the probability for that particular power level.

Instruments that perform CCDF measurements currently available on the market are high performance spectrum analysers, such as VSAs and PSAs, which demodulate the RF signal under test and then evaluate its CCDF curve by processing the samples of the baseband components.

Two alternative digital signal-processing approaches for CCDF measurements, based on original algorithms that are directly applied to the samples of the RF signal, are presented hereinafter. Both approaches (i) take advantage of proper sampling strategies developed during the research activity that is object of the thesis [58], which grant alias-free sampling and a digital downconversion of the RF signal and (ii) process the instantaneous power trajectory, suitably evaluated. In particular, to gain the instantaneous power trajectory, the first approach (time-domain approach) averages the quadratic values of the samples over a carrier period, while the second (time-frequency approach) applies TFRs [23], [59].

The two approaches do not require any demodulation of the signal under test and do not need special purpose high-performance instrumentation: only a processing unit and a DAS are, in fact, needed.

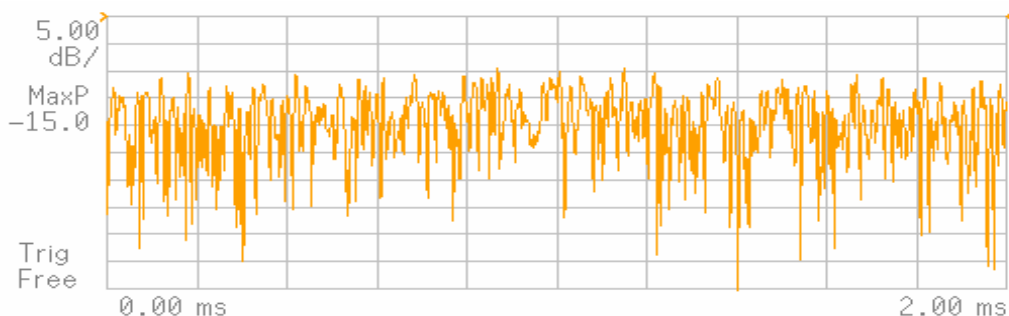


**Fig.II.5 - Envelope power of a W-CDMA signal; its high variability is due to the noise-like nature of the signal.**

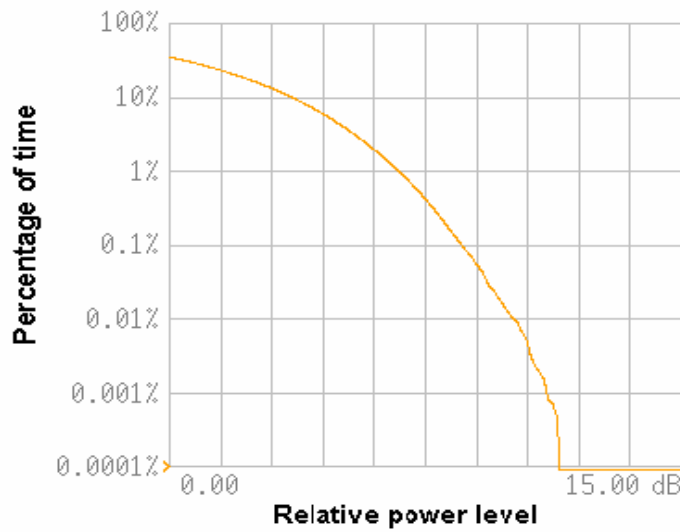


**Fig.II.6 - Power CCDF curve of the signal referred to in Fig.II.5.**

### *II.3.2 - Proposed Approaches*

As stated above, the two proposed approaches gain a measure of the CCDF from the instantaneous power trajectory. In particular, no analog downconversion and/or demodulation of the signal under test are needed; both approaches, in fact, simply process the samples of the RF signal. Specifically, they consist of three steps: (i) signal digitization, (ii) instantaneous power trajectory evaluation and (iii) CCDF curve determination.

#### *A. Signal digitization*

First, the RF signal,  $s(t)$ , is digitized by a DAS at the sampling frequency provided by one of the algorithms presented in [58]. The role played by such algorithm is quite important: it lets the user choose the integer ratio,  $p$ , between the sampling frequency,  $f_s$ , and the frequency at which the spectrum of the digitized signal will be centered, and then outputs the minimum value of the sampling frequency that satisfies such requirement. It is so possible to digitally downconvert the input signal thanks to a sampling frequency much lower than the carrier frequency, with consequent benefits in terms of frequency resolution. Equivalently, it is possible to analyse a larger time interval, given the number of samples. Moreover, as it will be clear soon with regard to the time-domain approach, it grants the advantage of acquiring an integer number of samples per carrier period.

### B. Instantaneous power trajectory evaluation

#### ➤ Time-domain approach

The first proposed approach moves from the following consideration: the carrier frequency is higher than the symbol rate (or chip rate, with regard to 3G signals [2]) and consequently one symbol modulates several carrier periods. It therefore makes sense to average the square voltage values over one carrier period, which represents the minimum averaging interval for gaining a non trivial instantaneous power value.

Thanks to the application of *algorithm I* presented in [58], the same number of samples,  $p$ , are acquired per each carrier period. Then, the  $N$  acquired samples are divided into groups of  $p$  and each point of the power trajectory  $P(k)$  is determined as the mean square value over  $p$  consecutive samples:

$$P(k) = \frac{1}{p} \sum_{n=1}^p s^2 \left( \frac{n + (k-1)p}{f_s} \right) \quad (\text{II.28})$$

#### ➤ Time-frequency approach

The second approach is based on the application of a particular TFR, the STFT (Short-Time Fourier Transform) [23]. The instantaneous power of the signal under analysis is, in fact, evaluated by applying the STFT, which is defined for discrete-time signals as

$$STFT_s(m, n) = \sum_{k=0}^{N-1} w(k-n) s(k) e^{-j2\pi \frac{m}{N} k} \quad (\text{II.29})$$

where  $w(k)$  is the window function, and  $N$  is the number of samples on which  $STFT_s$  is performed;  $k$  stands for the discrete-time variable.

The signal  $s(k)$  is divided into a number of segments, each of which, weighted by the window function  $w(k)$ , is treated separately in order to evaluate its spectral content. Expression (II.29) is computed via an FFT-based algorithm; the results are then taken in modulus and squared in order to attain the so-called spectrogram. In the presence of discrete-time signals, the spectrogram is represented by means of a matrix; row index is connected to frequency, while column index represents time. By visualizing the matrix along a time-frequency plane, the evolution versus time of the power spectral contents of the analyzed signal can be observed. By summing the values along each column, the instantaneous power of the signal as a function of time can be calculated.

It is worth noting that spectrogram results depend on the particular windowing function

adopted. The results of the experimental activity aimed at singling out the optimal tuning of window parameters are given in the next subsection.

### *C. CCDF curve determination*

Finally, the mean and peak signal power levels are evaluated and the CCDF is measured by determining a set of levels, distanced one to another of 0.01 dB, between the mean and the peak signal power level, and calculating the percentage of time during which the signal is above each level. For the sake of clarity, Fig.II.7 shows the evolution of the instantaneous power of a 3G signal versus time. The bold line represents the mean power level, while the thin solid one represents a power level of 1.0 dB above the mean. The value of  $CCDF(x)$ , for  $x = 1.0$  dB, is evaluated as the ratio of the time during which the signal is above the thin dotted line to the observation interval.

### *II.3.3 - Performance assessment*

A suitable measurement station has been set up in order to validate the approaches with regard to real 3G signals characterized by different carrier frequencies and average power levels. In particular, the performance of the two approaches has been evaluated as a function of the number of samples per carrier period,  $p$ . To this aim, CCDF measures gained through

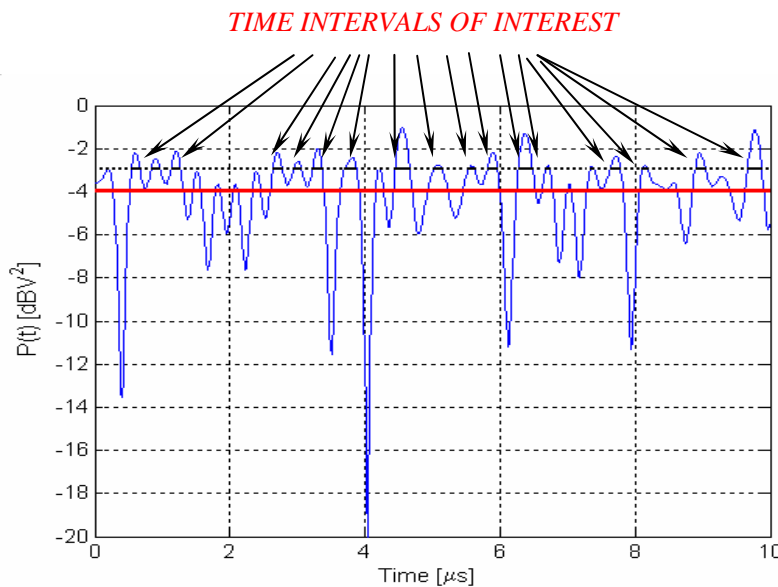


**Fig.II.7 - Evaluation of the CCDF from the instantaneous power trajectory: the bold line is the mean power level, while the thin dotted line is 1 dB above. The value of  $CCDF(x)$ , with  $x=1$  dB, is computed as the ratio between the duration of all the time intervals indicated by the arrows and the overall duration of the signal.**

the application of the proposed approaches have been compared to those provided by a VSA.

#### A. Measurement station

The measurement station adopted for the experimental tests is shown in Fig.II.8. It consists of (i) a processing and control unit, namely a personal computer; (ii) a digital RF signal generator *Agilent Technologies E4432B<sup>TM</sup>* [55] (250 kHz - 3.0 GHz output frequency) equipped with 3G standard-compliant signal generation capability; (iii) a DSO *LeCroy LC 584AL<sup>TM</sup>* [49] (8-bit resolution, 1 GHz bandwidth, 8 GS/s maximum sample rate), and (iv) a synthesized arbitrary waveform generator (0.26 - 1030 MHz output frequency). They are all interconnected by means of an IEEE-488 standard interface bus.

The RF signal, provided by the digital signal generator and complying with the 3G specifications, is digitized according to the following procedure: the optimal sampling frequency,  $f_s$ , is provided by the algorithms presented in [58], and a sinusoidal signal at frequency  $f_s$  is generated by the synthesized signal generator to drive the DSO sampling clock (external clock). Subsequently, the CCDF is measured through the application of the proposed approaches to the acquired samples.

#### B. Optimal choice of time-frequency parameters

As stated before, spectrogram results depend on the particular window function adopted for STFT in (II.29); an optimal choice of the type and size of the window has to be made. To this aim, preliminary measurements on test signals have been carried out considering rectangular, Hanning and Blackman windows, which are some of the most common ones; different window sizes have been taken into account, too. The optimal window type and size have been singled out as those that minimise the *rmse* (root mean square error) between the CCDF measured by applying the proposed approach and that given by the VSA, which has

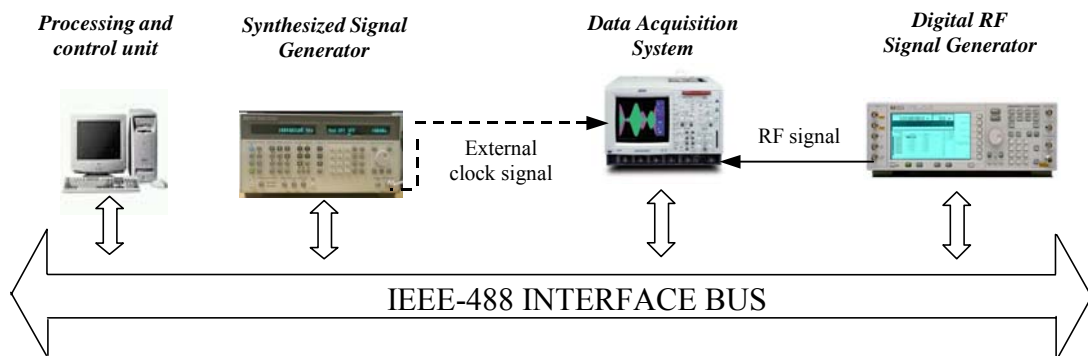


Fig.II.8 - Measurement station.

been taken as the reference curve. Even though both curves to be compared have been evaluated at power levels distanced of 0.01 dB one to another, the value of the peak-to-average power ratio (PAR) measured by the proposed approach and that furnished by the VSA have sometimes been not equal. In such cases,  $P$  and  $Q$ , the number of points constituting, respectively, the measured CCDF curve and the nominal one, were different; consequently, the  $rmse$  has been evaluated as

$$rmse = \sqrt{\frac{1}{M} \sum_{i=1}^M [y(i) - y_r(i)]^2} \quad (II.30)$$

where  $y(i)$ ,  $i = 1, 2, \dots, P$  are the values of the CCDF measured through the proposed approach,  $y_r(i)$ ,  $i = 1, 2, \dots, Q$ , are the values of the CCDF given by the VSA, and  $M = \min(P, Q)$ .

Table II.4 shows the average  $rmse$  values achieved for the considered window type and size, as resulting from measurements carried out on several 3G signals characterized by different carrier frequencies and average power levels. Note that window size is expressed in terms of  $T_c$ , the carrier period. The experimental results show that shorter windows have provided lower values of  $rmse$ . This is not unexpected because the better time resolution granted by shorter windows, at the expenses of frequency resolution, is preferable for our purpose of gaining the instantaneous power trajectory. In particular, the  $2 T_c$ -long Hanning window, which grants the lowest  $rmse$ , turns out to be the most suitable windowing function.

*C. Results*

A second set of experimental tests have then been carried out on 3G signals, in order to assess the performance of the two proposed approaches. Each generated signal has been digitized at different sampling frequencies, with the aim of investigating the role of the parameter  $p$ . For each signal and each given sampling frequency, several acquisitions have been made and the related CCDF curves have been evaluated. Then, the measurement result for the considered signal has been expressed in terms of the average CCDF curve, which has

**Table II.4 - Average values of  $rmse$  between measured and reference CCDF curves.**

		WINDOW SIZE				
		$T_c$	$2T_c$	$3T_c$	$4 T_c$	$5 T_c$
WINDOW TYPE	<i>Rectangular</i>	1.20	1.07	2.08	2.42	2.89
	<i>Hanning</i>	0.89	0.81	0.99	1.28	2.02
	<i>Blackman</i>	0.85	0.83	0.86	1.27	1.98

been obtained by calculating the average value for each abscissa (i.e. for each power level).

For the sake of brevity, Fig.II.9 shows the outcomes of the application of the two approaches to a 3G signal modulating a carrier at 449.4 MHz; in particular, Fig.II.9a is related to the time-domain approach, while Fig.II.9b refers to the time-frequency approach. The two figures compare the CCDF curves gained through the proposed approaches, when different sampling frequencies have been utilized, to the CCDF curve provided by the VSA. In all the cases, the digitized signal has been downconverted to 21.4 MHz with different values of the integer  $p$ . Specifically, in each figure, (i) the dashed line is the CCDF curve achieved when the RF signal is sampled at  $f_s = 428$  MS/s ( $p = 20$ ), (ii) the dotted line is related to a sampling

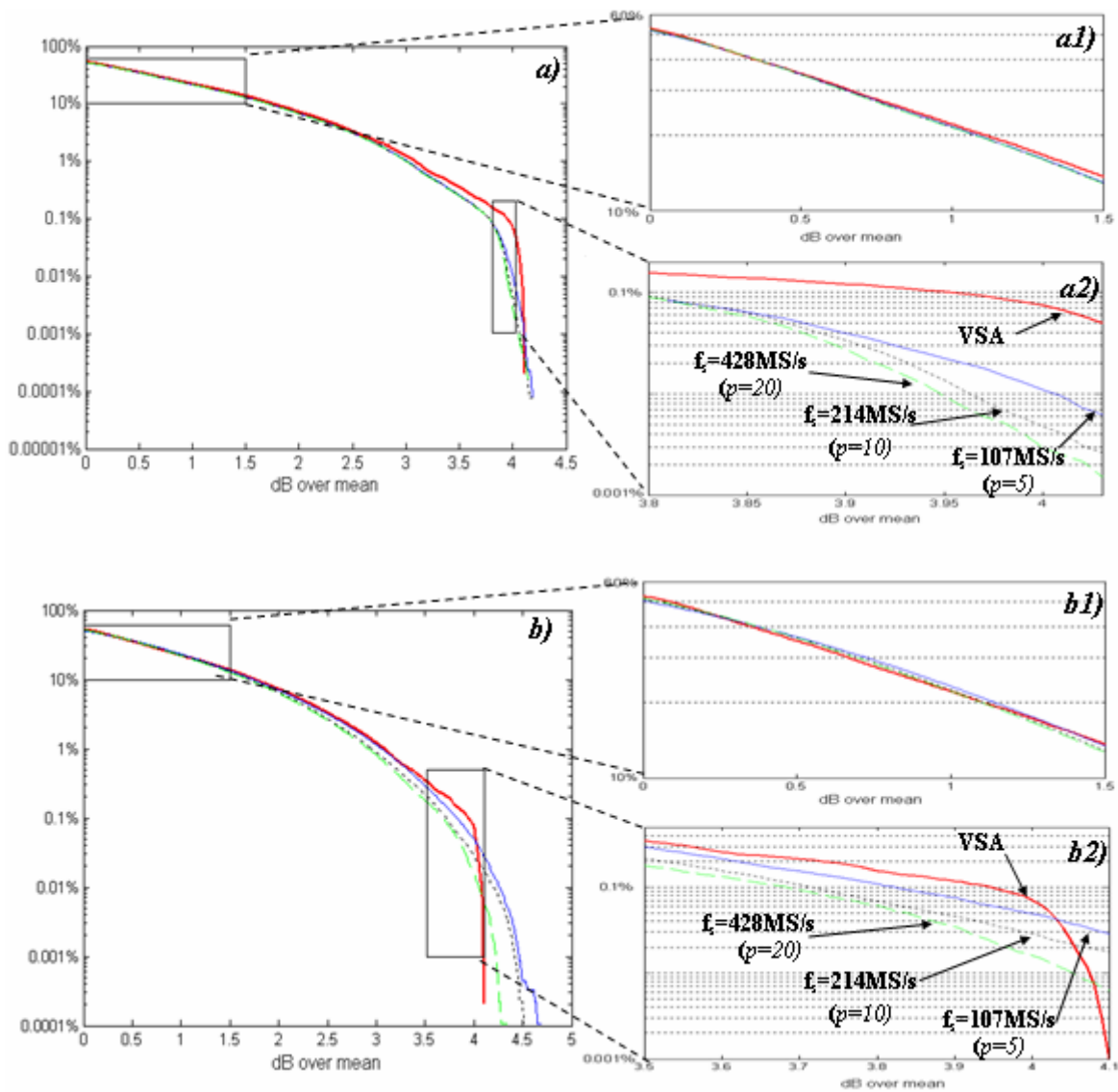


**Fig.II.9 - Comparison between the CCDF provided by the VSA and those provided by a) the time-domain approach, and b) the time-frequency approach, when different values of the sampling frequency,  $f_s$ , and therefore of the ratio  $p$ , are taken into account. Details of low and high power levels are given in a1), a2), b1), b2).**

frequency equal to 214 MS/s ( $p = 10$ ), (iii) the solid line refers to a sampling frequency equal to 107 MS/s ( $p = 5$ ) and, finally, (iv) the bold line is the CCDF curve provided by the VSA.

The results show that the correspondence between the CCDF curve gained through the application of the proposed approaches and that provided by the VSA is greater than that assured by analogous attempts recently made [60]. In particular, as the magnified subfigures prove, the point-to-point difference is particularly small for power levels in proximity to the mean value and is substantially independent from  $p$ . With regard to higher power values, lower values of  $p$  ( $p = 5$  in Fig.II.9) seem to provide better results. It is worth noting that the  $y$ -axis is logarithmically scaled and, therefore, the point-to-point difference that seems to be considerable above 3 dBm is, on the contrary, irrelevant. In other words, the discrepancy between the two curves that appears to be significant over 3 dBm is referred to power levels that are seldom reached by the RF signal. In conclusion, low values of  $p$  ( $p \in \{4, 5\}$ ) are generally preferable, even though higher values have also provided good results. Similar outcomes have been experienced with regard to other considered signals.

## **II.4 - Transmitter transient measurement**

### *II.4.1 - Introduction*

As well known, typical functioning of wireless transmitters generally involves power and/or frequency transients. Both transients are experienced at the transmitter switching on, and, similarly, during bursty transmissions. Another example is provided by TDMA and spread spectrum systems, where rapid and continuous carrier power changes, intended to maximize spectrum utilization and battery life, naturally determine power transients. Moreover, frequency transients occur when transmitters switch from one channel to another.

The main problem connected with transmitter transients is possible interference to other stations. To avoid such interference, transmitter attack time, i.e. the time it takes to switch its output power on, should be short enough. The standard issued by ETSI (European Telecommunication Standard Institute) on electromagnetic compatibility and radio spectrum matters includes a section on measurements of transmitter transient behavior [61]. In particular, the standard defines transmitter attack time in terms of power and frequency transients, establishes its maximum duration, and proposes a related measurement setup. The standard measurement setup is sketched in Fig.II.10. It requires the employment of several instruments, such as an RF detector or a spectrum analyzer, an FM (Frequency Modulation)

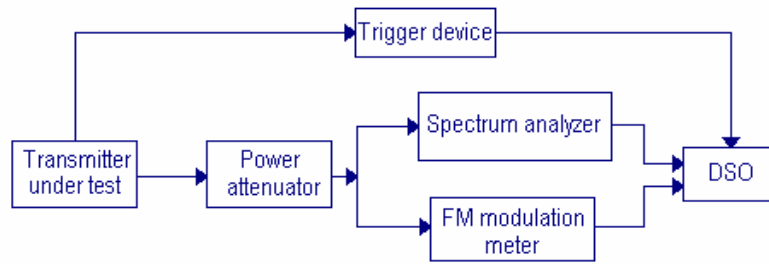


**Fig.II.10 - Standard measurement setup.**

modulation meter, and a DSO. Some major manufacturers have recently proposed the use of VSA, equipped with demodulation capability, to measure transmitter transients with a single instrument and simultaneously display amplitude and frequency versus time [62],[63]. Such instruments, however, demodulate output signal to measure transmitter transient, and therefore need some information on the transmitted signal, such as carrier frequency and modulation type. In the following, a digital-signal processing method, based on TFRs [23] and optimal sampling strategies [58], is proposed for measuring transmitter attack time. The method, which simultaneously measures both power and frequency transients, requires no signal demodulation, thus overcoming VSA limitation. Moreover, it simply processes a few thousand signal samples acquired by means of a common data acquisition system, rather than involving the use of several instruments, as recommended by the standard.

#### *II.4.2 - Proposed method*

The proposed method is mandated to the measurement of wireless transmitter attack time without demodulating its output signal, and without needing special-purpose instrumentation. The method, based on digital-signal processing, consists of three fundamental stages, which are described in the following: (i) sample rate selection and signal digitization, (ii) TFR application to gain instantaneous power and frequency trajectories, and (iii) measurement of power and frequency transients.

##### *A. Sample rate selection and signal digitization*

First, the transmitted signal has to be digitized by the DSO at the sample rate provided by one of the algorithms presented in [58]. In particular, the algorithm receives in input some information on the signal, such as its bandwidth and carrier frequency, and then outputs the minimum sample rate,  $f_s$ , that satisfies user's requirement in terms of spectral allocation of the sampled signal. It is so possible to digitally downconvert the input signal thanks to a sampling

frequency much lower than the carrier frequency, with consequent benefits in terms of frequency resolution. Equivalently, it is possible to analyze a larger time interval, given the number of samples.

### *B. TFR application*

To evaluate instantaneous power and frequency trajectories, a TFR has to be preliminarily applied. A linear TFR should, in particular, be chosen in order to avoid cross terms peculiar to quadratic ones [23]. Two linear TFRs have been considered, and related results compared: the STFT [23], and a modified version of the chirplet transform (CT) [64],[65].

The discrete short-time Fourier transform of the digitized signal  $s(k)$ ,  $STFT_s$ , is evaluated according to (II.29). The modified version of CT is calculated, in accordance to [65], as

$$CT_s(m, n) = \sum_{k=0}^{N-1} g(k-n)s(k)e^{-j2\pi\frac{m}{N}k} \quad (II.31)$$

where  $g(k)$  is a modulated Gaussian window given by

$$g(k) = \sqrt{\frac{1}{\sqrt{2\pi}a}} e^{-\frac{1}{2}\left(\frac{k}{a}\right)^2} e^{-j\pi\left[c(kT)^2 + \frac{b}{3}(kT)^3\right]} \quad (II.32)$$

in which  $a$ ,  $b$ , and  $c$  are respectively the scaling, bending, and chirping factor, whereas  $T$  is the sample period characterizing the acquired signal.

As with regard to STFT, modified CT in (II.31) is computed via an FFT-based algorithm, and results are taken in modulus and squared in order to achieve the evolution versus time of the power spectral contents of the analyzed signal.

### *C. Power and frequency transient measurement*

ETSI standard [61] defines transmitter attack time,  $t_a$ , as the maximum between power and frequency transient durations, defined, respectively, as

a) the time which elapses between the initiation of the "transmitter on" function and the moment when the transmitter output power has reached a level 1 dB below or 1.5 dB above the steady state power,  $P_c$ , and maintains a level within +1,5 dB/-1 dB from  $P_c$ ;

b) the time which elapses between the initiation of the "transmitter on" function and the moment after which the frequency of the carrier always remains within  $\pm 1$  kHz of its steady state frequency,  $f_c$ .

The standard prescribes that  $t_a$  shall not exceed 25 ms.

Instantaneous power and frequency trajectories are evaluated by suitably processing the matrix obtained at the end of the previous step. Instantaneous power of the signal as a function of time can, in particular, be calculated by summing the values along each column of the matrix, and multiplying the result by the frequency resolution, which is equal to  $(NT)^{-1}$ . As the maximum value of the power spectrum is, in each time instant, associated to the instantaneous frequency of the signal, the frequency trajectory can be evaluated by applying a proper peak location algorithm to the matrix [24]. Specifically, for each column, the row index in correspondence of which the power spectrum reaches its maximum is collected in an array, which consequently accounts for the evolution versus time of the frequency of the analyzed signal. No demodulation is thus needed to gain the desired instantaneous power and frequency trajectories. Transmitter attack time is finally measured according to its definition.

### *II.4.3 - Performance assessment*

Typical evolutions of power and frequency transients are given by the standard [61]. The authors have synthesized a signal characterized by such trajectories to properly select the value of each parameter involved in the evaluation of the considered TFRs (e.g. window function, scaling factor, chirp rate and bending factor).

#### *A. Test Signal*

As highlighted by the standard, common features characterizing the time domain evolution of real power and frequency trajectories during transmitter transients are overshoot and ringing. Suitable test signals should assess the capability of the method to accurately measure power and frequency trajectories exhibiting such features. In detail, some significant points characterizing the evolution versus time of power and frequency, that is, respectively, significant values of instantaneous power and frequency, are fixed in correspondence of certain time instants elapsed from the initiation of the "transmitter on" function. The whole trajectory is then synthesized by interpolating between and re-sampling data at the same rate that is intended to be used in the generation process. In particular, piecewise cubic interpolation allows the significant points to pass through unchanged. Finally, test signals are accomplished by imposing the so synthesized trajectories to sinusoidal carriers.

As an example, typical instantaneous frequency and power trajectories of the adopted test signals utilized to assess the performance of the method are shown, respectively, in Fig.II.11 and Fig.II.12. Steady state power and frequency values,  $P_c$  and  $f_c$ , are chosen equal to,

respectively,  $0 \text{ dBV}^2$  and  $25 \text{ kHz}$ . Fig.II.13 shows the evolution versus time of the test signal, which will be generated in analog form, related to the initial transient.

### *B. Experimental Setup*

The measurement station set up for assessing the performance of the method consists of a DSO, a processing and control unit, namely a PC, and an AWG that provides the emulated signal. All instruments are interconnected by means of an IEEE-488 standard interface bus.

The digitally synthesized signal is downloaded into the internal memory of the AWG, which converts it in analog form. The synchronization pulse emitted by the AWG at the beginning of the generation is routed to the trigger channel of the DSO, which performs a single acquisition at a sample rate equal to  $100 \text{ kS/s}$ . The acquired samples are then transferred to the PC, which applies the proposed method to measure the transmitter attack

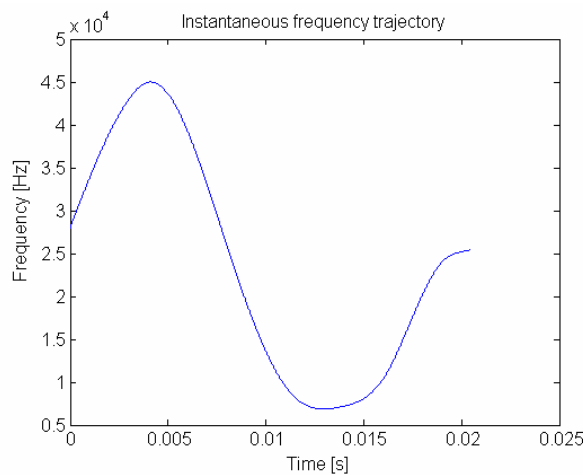


**Fig.II.11 - Instantaneous frequency trajectory of the test signal.**

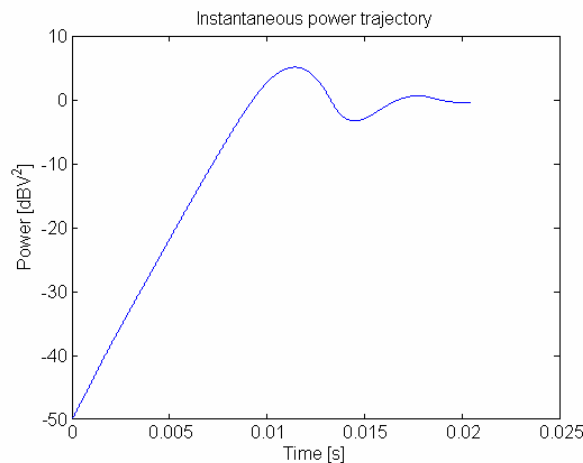


**Fig.II.12 - Instantaneous power trajectory of the test signal.**

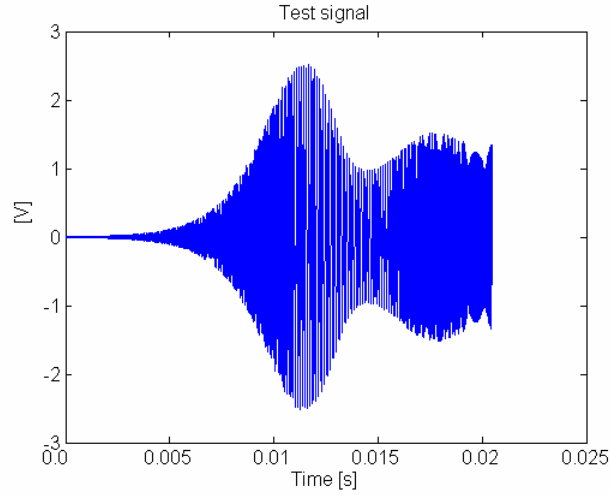


**Fig.II.13 - Evolution versus time of the test signal.**

time.

### C. STFT optimal window function

STFT results depend on the particular window function adopted. Hence, an optimal choice of the type and size of the window is desirable. Common window functions, such as Gaussian, Hanning, Hamming and Blackman, have been considered [66]. Different window sizes have been taken into account, too. In particular, measurements have been carried out using all possible combinations of the four considered window types, and window sizes ranging from 20 to 120 samples. For each parameter combination, frequency, power, and combined *rmse* have been evaluated, which are defined, respectively, as

$$rmse_{freq} = \sqrt{\frac{1}{N} \sum_{i=1}^N [f(i) - \hat{f}(i)]^2} \quad (\text{II.33})$$

$$rmse_{pot} = \sqrt{\frac{1}{N} \sum_{i=1}^N [P(i) - \hat{P}(i)]^2} \quad (\text{II.34})$$

$$rmse = \sqrt{\left(\frac{rmse_{freq}}{f_{rms}}\right)^2 + \left(\frac{rmse_{pot}}{P_{rms}}\right)^2} \quad (\text{II.35})$$

where  $f(i)$  and  $P(i)$  are the nominal frequency and power trajectories, and  $\hat{f}(i)$  and  $\hat{P}(i)$  are the measured ones. Moreover,  $f_{rms}$  and  $P_{rms}$  are, respectively, nominal frequency and power *rms* values.

The optimal window function is the one characterized by the lowest *rmse*. For each type of window function, Table II.5 indicates the optimal window length along with related values of *rmse*. Results reported in Table II.5 show that each window actually provides the same minimum *rmse*. Therefore, any of the considered windows can equivalently be utilized, provided that the respective optimal length is selected. In the experiments, a 37-tap Gaussian window has been utilized, as it comes out to be the optimal choice with regard to both power and frequency *rmse*. In particular, optimized TFR provide an *rmse* value equal to 0.032, thus showing the efficacy and reliability of the proposed method.

Fig.II.14 and Fig.II.15 show a superposition of measured and nominal power and frequency trajectories, when the optimal window function is utilized. In particular, Fig.II.14 is related to frequency transient, whereas Fig.II.15 accounts for power transient. In both figures, the solid line is the measured trajectory and the dotted line is the nominal one. Looking at the figures, significant differences between measured and nominal trajectories can be appreciated at the beginning of two trajectories. This is not an unexpected result; due to the very low power level characterizing the signal at the beginning of the transient, in fact, the random quantization noise introduced by DSO significantly degrades the acquired signal. The maximum value in the corresponding columns of the TFR matrix is, thus, related to the aforementioned noise rather than to the input signal. For the same reason, the measured power trajectory significantly differs from the nominal one during the first portion of the signal. As a consequence, *rmse* values, which are at the basis of the window function choice, are calculated excluding the first portion of instantaneous trajectories, in order to avoid worthless outcomes and achieve the intended result.

*D. Chirplet optimal parameter choice*

To exploit CT’s capabilities its parameters must be suitably tuned according to the local characteristics of the analyzed signal.

**Table II.5 - Results achieved with optimal windows.**

	<i>Optimal length</i>	<i>rmse</i>	<i>rmse<sub>freq</sub></i> [kHz]	<i>rmse<sub>pot</sub></i> [V <sup>2</sup> ]	<i>rmse<sub>freq</sub>/f<sub>rms</sub></i>	<i>rmse<sub>pot</sub>/p<sub>rms</sub></i>
<i>Hanning</i>	25	0.032	0.138	0.049	0.92 %	3.1 %
<i>Hamming</i>	27	0.032	0.139	0.049	0.93 %	3.1 %
<i>Blackman</i>	23	0.032	0.137	0.049	0.91 %	3.1 %
<i>Gaussian</i>	37	0.032	0.136	0.049	0.91 %	3.1 %

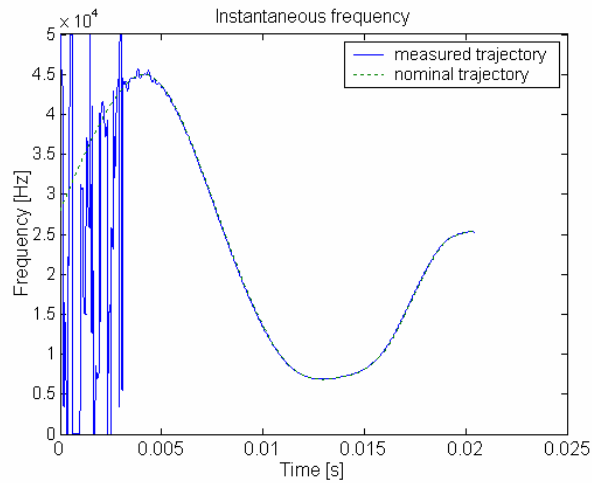


**Fig.II.14 - Instantaneous frequency trajectory gained when optimal values of STFT parameters are used. Measured (solid line) and nominal (dotted line) trajectories are compared.**

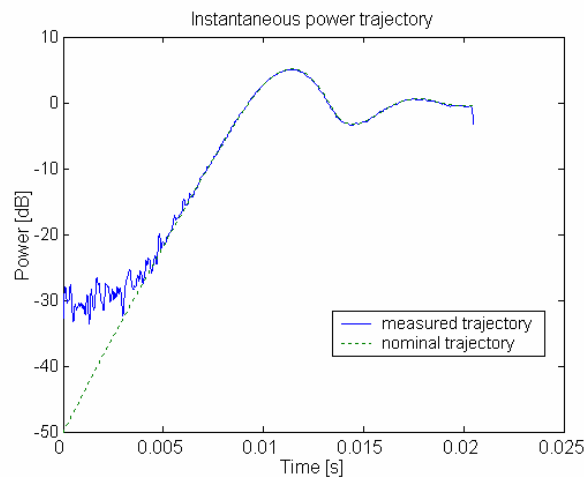


**Fig.II.15 - Instantaneous power trajectory gained when optimal values of STFT parameters are used. Measured (solid line) and nominal (dotted line) trajectories are compared.**

With regard to window type, the 37-tap Gaussian window, which has come out to be optimal for STFT, has been used also for CT.

Concerning chirp rate,  $c$ , and bending factor,  $b$ , their values have been determined from the analysis of a reference frequency trajectory. The same frequency trajectory considered for STFT optimization has been used for the purpose. In detail, it has been digitized at the same sample rate characterizing the acquired signal, and its local characteristics have been expressed in terms of slope (chirp rate), and curvature (bending factor), given by, respectively, the first and second order finite difference.

Finally, a number of frequency and power transient measurements have been carried out to determine the optimal mother chirplet scaling factor,  $a$ , which is the value that minimizes  $rmse$  given in (II.35). In particular, the plot of  $rmse$  values versus  $a$  exhibits a minimum equal to 0.021 in correspondence of a mother chirplet scaling factor equal to 4.0.

#### *II.4.4 - Tests on real transmitters*

Once optimal parameter combinations have been singled out, the proposed method has been applied to real transmitters operating in the range [30 MHz – 1 GHz], to which ETSI standard [61] is addressed. In particular, attack times of (i) a transmitter intended to be part of a bug and (ii) a walkie-talkie have been measured.

##### *A. Bug transmitter*

The transmitter under test has been set to a steady state carrier frequency  $f_c$  equal to 75.827 MHz. Its output signal has been sampled at 250 kS/s, so as to center the sampled signal at 77 kHz. A short pre-trigger has been imposed in order to capture the whole power and frequency transients. Fig.II.16 plots the evolution versus time of the acquired signal, whereas Fig.II.17 and Fig.II.18 respectively show instantaneous frequency and power trajectories provided by the method, when CT is applied. Very similar trajectories are obtained through STFT. The measurement has been repeated after tuning transmitter steady state carrier frequency  $f_c$  to 85.817 MHz, when the signal, sampled at 250 kS/s is centered at 67 kHz. Table II.6 enlists achieved results, expressed in terms of power and frequency transient duration, respectively  $t_p$  and  $t_f$ , and transmitter attack time,  $t_a$ , which is equal to  $\max(t_p, t_f)$ , in accordance to the standard definition. Results show that attack time is basically

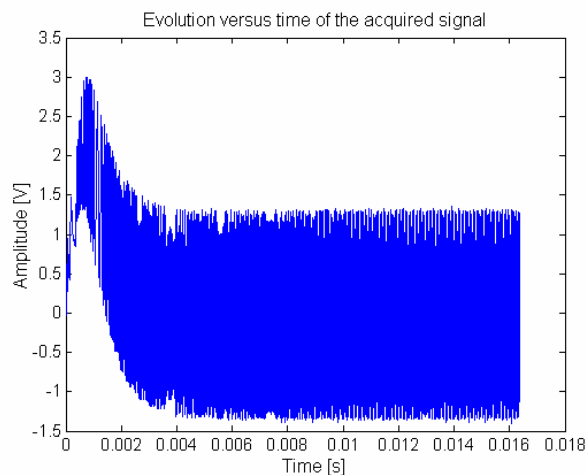


**Fig.II.16 - Evolution versus time of the signal acquired from the bug transmitter.**

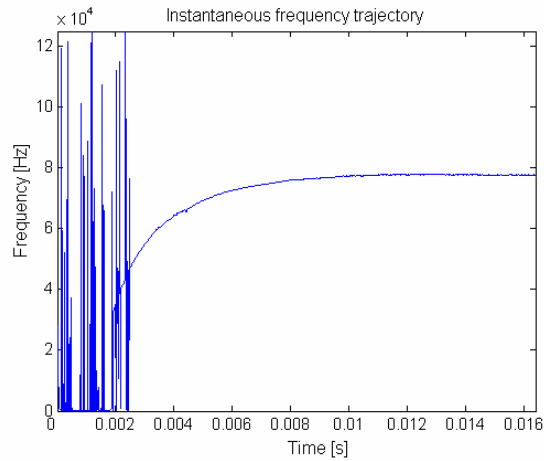


**Fig.II.17 - Instantaneous frequency trajectory, obtained through the use of CT, of the signal at the output of the bug transmitter.**

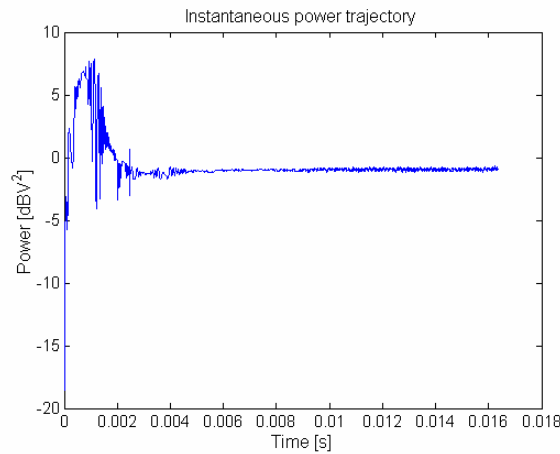


**Fig.II.18 - Instantaneous power trajectory, obtained through the use of CT, of the signal at the output of the bug transmitter.**

determined to frequency transient. No significant discrepancy in the results emerges when the adopted TFR is either CT or STFT; differences between related results are, in fact, within 2%. STFT is therefore preferable, because its computational burden is much lower than that characterizing the CT.

**Table II.6 - Measurement results related to the bug transmitter.**

<i>Steady state <math>f_c</math></i>	<i>TFR</i>	<i>t<sub>f</sub> [ms]</i>	<i>t<sub>p</sub> [ms]</i>	<i>t<sub>a</sub> [ms]</i>
<b>75.827 MHz</b>	<b>CT</b>	14.33	2.64	14.33
	<b>STFT</b>	14.17	2.66	14.17
<b>85.817 MHz</b>	<b>CT</b>	6.61	2.44	6.61
	<b>STFT</b>	6.61	2.48	6.61

*B. Walkie-talkie*

The proposed method has been applied also to measure the attack time of a walkie-talkie, when receiving a sinusoidal 20 kHz signal in input. The steady state carrier frequency  $f_c$  of the transmitter under test is equal to 30.225 MHz. Its output signal has been sampled at  $f_s = 200$  kS/s, the sampled signal being consequently centered at  $f_s/8$ . The evolution versus time of the acquired signal is shown by Fig.II.19. Measurement results for both TFRs are reported in Table II.7, expressed in terms of transmitter attack time,  $t_a$ , and frequency and power transient durations,  $t_f$  and  $t_p$ . In this case, power transient is longer than frequency one, and therefore determines the walkie-talkie attack time, which is largely within the limits imposed by the standard. Table II.7 also shows that the difference between transient durations measured through the application of CT and that provided by the use of STFT is inferior to 2%. STFT is therefore preferable, because its computational burden is much lower than that characterizing the CT.

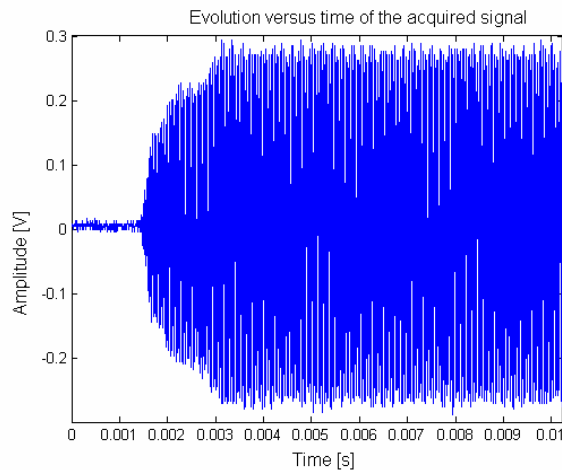


**Fig.II.19 - Evolution versus time of the signal acquired from the walkie-talkie.**

**Table II.7 - Measurement results related to the walkie-talkie.**

<i>TFR</i>	$t_f$ [ms]	$t_p$ [ms]	$t_a$ [ms]
<b>CT</b>	1.55	2.90	2.90
<b>STFT</b>	1.58	2.90	2.90

*II.4.5 - Conclusion*

A digital-signal processing method, based on linear TFRs, has been proposed to measure wireless transmitter attack time. The method simultaneously measures both power and

frequency transients, and requires neither signal demodulation, nor costly special-purpose instrumentation. Moreover, thanks to the use of band-pass sampling strategies, just a few thousand samples, acquired by means of a common laboratory DSO, are needed for the scope.

To single out the optimal values of TFR parameters, proper signals have been digitally synthesized, whose instantaneous power and frequency trajectories evolve in accordance to those reported in [61]. Optimal parameter values have then been selected as those granting the minimum *rmse* with regard to nominal trajectories.

Experimental results have assessed the reliability and efficacy of the method in measuring instantaneous power and frequency trajectories. Experienced values of *rmse* for optimized STFT and CT are equal respectively to 0.032 and 0.021. Moreover, transmitter attack time measurements carried out on real wireless transmitters, utilizing either one of the linear TFRs considered, provide concurring results.



## **CHAPTER III**

### **I/Q IMPAIRMENTS DETECTION AND EVALUATION**

#### **III.1 - Introduction**

Proper functioning of RF digital transmitters mainly relies upon the performance of the I/Q modulator they are normally equipped with. Impairments in the I/Q modulation section, also called I/Q impairments, such as gain imbalance, quadrature error, and voltage offsets, can severely degrade the quality of transmitter output signal, with a consequent reduction of transmission efficiency. Detection of I/Q impairments and evaluation of their amount is therefore crucial for transmitter troubleshooting, and in every stage of transmitter lifecycle. A significant part of the research activity at the basis of this thesis has been devoted to that: three different solutions for I/Q impairments detection and evaluation are presented in the following, each of which is designed to be particularly effective in one or more cases of practical interest. The proposed solutions have been extensively tested on telecommunication signals to assess their performance.

#### **III.2 - A measurement method based on clustering**

##### *III.2.1 - Introduction*

Due to the high degree of integration, direct access to the I/Q modulation section of a digital transmitter is precluded; only the transmitter output signal, generally at radiofrequency,

is often available for the analysis. Unfortunately, the overall effect observable on the output signal is normally due to different simultaneous impairments, which must be separated one from the other. In addition, combined impairments could drive one or more symbols out of their own decision regions, causing impairment evaluation to fail.

The aforementioned problems do not seem to be adequately faced by standard measurement guidelines [34] and test and measurement solutions proposed by major manufacturers [29],[57],[32]. In particular, (i) neither rules for distinguishing the specific contribution of each impairment in the output signal are provided, (ii) nor the possibility of symbols outside their own decision regions is taken into account.

In particular, the occurrence of condition (ii) may make inapplicable troubleshooting procedures [29] and measurement methods presented in the literature [67], which are based on a decision-directed strategy. This is particularly critical when constellation diagrams are characterized by high cardinality, as the minimum distance  $d$  between ideal symbol position and decision region boundary decreases with cardinality (see Fig.III.1 and Fig.III.2).

An original measurement method for a comprehensive evaluation of I/Q impairments also in the aforementioned critical conditions is presented hereinafter. It follows a digital signal processing approach that operates on the transmitter output signal, properly digitized by means of a DAS. In particular, it is based on a suitable clustering procedure, mandated to the correction of the distorted pattern of received symbols, and on an original measurement algorithm, which faces the problem of separating the effects of different impairments acting at the same time, in order to proceed to an accurate evaluation of their amount.

The method consists of three fundamental stages: signal demodulation, clustering, and

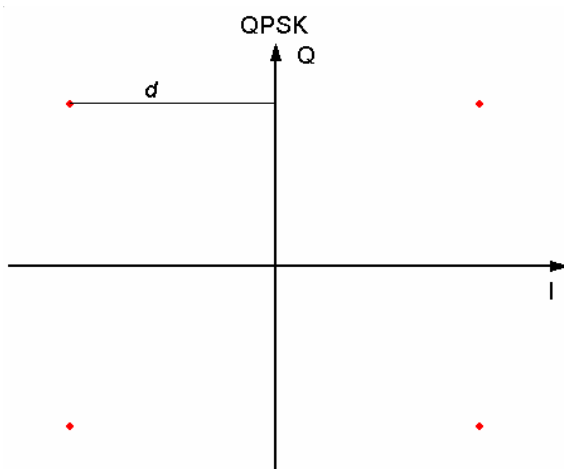


**Fig.III.1 – I/Q diagram for QPSK signal.**

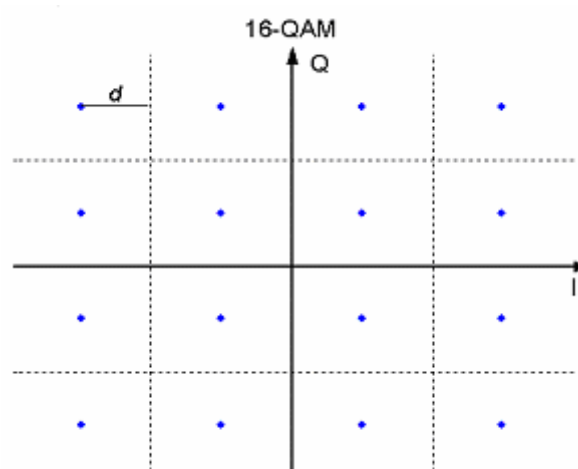


**Fig.III.2 – I/Q diagram for 16-QAM signal.**

impairment amount evaluation. In particular, signal demodulation detects the actual positions that symbols affected by impairments have on the I/Q diagram. The clustering procedure suitably pre-processes the recovered symbols to univocally reveal the deviation of each of them from its ideal position on the I/Q diagram. Finally, the contribution of each impairment to the deviations of all symbols is singled out, and correctly evaluated according to a straightforward measurement algorithm.

### III.2.2 - Impairments affecting I/Q modulators

I/Q modulator combines I and Q signals coming from the baseband stage. Due to potential different behavior exhibited by the I and Q paths [29], several impairments can take place, which show up as anomalies in the transmitted signal.

The scheme in Fig.III.3 is generally adopted to model the presence of I/Q impairments in a digital transmitter. In particular, it accounts for:

- gain imbalance  $\beta$ , which is defined as

$$\beta = \frac{\max(G_I, G_Q)}{\min(G_I, G_Q)} - 1 \quad (\text{III.1})$$

where  $G_I$  and  $G_Q$  are the gain, respectively, of the I and Q branch;

- quadrature error  $\phi$ , which reveals an angle between the two quadrature carriers different from  $\pi/2$ ;
- voltage offsets on the two branches,  $c_I$  and  $c_Q$ .

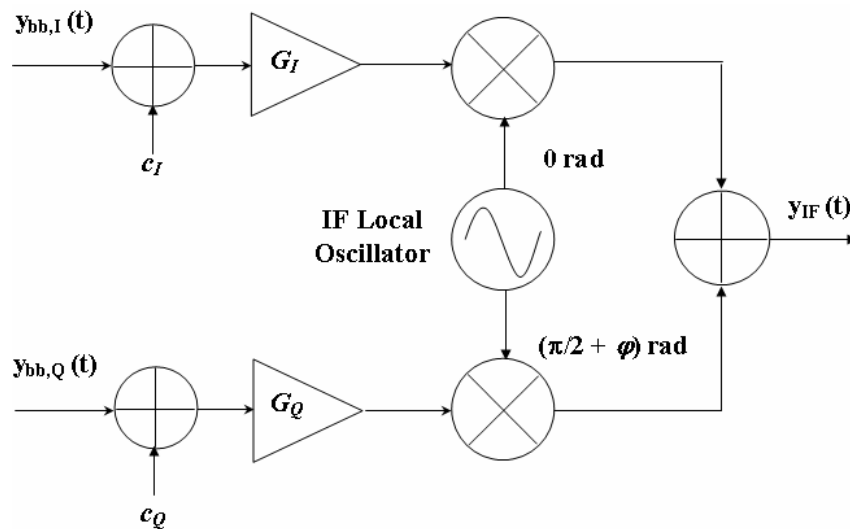


Fig.III.3 – I/Q impairment model.

A general expression for the IF signal,  $y_{IF}(t)$ , at the output of an I/Q modulator affected by such impairments is given by

$$y_{IF}(t) = G_I (c_I + y_{bb,I}(t)) \cos(2\pi f_{IF}t) - G_Q (c_Q + y_{bb,Q}(t)) \sin(2\pi f_{IF}t + \phi) \quad (III.2)$$

where impairments are assumed not to vary in the observation interval.

The contributions of the considered impairments are evident from the analysis of Fig.III.4, which refers to the constellation diagram of a 64-QAM signal. In particular, crosses represent the actual positions of symbols as the outcome of a modulator affected by impairments, whereas dots are their ideal ones. Fig.III.4 shows that some symbols cross the boundaries of their own decision regions as a consequence of impairments.

### III.2.3 - Proposed method

#### A. Signal demodulation

To recognize the actual I/Q constellation diagram characterizing the transmitter under test, the output signal is suitably digitized and demodulated. If the signal is outside the bandwidth of the data acquisition system a prior downconversion stage is required.

As nominally identical symbols are slightly spread, the acquisition of a number of

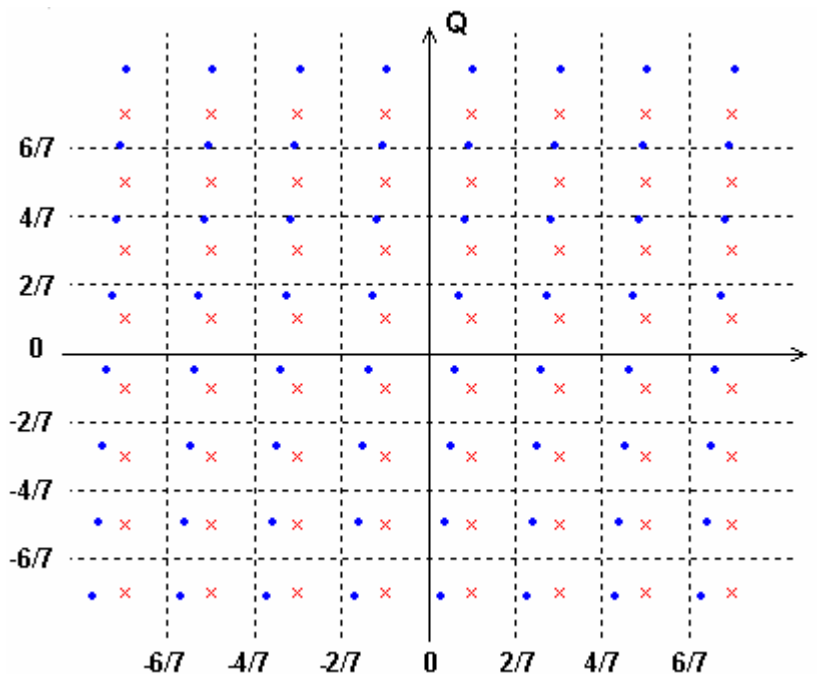


**Fig.III.4 – Ideal 64-QAM constellation with amplitude imbalance ( $\beta=0.1$ ), quadrature error ( $\phi=\pi/64$ ), and voltage offsets ( $c_I=-0.05$ ,  $c_Q=0.075$ ). Red crosses and blue dots represent nominal and actual symbol positions, respectively. I and Q components are normalized to their maximum value.**

symbols,  $N$ , much greater than the constellation cardinality,  $M$ , is required. The  $N$  symbols are then grouped into  $M$  clusters by means of a clustering procedure [68],[69], and for each cluster a single representative point is chosen in order to prevent symbol spread from affecting impairment evaluation.

### B. Clustering procedure

A clustering procedure involves dividing a set of points into separated groups, or clusters, where points in a cluster are *more similar* to one another than to points in other clusters. The expression *more similar*, in this case, means *closer* by some measure of proximity.

As the outcome of a clustering procedure, every point is assigned to some cluster, and every cluster can be characterized by a single representative point.

The clustering procedure utilized is based on an agglomerative approach. It calculates the pair-wise distance between all the  $N$  points,  $d(i,j)$ , and stores them in a vector  $Y$ , named similarity vector. The  $N(N-1)/2$  elements in the vector  $Y$  are then sorted according to

$$Y = [d(1,2), d(1,3), \dots, d(1,N), d(2,3), \dots, d(N-1,N)] \quad (\text{III.3})$$

where the distance between the points  $i$  and  $j$  ( $i < j$ ) is the element

$$d(i,j) = Y[(i-1)(N-i/2)+j-i] \quad (\text{III.4})$$

The sorted vector is passed to an algorithm, named single linkage algorithm, that merges the  $N$  points into  $M$  clusters ( $N$  has to be large enough to grant that each symbol in the constellation occurs at least once). In detail, at the first step the  $N$  points are considered as clusters made up of a single point. At the  $i$ -th step, the single linkage procedure finds the two nearest clusters and merges them, so that  $N-i$  clusters are left. The algorithm stops at the  $(N-M)$ th step, when the  $N$  points are collected into  $M$  clusters.

### C. Choice of the representative points

Representative points are chosen so as to minimize the average distance from all the points in the cluster. It can be easily shown that this criterion leads to the choice of the points characterized by the coordinates

$$\begin{cases} I_r^k = \frac{1}{N_k} \sum_{j=1}^{N_k} I_j^k \\ Q_r^k = \frac{1}{N_k} \sum_{j=1}^{N_k} Q_j^k \end{cases}, \quad k = 1, 2, \dots, M \quad (\text{III.5})$$

where  $I_j^k$  and  $Q_j^k$  are the coordinates of the  $N_k$  points belonging to the  $k$ -th cluster.

#### *D. Impairment evaluation*

Each representative point  $(I_r^k, Q_r^k)$  is matched to its own ideal position  $(I_{id}^k, Q_{id}^k)$  in the I/Q diagram. In particular, representative and ideal points are both numbered following a top-down left-to-right order, and matched accordingly. It is worth noting that the required matching cannot be correctly attained through a common threshold decision rule when one or more representative points are outside their correct decision region.

Named  $y_{bb}=I_{id}+jQ_{id}$  the ideal baseband signal, unaffected by I/Q impairments, the signal expression at IF (III.2) can be rewritten as

$$y_{IF}(t)=[c_I+I_{id}(t)]\cos(2\pi f_{IF}t)-(1+\beta)\cdot[c_Q+Q_{id}(t)]\sin(2\pi f_{IF}t+\phi) \quad (III.6)$$

where  $G_Q > G_I = 1$  is supposed. An equivalent expression is

$$y_{IF}(t)=[c_I-c_Q(1+\beta)\sin\phi+I_{id}(t)-(1+\beta)\sin\phi Q_{id}(t)]\cos(2\pi f_{IF}t)+ \\ -[c_Q(1+\beta)\cos\phi+(1+\beta)\cos\phi Q_{id}(t)]\sin(2\pi f_{IF}t) \quad (III.7)$$

Despite their non-linear combination, all the impairments are estimated without previously separating them, thus overcoming one of the limitations of ETSI guidelines.

In detail, the coordinates  $(O_I, O_Q)$  of the barycentre of the set of representative points  $(I_r^k, Q_r^k)$  are first evaluated. It is worth highlighting that the barycentre can be different from the origin of the axes because of the presence of impairments. With reference to the discrete-time version of the expression (III.7), the following equations for the barycentre coordinates can be derived:

$$O_I = c_I + c_Q(1+\beta)\sin\phi \quad (III.8)$$

and

$$O_Q = c_Q(1+\beta)\cos\phi \quad (III.9)$$

Subsequently, taking into account (III.8) and (III.9), the substitution of the ideal coordinates  $(I_{id}^k, Q_{id}^k)$  into the time-discrete version of the expression (III.7) yields

$$(1+\beta)\sin\phi Q_{id}^k = I_{id}^k + O_I - I_r^k \quad , \quad k = 1, 2, \dots, M \quad (III.10)$$

and

$$(1 + \beta) \cos \phi Q_{id}^k = Q_r^k - O_Q \quad , \quad k = 1, 2, \dots, M \quad . \quad (III.11)$$

In order to solve the system of  $2M$  equations composed by (III.10) and (III.11), an estimate of the angle  $\phi$  is determined by evaluating the average value of the incremental ratios of the points  $(I_r^k, Q_r^k)$  along the Q coordinate. For the sake of clarity, let us consider two generic representative points  $(I_r^a, Q_r^a)$  and  $(I_r^b, Q_r^b)$ , which are adjacent on the Q axis. Their

ideal coordinates satisfy  $I_{id}^a = I_{id}^b$  and  $Q_{id}^a = Q_{id}^b + \frac{2}{\sqrt{M} - 1}$ , and their incremental ratio, defined as  $\frac{I_r^b - I_r^a}{Q_r^b - Q_r^a}$ , is consequently equal to  $-\tan(\phi)$ .

The estimated value for  $\phi$  is substituted into relations (III.10) and (III.11), which are then solved by imposing the minimum average squared error on the estimate of  $\beta$ .

Voltage offsets,  $c_I$  and  $c_Q$ , are finally evaluated from (III.8) and (III.9), according to

$$c_I = O_I - O_Q \tan \phi \quad (III.12)$$

and

$$c_Q = \frac{O_Q}{(1 + \beta) \cos \phi} \quad . \quad (III.13)$$

### III.2.4 - Performance assessment

The performance of the proposed method has been assessed through a number of experiments on RF signals characterized by different baseband modulations. In particular, QPSK, 16-QAM and 64-QAM signals have been taken into consideration.

#### A. Measurement station

A suitable automatic measurement station has been set up, which is depicted in Fig.III.5. It consists of an AWG, a DSO, and a control and processing unit (PC), which are all interconnected by means of an IEEE-488 standard interface bus.

The following operative steps have been taken.

1. The baseband signal has been synthesized in digital form by means of a suitable algorithm running on the PC.
2. Calibrated I/Q impairments have been introduced on the digital sequence of samples; impairments have been assumed to be constant in the observation interval.

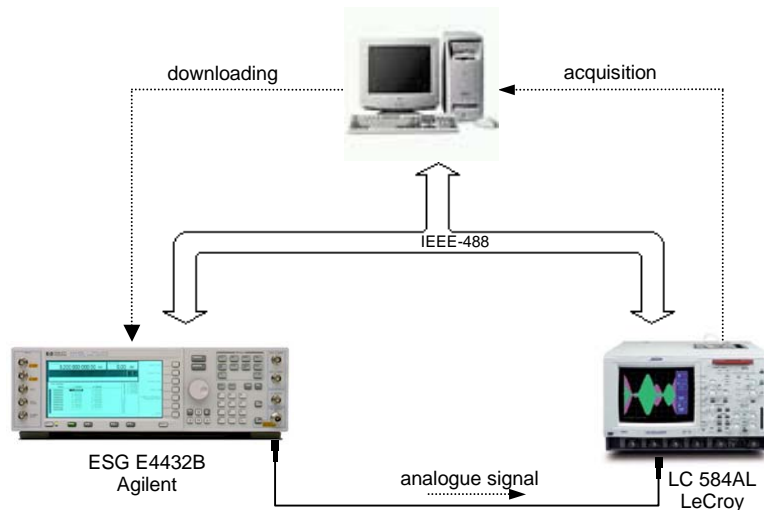


**Fig.III.5 – Measurement station.**

3. The generated samples have been downloaded into the memory of the AWG, which has operated the conversion in analog form.
4. The analog modulated signal has been digitized by the DSO; the acquired samples have been transferred to the PC.
5. The PC has demodulated the signal, and evaluated I/Q impairments through the proposed algorithms.

#### *B. Experimental results*

Three sets of experiments have been carried out. In each set, for a given amount of I/Q impairments involved, about one hundred signals characterized by the same baseband modulation, with different bit sequences, have been considered in order to achieve a reliable analysis. In particular, in the first set of experiments, a single impairment has been considered. In the second set, two simultaneous impairments have been imposed on the synthesized signal, with the aim of analyzing the influence of an interfering impairment when the measurement of the other impairment is addressed. The last set of experiments has been focused on the most general situation in which gain imbalance, quadrature error and I/Q offsets were all simultaneously present.

For the sake of brevity, only the results attained in the second and the third sets of experiments are given. Results are expressed in terms of difference  $\Delta$  between imposed and measured impairment values (averaged over the one hundred measurements), and experimental standard deviation  $\sigma$ .

With reference to the second set of experiments, Fig.III.6 shows the results attained on 64-QAM signals simultaneously affected by gain imbalance and quadrature error. Specifically, it provides a histogram representation of  $\Delta\%$  and  $\sigma\%$  related, respectively, to gain imbalance (Fig.III.6.a,c) and quadrature error (Fig.III.6.b,d) measurements, as functions of imposed impairment amounts.

Table III.1 enlists results achieved on 64-QAM signals, with regard to the most general case, when all the impairments were simultaneously present; both  $\Delta$  and  $\sigma$  are expressed in percentage relative terms.

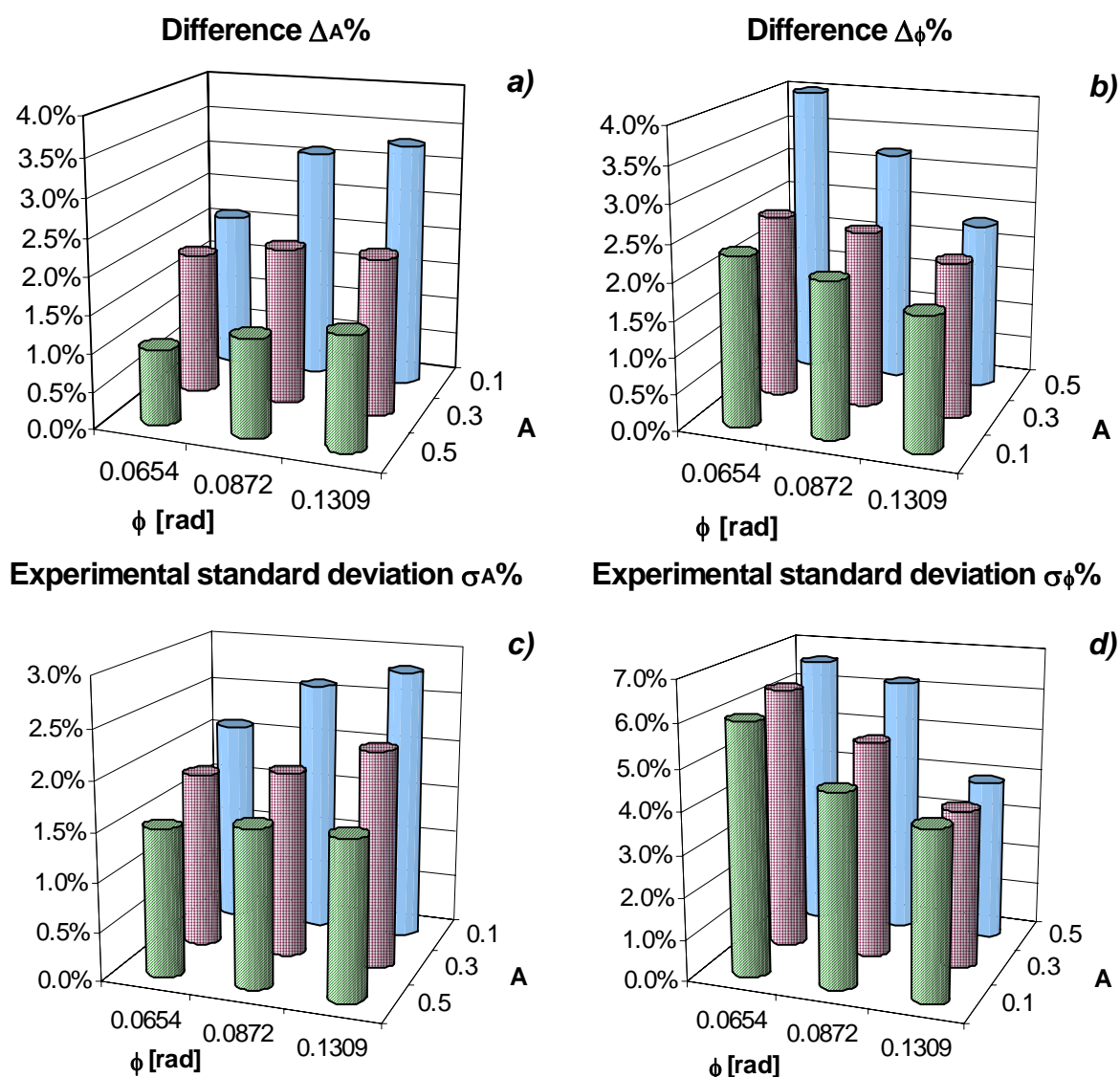


Fig.III.6 – Difference  $\Delta\%$ , in percentage relative terms, between measured and imposed a) amplitude imbalance ( $A\equiv\beta$ ) and b) quadrature error; experimental standard deviation  $\sigma\%$ , in percentage relative terms, related to c) amplitude imbalance and d) quadrature error.

**Table III.1 - Results of experimental tests on signals affected by different combinations of impairments.**

Imposed impairments				$\Delta$ %				$\sigma$ %			
$\beta$	$\phi$ [rad]	$c_I$	$c_Q$	$\beta$	$\phi$ [rad]	$c_I$	$c_Q$	$\beta$	$\phi$ [rad]	$c_I$	$c_Q$
0.1	0.0654	0.05	0.05	2.1%	2.3%	1.2%	1.6%	2.1%	6.0%	3.2%	3.4%
0.1	0.0872	0.05	0.05	3.1%	2.1%	1.0%	1.8%	2.6%	4.6%	2.4%	3.2%
0.1	0.1309	0.05	0.05	3.3%	1.8%	1.2%	2.4%	2.8%	4.0%	2.7%	3.8%
0.3	0.0654	0.1	0.1	1.9%	2.5%	2.6%	4.5%	1.8%	6.3%	2.3%	2.0%
0.3	0.0872	0.1	0.1	2.1%	2.4%	1.4%	3.5%	1.9%	5.2%	3.0%	2.1%
0.3	0.1309	0.1	0.1	2.1%	2.1%	1.2%	4.6%	2.2%	3.8%	2.7%	2.2%
0.5	0.0654	0.05	0.05	1.0%	4.0%	4.5%	2.8%	1.5%	6.6%	3.6%	3.0%
0.5	0.0872	0.05	0.05	1.3%	3.2%	3.9%	4.2%	1.6%	6.2%	2.6%	3.2%
0.5	0.1309	0.05	0.05	1.5%	2.3%	3.3%	4.4%	1.6%	3.9%	2.4%	3.0%

From the analysis of the results, the following considerations can be drawn.

- The proposed method provides good results in terms of difference between imposed and measured impairments;  $\Delta\%$  is, in fact, always inferior to 5%.
- It also offers satisfying repeatability, since  $\sigma\%$  is inferior to 7% for quadrature error measurements and lower than 4% with regard to all the other impairments.
- Both  $\Delta\%$  and  $\sigma\%$  values (i) decrease upon the increasing of the amount of the impairment, and (ii) increase upon the increasing of the amount of the other impairments.
- The performance of the method is slightly worse for higher I/Q diagram cardinality.
- The method is capable of detecting and evaluating the amounts of more than two impairments that simultaneously affect the modulator, and its range of application is not limited to I/Q diagrams characterized by low cardinality.

### III.2.5 - Conclusion

A new digital-signal processing approach aimed at troubleshooting transmitters in QAM-based telecommunication systems has been discussed. In particular, a measurement method capable of estimating gain imbalance, quadrature error and voltage offsets, has been presented and its performance experimentally assessed.

The main advantages of the method are its capability of (i) univocally revealing each symbol deviation from its ideal position, even when impairment combination leads some symbols outside their own original decision region, and (ii) separating different simultaneous I/Q impairments, thus overcoming a major limitation of ETSI guidelines.

A suitable measurement station has been set up with the aim of assessing the performance of the method through a number of experiments on different types of signals and with regard to different impairment combinations and amounts. The experimental activity has proved effectiveness and repeatability of the proposed method; experienced values of  $\Delta\%$  and  $\sigma\%$  are, in fact, lower than few percents. Experimental results give also evidence of the robustness of the method with regard to the possible presence of interfering tones or phase jitter; in such critical conditions, in fact,  $\Delta\%$  and  $\sigma\%$  are generally lower than 6% and 9%, respectively.

### **III.3 - A measurement method based on error vector analysis**

#### *III.3.1 - Introduction*

To estimate most common impairments (gain imbalance, quadrature error and voltage offsets) that affect the I/Q modulator in a digital transmitter through measurements performed at its RF output, leading manufacturers suggest looking at the constellation diagram of the transmitted RF signal [29]. Besides being impracticable when more than two impairments are present at the same time, this solution allows only qualitative estimation of impairment amount because no appropriate relations are put at user's disposal. ETSI measurement guidelines concerning DVB provide, on the contrary, useful relations, which are, however, effective only in the case that a single impairment affects the I/Q modulator [34].

Two different methods allow overcoming the aforementioned limitations: the method proposed in [67], and the one presented in the previous section. Both of them are capable of separating and estimating all I/Q impairments simultaneously present. In particular, the presented in the previous section assures better accuracy for high signal space cardinality, and works properly even when received symbols are outside their correct decision regions, whereas the method described in [67] is more accurate in the case of a low cardinality. Computational load of both methods, however, could be too heavy, also in some uncomplicated situations (very frequent in practice), such as those in which only one or two impairments are predominant, and received symbols do not cross the boundaries of their original decision regions.

To grant lighter computational burden and, consequently, reduced test and measurement time in such uncomplicated situations, a new and straightforward measurement method is proposed hereinafter. After a preliminary analysis of the constellation diagram with the aim of singling out the predominant (one or two) I/Q impairments, the method provides for the

calculation of the error vector for each transmitted symbol. The amount of the detected I/Q impairments is then evaluated through the application of original and simple algebraic relations, which involve the components of the error vector and the considered impairments.

### *III.3.2 - Theoretical background*

#### *A. Error Vector*

As well known, an I/Q modulator allows a discrete set of symbols to be represented by a specific constellation diagram on a bidimensional space, namely the I/Q plane. Impairments affecting the transmitter, system non-idealities, as well as thermal noise, can result in a deviation of the actual symbols from their ideal positions on the diagram.

EV is defined as the vector difference between the actual and ideal symbol position on the I/Q plane (Fig.I.3); its components along the I and Q axes are generally referred respectively to as the EV real and imaginary part. Several international standards, specifications, and technical literature [29],[34],[70],[71],[72],[73],[74] consider the magnitude of the error vector, EVM, a key metric for RF transmitter testing and troubleshooting. EVM is also important in transceiver characterization [75],[35],[76], as it provides information on the overall modulated signal quality, bearing traces of possible causes of signal distortion, ranging from I/Q impairments to phase noise and power amplifier non-linearity [77],[78],[79],[80],[81],[82],[83].

#### *B. I/Q impairments model*

Expression (III.2) for the IF signal,  $y_{IF}(t)$ , at the output of an I/Q modulator affected by such impairments can equivalently be rewritten as

$$y_{IF}(t) = G(1-g)(c_I + y_{bb,I}(t)) \cos(2\pi f_{IF}t) + \\ - G(1+g)(c_Q + y_{bb,Q}(t)) \sin(2\pi f_{IF}t + \phi) \quad (III.14)$$

where  $g$  is the semi-difference between the gains on the two branches, normalized to their average value  $G$ , i.e.

$$g = \frac{G_Q - G_I}{G_Q + G_I} \quad (III.15)$$

and

$$G = \frac{G_Q + G_I}{2} \quad (III.16)$$

In the case of unity average gain ( $G = 1$ ), relation (III.14) yields the following expression for the equivalent baseband signal affected by impairments,  $z_{bb}(t)$ :

$$z_{bb}(t) = (1 - g) \cdot (c_I + y_{bb,I}(t)) + j \cdot (1 + g) \cdot (c_Q + y_{bb,Q}(t)) e^{j\phi} \quad (III.17)$$

*C. Limits of currently available proposals*

As stated above, the analysis of the constellation diagram, suggested by troubleshooting procedures of leading manufacturers, is effective only in the case that no more than two impairments simultaneously affect the I/Q modulator. Indeed, in the presence of one or two impairments, it provides only qualitative information. For the sake of clarity, Fig.III.7 shows the constellation diagram of a QPSK signal when a gain imbalance,  $g = 0.1710$ , and a quadrature error,  $\phi = \pi/32$  rad, are jointly present; dots are the actual symbol positions, while crosses are the expected ideal ones. Although it can be clearly stated from a look at the dashed diagram that a rotation and an unevenness between the two axes are simultaneously present, no quantitative information can be gained concerning the impairment amounts. At the same time, analytical relations suggested in [34] are of no use, since the required separation of the effects of different impairments is impractical.

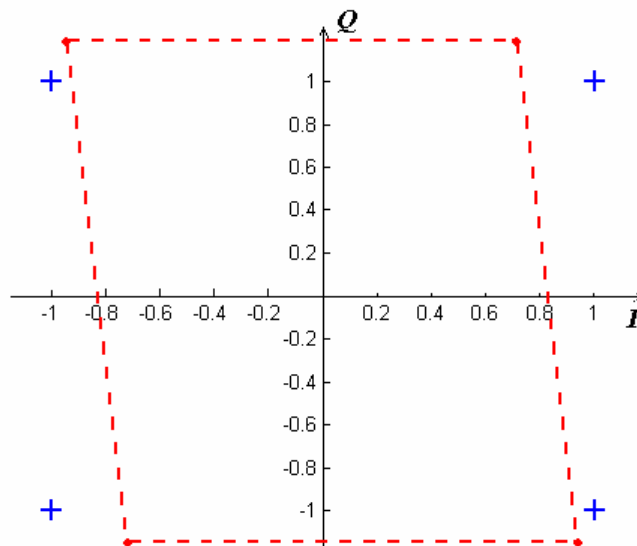


**Fig.III.7 – Effect of joint gain imbalance and quadrature error on the constellation diagram of a QPSK signal;  $g$  and  $\phi$  are, respectively, equal to 0.1710 and  $\pi/32$  rad.**

### *III.3.3 - Proposed method*

Besides overcoming the limits of manufacturers' troubleshooting procedures and measurement guidelines, the proposed method aims at estimating the amount of I/Q impairments that affect a digital transmitter in a reduced measurement time. It is, in particular, effective when one or two impairments are predominant and received symbols do not cross the boundaries of their original decision regions, which are very frequent conditions with digital transmitters troubleshooting.

The fundamental stages of the method can be summarized as follows. The presentation order given below reflects a typical execution order.

a) *Demodulation*. The RF output of the digital transmitter under analysis is demodulated in order to recover the time domain evolution of its baseband (I/Q) signals and, accordingly, actual and nominal position of transmitted symbols on the constellation diagram.

b) *Impairment detection*. The actual constellation diagram should be analyzed in order to detect the presence of I/Q impairments and establish whether one or two impairments prevail. To this end, suitable approaches can be exploited [84].

c) *Impairment evaluation*. For each transmitted symbol, the real and imaginary part of the error vector are first calculated and then put into original algebraic relations, which allow the estimation of the amount of the occurred impairments. The measurement result is finally obtained as the average of all gained estimates, according to the size of the considered set of consecutive symbols.

With regard to the last stage, different relations are given depending upon which impairment or pair of impairments is singled out as predominant. For the sake of clarity, details concerning all proposed relations are separately given below.

#### *A. Single impairment*

Fig.III.8. Fig.III.9 and Fig.III.10 show the effects, on the I/Q diagram of a QPSK, of the presence of, respectively, (i) a gain imbalance,  $g$ , equal to 0.1146, (ii) a quadrature error,  $\phi$ , equal to  $\pi/16$  rad and (iii) a normalized voltage offset on component I,  $c_I$ , equal to 0.15. With reference to the notations introduced in the previous section, the continuous line vectors represent the ideal signal  $y_{bb}$ , while the dashed line vectors represent the signal with impairments,  $z_{bb}$ , and the dotted line vectors represent the EV.

##### *A.1. Gain imbalance*

When only the gain imbalance,  $g$ , is present, the error vector,  $EV_{gain}$ , can be written as

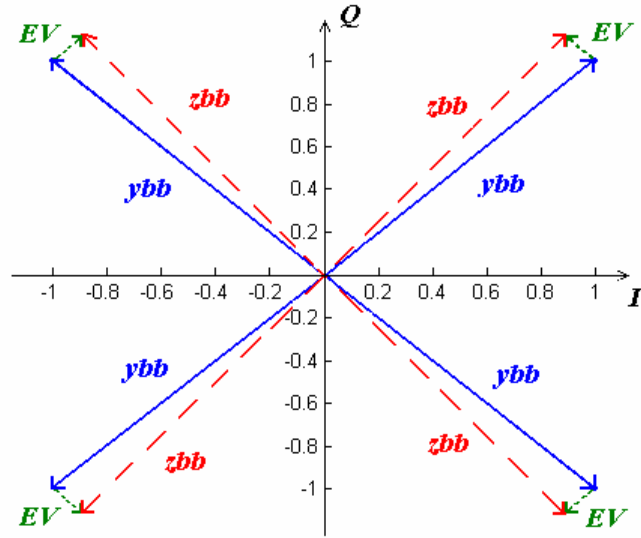


Fig.III.8 – EV components due to a gain imbalance,  $g$ , equal to 0.1146.

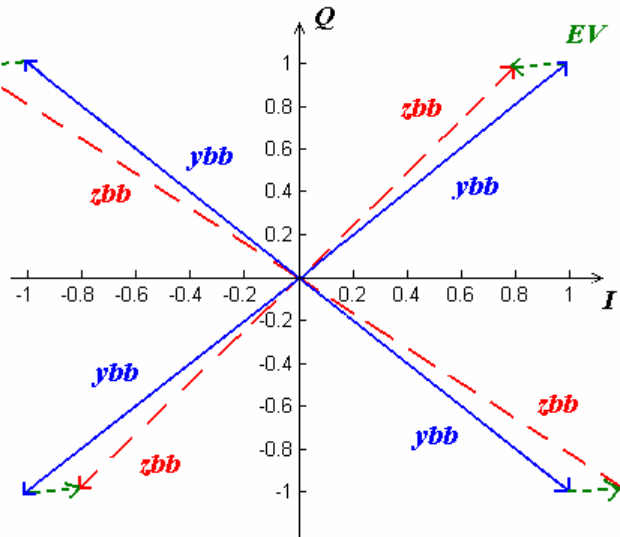


Fig.III.9 – EV components due to a quadrature error,  $\phi$ , equal to  $\pi/16$  rad.

$$EV_{gain} = z_{bb} - y_{bb} = -y_{bb,I} \cdot g + j \cdot y_{bb,Q} \cdot g \quad (III.18)$$

and, therefore,  $g$  can be estimated as

$$g = \frac{\text{Im}\{EV_{gain}\}}{y_{bb,Q}} = -\frac{\text{Re}\{EV_{gain}\}}{y_{bb,I}} \quad (III.19)$$

The operators  $\text{Re}\{x\}$  and  $\text{Im}\{x\}$  respectively give the real and imaginary part of input  $x$ .

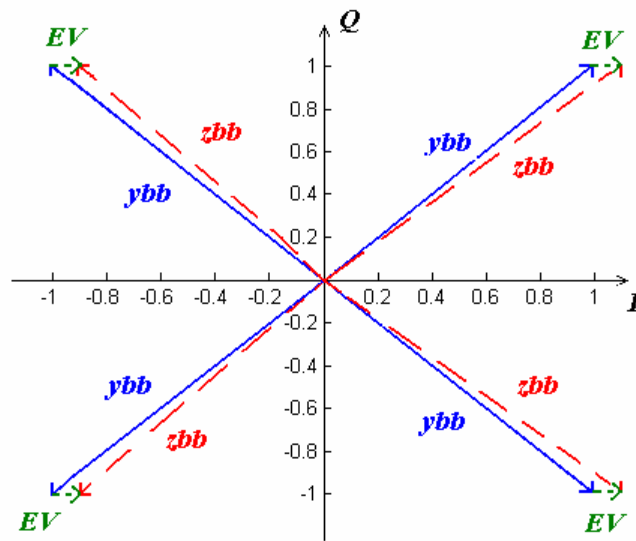


Fig.III.10 – EV components due to a voltage offset on component I,  $c_I$ , equal to 0.15.

### A.2. Quadrature error

In the case that only quadrature error occurs, the error vector,  $EV_\phi$  is given by

$$EV_\phi = -y_{bb,Q} \cdot \sin\phi + j \cdot y_{bb,Q} \cdot (\cos\phi - 1) \quad (III.20)$$

which can be approximated as follows, when  $\phi \ll 1$ ,

$$EV_\phi \approx -y_{bb,Q} \cdot \phi \quad (III.21)$$

hence

$$\phi \approx -\frac{\text{Re}\{EV_\phi\}}{y_{bb,Q}} \quad (III.22)$$

### A.3. Offset

Finally, a straightforward relation links the error vector,  $EV_{offset}$ , to the voltage offsets,  $c_I$  and  $c_Q$ , when other impairments are negligible:

$$EV_{offset} = c_I + j \cdot c_Q \quad (III.23)$$

The values of  $c_I$  and  $c_Q$  can therefore be evaluated respectively as

$$c_I = \text{Re}\{EV_{offset}\} \quad (III.24)$$

and

$$c_Q = \text{Im}\{EV_{\text{offset}}\} \quad . \quad (\text{III.25})$$

## B. Two impairments

### B.1. Gain imbalance and quadrature error

Fig.III.7 shows a QPSK constellation diagram in the presence of gain imbalance and quadrature error; in such cases, the analytical expression for the error vector,  $EV_{\text{gain},\phi}$  is

$$EV_{\text{gain},\phi} = -g \cdot y_{bb,I} - y_{bb,Q} (1+g) \sin \phi + j \cdot y_{bb,Q} [(1+g) \cos \phi - 1] \quad . \quad (\text{III.26})$$

If  $\phi \ll 1$ , relation (III.26) reduces to

$$EV_{\text{gain},\phi} \approx -g \cdot y_{bb,I} - y_{bb,Q} (1+g) \cdot \phi + j \cdot g \cdot y_{bb,Q} \quad . \quad (\text{III.27})$$

Consequently,  $g$  and  $\phi$  can be obtained respectively from

$$g = \frac{\text{Im}\{EV_{\text{gain},\phi}\}}{y_{bb,Q}} \quad (\text{III.28})$$

and

$$\phi \approx -\frac{\text{Re}\{EV_{\text{gain},\phi}\} + g \cdot y_{bb,I}}{y_{bb,Q} (1+g)} \quad . \quad (\text{III.29})$$

### B.2. Gain imbalance and offset $c_I$

When gain imbalance and  $c_I$  are present at the same time, the error vector,  $EV_{\text{gain},c_I}$ , can be written as

$$EV_{\text{gain},c_I} = (1-g) \cdot c_I - g \cdot y_{bb,I} + j \cdot y_{bb,Q} \cdot g \quad . \quad (\text{III.30})$$

Therefore,  $g$  is given by

$$g = \frac{\text{Im}\{EV_{\text{gain},c_I}\}}{y_{bb,Q}} \quad (\text{III.31})$$

and  $c_I$  can be obtained from

$$c_I = \frac{\text{Re}\{EV_{\text{gain},c_I}\} + g \cdot y_{bb,I}}{1-g} \quad . \quad (\text{III.32})$$

### B.3. Gain imbalance and offset $c_Q$

When gain imbalance and  $c_Q$  are present at the same time, the error vector  $EV_{gain,c_Q}$ , has the following expression:

$$EV_{gain,c_Q} = -g \cdot y_{bb,I} + j [c_Q(1+g) + y_{bb,Q} \cdot g] \quad . \quad (III.33)$$

Impairments can thus be estimated as

$$g = -\frac{\operatorname{Re}\{EV_{gain,c_Q}\}}{y_{bb,I}} \quad (III.34)$$

and

$$c_Q = \frac{\operatorname{Im}\{EV_{gain,c_Q}\} - g \cdot y_{bb,Q}}{1+g} \quad . \quad (III.35)$$

### B.4. Quadrature error and offset $c_Q$

The combination of quadrature error and  $c_Q$  leads to the following expression for the error vector  $EV_{\phi,c_Q}$ :

$$EV_{\phi,c_Q} = -(c_Q + y_{bb,Q}) \sin \phi + j[(c_Q + y_{bb,Q}) \cos \phi - y_{bb,Q}] \quad . \quad (III.36)$$

Therefore, impairment amounts can be estimated as

$$\phi = -\operatorname{atan}\left(\frac{\operatorname{Re}\{EV_{\phi,c_Q}\}}{\operatorname{Im}\{EV_{\phi,c_Q}\} + y_{bb,Q}}\right) \quad (III.37)$$

and

$$c_Q = -\frac{\operatorname{Re}\{EV_{\phi,c_Q}\}}{\sin \phi} - y_{bb,Q} \quad . \quad (III.38)$$

### B.5. Quadrature error and offset $c_I$

If quadrature error and offset  $c_I$  jointly act, the error vector,  $EV_{\phi,c_I}$ , is expressed as

$$EV_{\phi,c_I} = c_I - y_{bb,Q} \cdot \sin \phi + j \cdot y_{bb,Q} \cdot (\cos \phi - 1) \quad (III.39)$$

and to estimate the amount of the considered impairments, the following steps have to be taken.

1. Received symbols are separated into groups characterized by the same  $y_{bb,Q}$ .

2. For each group the average of  $\text{Re}\{EV_{\phi,c_I}\}$ , namely  $\overline{\text{Re}\{EV_{\phi,c_I}\}}^{y_{bb,Q}}$ , is computed.
3. Differences  $\Delta^{|y_{bb,Q}|}$  between  $\overline{\text{Re}\{EV_{\phi,c_I}\}}^{y_{bb,Q}}$  of the two groups characterized by the same  $|y_{bb,Q}|$ , i.e.  $\Delta^{|y_{bb,Q}|} = \overline{\text{Re}\{EV_{\phi,c_I}\}}^{|y_{bb,Q}|} - \overline{\text{Re}\{EV_{\phi,c_I}\}}^{-|y_{bb,Q}|}$ , are computed.
4. Then, impairment amounts can be estimated by observing that  $\Delta^{|y_{bb,Q}|} = -2y_{bb,Q} \sin \phi$ , due to the symmetry of the constellation. Specifically,

$$\phi = -\arcsin\left(\frac{\Delta^{|y_{bb,Q}|}}{2y_{bb,Q}}\right) \quad (\text{III.40})$$

and

$$c_I = \text{Re}\{EV_{\phi,c_I}\} + y_{bb,Q} \sin \phi \quad (\text{III.41})$$

### III.3.4 - Performance assessment

The method has been validated through a wide experimental activity, carried out on signals characterized by different types of digital modulation schemes. Both high and low cardinality signal spaces have been taken into consideration. In particular, the following test signals have been adopted: (i) WCDMA signals, which characterize UMTS, the European proposal for a third generation communication system, and (ii) 16-QAM and 32-QAM signals, peculiar to DVB standards [10],[11].

#### A. Measurement station

A suitable measurement station has been set up (Fig.III.11). It consists of (i) a processing and control unit, namely a personal computer, (ii) a digital RF signal generator, *Agilent E4432B*<sup>TM</sup> [55], (250 kHz-3 GHz output frequency) with AWG capability (14-bit vertical resolution, 1 MS memory depth, 40 MHz maximum generation frequency), and (iii) a VSA *Agilent 4460A*<sup>TM</sup> [52] (7 MHz-4.0 GHz input frequency range, I/Q signal demodulation personality); these are all interconnected by means of an IEEE-488 standard interface bus.

Taking advantage of the features of the chosen RF generator, impairments having a known amplitude have been imposed on its I/Q modulator. The choice of the impairment amount to be introduced is, in fact, possible from the generator user panel. The VSA then downconverts the RF generated signal to IF, and demodulates it, thus extracting the baseband components (I and Q). To this end, the VSA needs to be synchronized to the signal generator:

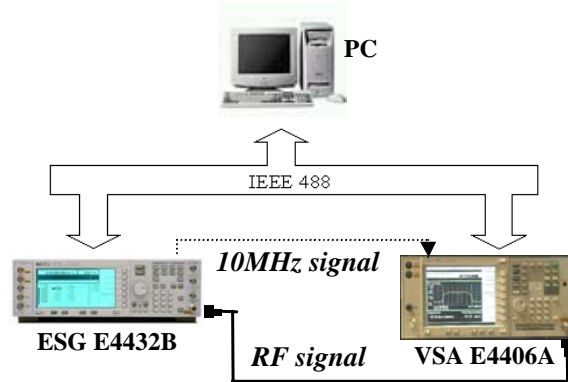


**Fig.III.11 – Measurement station.**

they both have the same 10 MHz reference clock. The I and Q components, made available by the VSA as 30,001 samples taken at a rate of 15 MS/s, are finally transferred, via the IEEE-488 bus, to the processing unit, which calculates the components of the error vector and provides the final estimate of the detected impairments according to the proposed relations.

*B. Experimental results*

Table III.2 and Table III.3 report imposed impairment amounts when, respectively, WCDMA and DVB signals are generated. For each impairment, sets of equally distributed values within reported ranges are taken into consideration. It is worth noting that voltage offsets are expressed in normalized terms, referenced to the maximum value of I and Q components. The imposed impairment amounts ensure that the generated symbols do not cross the boundaries of their decision boxes on the I/Q plane. This is the reason why impairment amounts for DVB signals are lower than the corresponding ones for WCDMA signals, as it is evident for gain imbalance and voltage offsets.

**Table III.2 - Impairment amounts for WCDMA signals.**

	<i>Single</i>	<i>Double</i>
$G_Q/G_I$ [dB]	0.5 - 2.0	0.5 - 2.0
$\varphi$ [rad]	0.021 - 0.168	0.084 - 0.126
$c_I$	0.04 - 0.40	0.08 - 0.32
$c_Q$	0.04 - 0.40	0.08 - 0.32

**Table III.3 - Impairment amounts for DVB signals.**

	<i>Single</i>	<i>Double</i>
$G_Q/G_I$ [dB]	0.5 - 2.0	0.5 - 2.0
$\phi$ [rad]	0.052 - 0.122	0.035 - 0.069
$c_I$	0.02 - 0.12	0.02 - 0.08
$c_Q$	0.02 - 0.12	0.02 - 0.08

As an example, Fig.III.12, Fig.III.13 and Fig.III.14 refer to a 32-QAM signal, generated at a symbol rate equal to 1.5 Msymbol/s with an imposed gain imbalance,  $g$ , equal to 0.129. In particular, Fig.III.12 and Fig.III.13 give respectively the I/Q polar diagram and baseband I

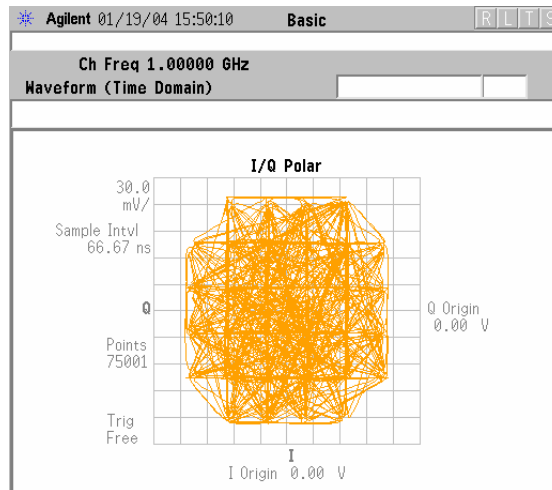


**Fig.III.12 – I/Q polar diagram of a DVB signal in the presence of gain imbalance.**

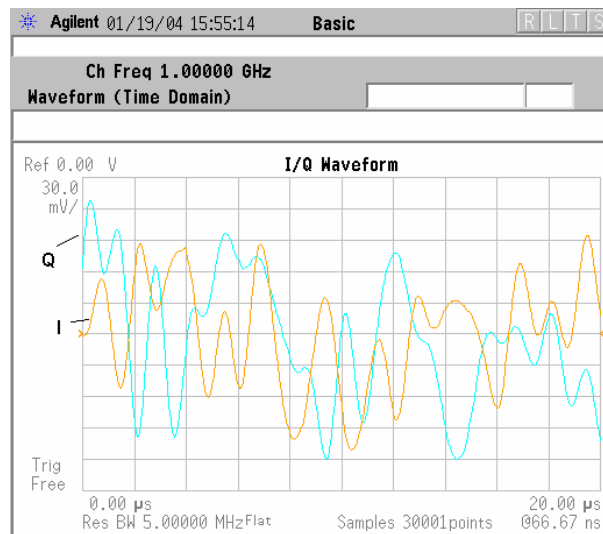


**Fig.III.13 – I and Q waveforms related to the signal in Fig.III.12.**

and Q waveforms (10 samples per symbol) provided by the VSA, while Fig.III.14 reports the symbol-by-symbol estimation of gain imbalance. The measurement result is the mean value of the symbol-by-symbol estimations.

Table III.4 and Table III.5 summarize the entire set of results for, respectively, WCDMA and DVB signals. They are presented in terms of difference from imposed values ( $\Delta$ ) and experimental standard deviation ( $\sigma$ ), both expressed in percentage relative terms. In particular, all measurement results fall within the lower and upper limits summarized in the tables.

From the analysis of the experimental results, the following considerations can be drawn.

- Values of  $\Delta$  % and  $\sigma$  % below 5% have been experienced in most cases.
- The lower the amount of the imposed impairment, the higher the related values of  $\Delta$  % and  $\sigma$  %.
- A comparison with the results achieved on WCDMA signals through the application of the method proposed in [67] shows that the values of  $\Delta$  % and  $\sigma$  %, respectively included in the ranges [0.53%-10%] and [0.9%-9.0%], concur with those experienced in [67], which are included in [0.50%-10%] and [0.51%-9.0%].

**Table III.4 - Measurement results for WCDMA signals.**

	$\Delta$ %		$\sigma$ %	
	<i>min</i>	<i>max</i>	<i>min</i>	<i>Max</i>
<b><i>g</i></b>	2.4%	8.0%	0.9%	8.0%
<b><math>\varphi</math></b>	3.8%	10%	1.5%	9.0%
<b><i>c<sub>I</sub></i></b>	0.88%	6.0%	1.3%	5.0%
<b><i>c<sub>Q</sub></i></b>	0.53%	5.0%	1.0%	5.0%

**Table III.5 - Measurement results for DVB signals.**

	$\Delta$ %		$\sigma$ %	
	<i>min</i>	<i>max</i>	<i>min</i>	<i>max</i>
<b><i>g</i></b>	2.3%	4.4%	1.0%	5.0%
<b><math>\varphi</math></b>	4.2%	7.2%	3.8%	9.0%
<b><i>c<sub>I</sub></i></b>	1.1%	6.7%	1.1%	4.0%
<b><i>c<sub>Q</sub></i></b>	0.9%	6.5%	1.0%	4.1%

- A comparison with the results achieved on DVB signals through the application of the method proposed in Section III.2 shows that the values of  $\Delta$  % and  $\sigma$  %, respectively included in the ranges [0.9%-6.7%] and [1.0%-9.0%], concur with those experienced in Section III.2, which are included in [1.0%-4.5%] and [1.5%-6.6%].
- The method based on EV is operational even for short input data streams. In particular, when it is compared to the real-time RLS algorithm proposed in [67], the same experimental standard deviation of the measurement results is typically accomplished for a 5-times shorter input data stream, which allows a 5-time reduction of the measurement time. Its fast execution is much more evident when it is compared to the method loaded by the clustering pre-processing described in Section III.2, especially in the presence of a high signal space cardinality.

### III.3.5 - Conclusion

An original method for estimating I/Q impairments in digital transmitters has been presented. It exploits the results of EV measurements, and is appropriate in various stages (production, installation, and maintenance) of transmitter life cycle. Simple and original algebraic expressions, which relate the amount of occurred impairments to EV components, represent the core of the method, and allow overcoming typical limitations of measurement approaches proposed by leading manufacturers or suggested by measurement guidelines.

An extended experimental activity has shown the reliability and effectiveness of the proposed method when only one or two I/Q impairments are significant (as it often occurs). In particular, the results achieved provide evidence of the same accuracy as the method presented in Section III.2, whereas measurement time is significantly reduced.

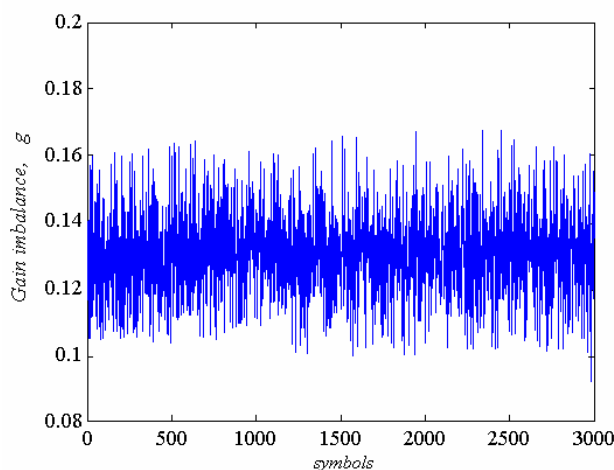


**Fig.III.14 – Symbol-by-symbol estimation of gain imbalance.**

### **III.4 - I/Q impairment detection and evaluation on OFDM transmitters**

#### *III.4.1 - Introduction*

Orthogonal Frequency Division Multiplexing (OFDM) is an emerging technology for high data rate transmission [85],[86],[87] which is expanding its application field to a variety of broadband communication schemes. OFDM is, in particular, adopted in the European standards for Digital Audio Broadcasting (DAB) [9] and Digital Video Broadcasting-Terrestrial (DVB-T) [12]. More recently, different Wireless Local Area Network (W-LAN) and Metropolitan Area Network (MAN) standards, in the USA and Europe, have converged on OFDM to achieve high data rates [7],[8],[88].

Detection and evaluation of I/Q impairments affecting an OFDM modulator, on the basis of their effects on the RF output signal, is not a trivial extension of procedures designed for generic I/Q modulators. The measurement method based on clustering, presented in Section III.2, as well as that proposed in [67], have proved to be effective with regard to generic QAM transmitters and in the presence of multiple I/Q impairments. The method based on the analysis of EV is particularly timesaving and grants the same performance as the former, but is applicable only in the presence of one or two predominant impairments. Such methods, however, as well as troubleshooting procedures proposed by major manufacturers and based on the analysis of I/Q diagram [29], are designed for traditional RF digital transmitters and cannot be profitably applied to OFDM transmitters. OFDM transmitters, in fact, exploit a multicarrier modulation scheme, I and Q components of which are, respectively, the real and imaginary part of the outcome of an IFFT (Inverse Fast Fourier Transform). As a consequence, not only are actual positions of symbols on the I/Q diagram of a certain carrier (generally called sub-carrier) affected by impairment amounts, but they also depend on symbols conveyed on the so-called mirror sub-carrier.

A new method for I/Q impairment detection and evaluation in OFDM transmitters is presented hereinafter. To rightly account for major effects induced on RF output signal by mirror sub-carrier interference in the presence of I/Q impairments, a proper analytical model is exploited. A similar model is at the basis of a method recently proposed for the compensation of I/Q impairments in OFDM receivers [89]. While the latter is only interested in evaluating the overall effect of impairments on the received signal and does not separate different impairment contributions, the proposed method, which is addressed to transmitter testing, allows for the automatic evaluation of the amount of each I/Q impairment.

Specifically, the original measurement procedure implemented by the method can be summarized as follows. The RF output signal is first demodulated to gain the symbols related to all sub-carriers. Then, for each sub-carrier but the so-called DC, an algebraic equation system, derived from the aforementioned model, and involving both impairments amounts, and in-phase and quadrature components of symbols conveyed by the sub-carrier and related mirror one, is solved in order to evaluate gain imbalance and quadrature error amounts. Concerning voltage offsets, their estimates are achieved by particularizing the same equation system to the DC sub-carrier. Measurement results for each impairment are finally obtained by averaging the different estimates. A number of experimental tests on OFDM signals are conducted to highlight the good performance of the method.

### III.4.2 - Problem statement

#### A. OFDM modulation

A simplified OFDM implementation diagram is sketched in Fig.III.15. Input serial bit sequence is parallelized into  $K$  groups, to each of which a QAM is applied. The  $K$  complex sequences of QAM symbols  $C_0(n), C_1(n), \dots, C_{K-1}(n)$  modulate orthogonal carriers. For a given  $n$ ,  $C_0(n), C_1(n), \dots, C_{K-1}(n)$  can be regarded as the FFT coefficients of the time-sequence  $c_0(n), c_1(n), \dots, c_{K-1}(n)$ , which constitutes an OFDM symbol. Real and imaginary parts of the complex sequence resulting from the serialization of the IFFT output are, respectively, I and Q component feeding the I/Q modulator. Their expression, in complex form, is

$$I_m(n) + jQ_m(n) = \sum_{k=0}^{K-1} C_k(n) e^{j2\pi k \frac{m}{K}}, \quad m = 0, 1, \dots, K-1 \quad \text{(III.42)}$$

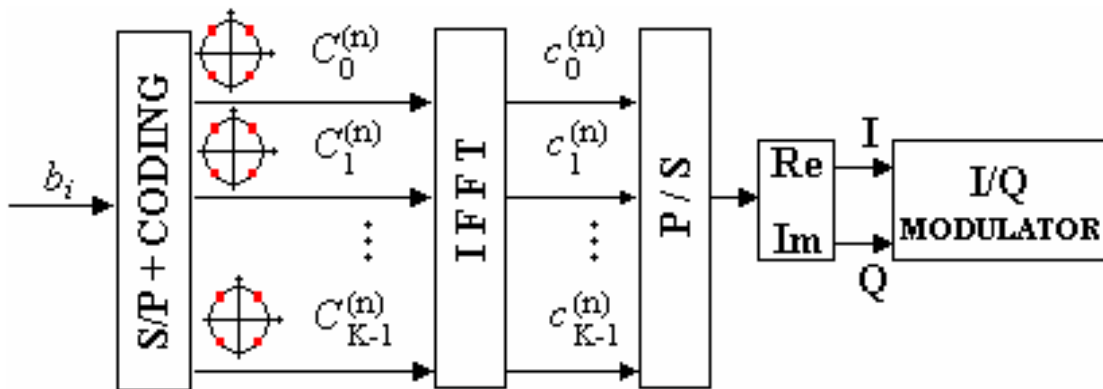


Fig.III.15 – Basic OFDM modulation scheme.

*B. OFDM signals affected by I/Q impairments*

As it is evident from Fig.III.16, I/Q diagram of an OFDM signal appears as a messy agglomeration of symbols, rather than a more familiar geometrical shape. This is the reason why no qualitative information on impairments affecting the modulator can be obtained from its analysis, in contrast to what happens for other modulation formats.

Expressions of sequences  $I'_m$  and  $Q'_m$ , which an ideal receiver would recover through its FFT block, are:

$$I'_m = (1 + \beta) \left\{ \sum_{k=0}^{K-1} \left[ A_k \cos\left(2\pi k \frac{m}{K}\right) - B_k \sin\left(2\pi k \frac{m}{K}\right) \right] + c_I \right\} + \phi \left\{ \sum_{k=0}^{K-1} \left[ A_k \sin\left(2\pi k \frac{m}{K}\right) + B_k \cos\left(2\pi k \frac{m}{K}\right) \right] + c_Q \right\} \quad (III.43)$$

$$Q'_m = \sum_{k=0}^{K-1} \left[ A_k \sin\left(2\pi k \frac{m}{K}\right) + B_k \cos\left(2\pi k \frac{m}{K}\right) \right] + c_Q \quad (III.44)$$

In expressions (III.43) and (III.44),  $G_I > G_Q = 1$  is assumed;  $A_k$  and  $B_k$  are, respectively, the real and imaginary part of  $C_k$ ;  $\cos(\phi)$  and  $\sin(\phi)$  are approximated with the first terms of their Maclaurin series, and index  $n$  is dropped, since the same considerations can be done for any OFDM symbol.

Expressions (III.43) and (III.44) yield

$$I'_m + jQ'_m = \sum_{k=0}^{K-1} \left\{ \left[ C_k + \frac{\beta}{2}(C_k + C_h^*) + j\frac{\phi}{2}(C_k - C_h^*) \right] e^{j2\pi k \frac{m}{N}} \right\} - \phi c_Q + (1 + \beta)c_I + j c_Q \quad (III.45)$$

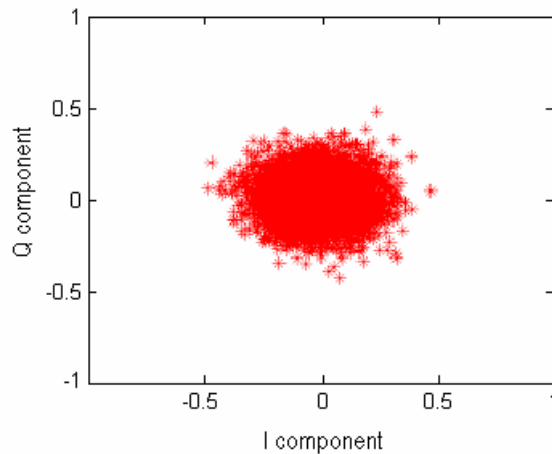


**Fig.III.16 – I/Q diagram of an OFDM signal.**

where  $x^*$  is the complex conjugate of  $x$ , and  $h = \text{mod}(K-k, K)$ , that is the remainder of  $\frac{K-k}{K}$ .

From expression (III.45) another significant difference between OFDM and classical QAM modulation emerges. If both channel and receiver are assumed to be ideal, the actual positions of received symbols on any of the  $K$  I/Q diagrams related to a single sub-carrier also depend on the symbols transmitted on the so-called mirror sub-carrier (referred to as  $h$ ). Consequently, for a given amount of I/Q impairments, actual symbol positions are not univocally determined.

As a clarifying example, let us suppose that the complex symbols  $C_0(n), C_1(n), \dots, C_{K-1}(n)$  at the input of the IFFT block be QPSK modulated, and let  $C'_0(n), C'_1(n), \dots, C'_{K-1}(n)$  be the  $n$ -th OFDM symbol recovered by an ideal receiver at the output of the FFT block. Fig.III.17 depicts the I/Q diagram related to the generic  $k^*$ -th sub-carrier, achieved from the sequence  $\{C'_{k^*}(n)\}$ ,  $n = 1, 2, \dots$  ( $n$  stands for time), when quadrature error and gain imbalance affect the transmitter; possible symbol locations on the diagram turn out to be 16, instead of 4. Let us now consider one of the 4 symbols in the original QPSK diagram. For a given amount of I/Q impairments, which is supposed to be constant over the observation interval, each successive occurrence of the symbol can assume a different position, depending on the particular symbol simultaneously conveyed by the mirror sub-carrier. With respect to a generic  $M$ -QAM diagram, possible symbol locations at the output of the FFT block turn out to be  $M^2$ . As a further example, Fig.III.18 shows the case of a 16-QAM diagram, where symbols can occupy 256 different locations; in particular, bold dots represent symbol original positions, whereas stars are all possible symbol positions under the effect of gain imbalance ( $\beta = 0.3$ ).

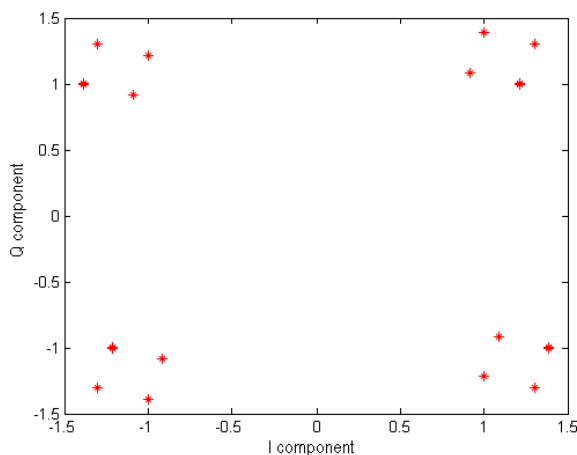


Fig.III.17 – I/Q diagram of an OFDM sub-carrier (QPSK).

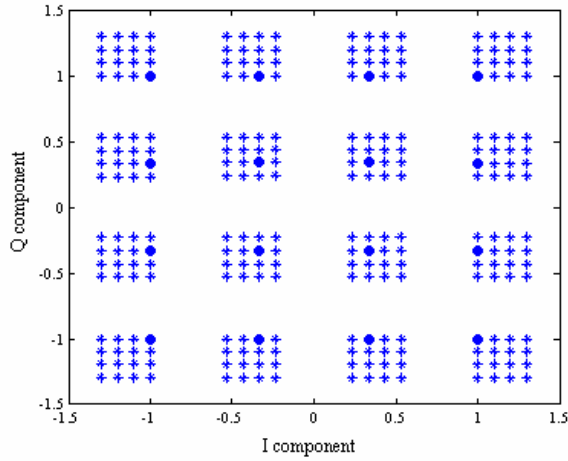


Fig.III.18 – I/Q diagram of an OFDM sub-carrier (16-QAM).

The aforementioned effects induced by I/Q impairments on a multicarrier modulation scheme make methods already proposed in [67], in Section III.2, and in Section III.3, as well as those suggested by major manufacturers, unreliable with regard to OFDM transmitters.

### III.4.3 - Proposed method

The measurement procedure is described in detail according to its fundamental stages. The presentation order reflects a typical execution order.

#### A. RF signal demodulation

The RF output signal of the digital transmitter under analysis is demodulated, and the  $K$  complex sequences  $C'_0(n), C'_1(n), \dots, C'_{K-1}(n)$  provided by the FFT block are extracted. The measurement algorithm, in fact, operates on such sequences. Let us drop index  $n$ , and consider the OFDM symbol at the output of the FFT block at a generic time instant, namely  $C'_0, C'_1, \dots, C'_{K-1}$ . According to (III.45), real and imaginary parts of coefficients  $C'_k$  are, respectively,

$$A'_k = \left(1 + \frac{\beta}{2}\right)A_k + \frac{\beta}{2}A_h - \frac{\phi}{2}(B_k + B_h) + \max(-k + 1, 0) \cdot [(1 + \beta)c_I - \phi c_Q] \quad (III.46)$$

and

$$B'_k = \left(1 + \frac{\beta}{2}\right)B_k - \frac{\beta}{2}B_h + \frac{\phi}{2}(A_k - A_h) + \max(-k + 1, 0) \cdot c_Q \quad (III.47)$$

The first step consists in estimating  $C_k=A_k+jB_k$ , for  $k=0,1,\dots,K-1$ , through typical threshold comparisons.

*B. Gain imbalance and quadrature error evaluation*

Some terms in (III.46) and (III.47) are present only when  $k=0$ , as accounted for by  $\max(k+1,0)$ , which is equal to 1 if  $k=0$ , and null else. Index  $k=0$  identifies the first entry of the IFFT, and is therefore often referred to as DC sub-carrier index. In other words, possible voltage offsets on I and Q branches have effect only on DC sub-carrier, as expected. Taking into account that, symbols related to all sub-carriers, except the DC, are processed in order to get an estimation of gain imbalance and quadrature error.

In detail, for each sub-carrier except the DC, (III.46) and (III.47) can be rewritten to yield the following system of two linear equations in the variables  $\beta$  and  $\phi$

$$\underline{\underline{\Theta}}^{(k)} \begin{pmatrix} \beta \\ \phi \end{pmatrix} = \underline{\underline{g}}^{(k)} \tag{III.48}$$

where

$$\underline{\underline{\Theta}}^{(k)} = \begin{pmatrix} A_k + A_h & -B_k - B_h \\ B_k - B_h & A_k - A_h \end{pmatrix} \tag{III.49}$$

and

$$\underline{\underline{g}}^{(k)} = 2 \begin{pmatrix} A'_k - A_k \\ B'_k - B_k \end{pmatrix} \tag{III.50}$$

The idea is to obtain an estimation of gain imbalance and quadrature error, respectively  $\hat{\beta}^{(k)}$  and  $\hat{\phi}^{(k)}$ , for each  $k$ .

As well known, if  $\det(\underline{\underline{\Theta}}^{(k)}) \neq 0$ , system (III.48) has a univocal solution, and impairment estimates are

$$\hat{\beta}^{(k)} = 2 \frac{(A'_k - A_k)(A_k - A_h) + (B'_k - B_k)(B_k + B_h)}{\det(\underline{\underline{\Theta}}^{(k)})} \tag{III.51}$$

$$\hat{\phi}^{(k)} = 2 \frac{(A_k + A_h)(B'_k - B_k) - (A'_k - A_k)(B_k - B_h)}{\det(\underline{\underline{\Theta}}^{(k)})} \tag{III.52}$$

It is worth noting that the case  $\det(\underline{\underline{\Theta}}^{(k)})=0$  is not infrequent, especially with regard to I/Q diagrams characterized by low cardinality;  $\det(\underline{\underline{\Theta}}^{(k)})$  is, in fact, always null when sub-carriers are QPSK modulated. Nevertheless, when  $\det(\underline{\underline{\Theta}}^{(k)})=0$ , it is still possible to estimate either gain imbalance or quadrature error, provided that one of the columns of (III.49) is identically null. In this case, in fact, system (III.48) collapses into two equations in the same variable, which are theoretically linearly dependent. As an example, if  $\underline{\underline{\Theta}}_{1,1}^{(k)} = \underline{\underline{\Theta}}_{2,1}^{(k)} = 0$ , (III.48) reduces to

$$\begin{cases} (-B_k - B_n) \phi = 2(A'_k - A_k) \\ (A_k - A_n) \phi = 2(B'_k - B_k) \end{cases} \quad . \quad (III.53)$$

In actual situations, a slight difference between the two equations in system (III.53) can occur, due to non-idealities that have effect on the terms  $A'_k$  and  $B'_k$  at the output of the FFT block. To contemplate this case, the two equations in (III.53) are separately solved, and  $\hat{\phi}^{(k)}$  is calculated as the average of their solutions.

Therefore, system (III.48) is solved for those  $k \in \{1, \dots, K-1\}$  that verify either  $\det(\underline{\underline{\Theta}}^{(k)}) \neq 0$  or  $\prod_j \sum_i |\underline{\underline{\Theta}}_{i,j}^{(k)}| = 0$ . Estimates  $\hat{\beta}^{(k)}$  and  $\hat{\phi}^{(k)}$  are then averaged to obtain a measure of gain imbalance,  $\hat{\beta}$ , and quadrature error,  $\hat{\phi}$ , for that particular OFDM symbol.

### *C. Voltage offset evaluation*

The final step of the proposed method consists in the estimation of voltage offsets. The values of  $\hat{\beta}$  and  $\hat{\phi}$ , attained at the previous step, are substituted into equations (III.46) and (III.47), which are evaluated for  $k = 0$ , yielding

$$A'_0 = (1 + \hat{\beta})(A_0 + c_I) - \hat{\phi} B'_0 \quad (III.54)$$

and

$$B'_0 = B_0 + c_Q \quad . \quad (III.55)$$

An estimate of  $c_I$  and  $c_Q$  can be obtained by simply inverting the two linear equations (III.54) and (III.55), which are split with regard to the variables  $c_I$  and  $c_Q$ :

$$\hat{c}_I = \frac{A'_0 + \hat{\phi} B'_0}{(1 + \hat{\beta})} - A_0 \quad (\text{III.56})$$

$$\hat{c}_Q = B'_0 - B_0 \quad (\text{III.57})$$

Assuming time-invariant impairments, the procedure is repeated for successive OFDM symbols, i.e. for successive values of time variable  $n$ , and I/Q impairment amounts evaluated for various symbols are averaged to achieve the desired measurement result.

#### *III.4.4 - Performance assessment*

A number of laboratory tests on OFDM signals have been carried out to experimentally assess the performance of the method. To this end, different combinations of impairment types and amounts, and different sub-carrier modulation patterns, i.e. modulation patterns characterizing the symbols  $C_0(n)$ ,  $C_I(n)$ , ...,  $C_{K-I}(n)$ , have been considered (QPSK, 16-QAM and 64-QAM).

##### *A. Measurement station and operative procedure*

A suitable measurement station has been set up, which the same as in Fig.III.11. It consists of (i) a processing and control unit, namely a personal computer, (ii) a digital RF signal generator, *Agilent Technologies E4432B*<sup>TM</sup> [55] (250 kHz-3 GHz output frequency) with AWG capability (14 bit vertical resolution, 1 Megasample memory depth, 40 MHz maximum sample clock), and (iii) a VSA *Agilent Technologies 4460A*<sup>TM</sup> [52] (7 MHz–4.0 GHz input frequency range, I/Q signal demodulation personality); they are all interconnected by means of an IEEE-488 standard interface bus.

The following operative steps have been taken.

- Baseband signals have digitally been synthesized through a suitable algorithm running on the processing and control unit. I/Q impairments of known amount are imposed on the digital sequence of samples. Impairments have been assumed to be constant in the observation interval.
- Generated samples have been downloaded into the volatile memory of the AWG, operating the D/A conversion and RF up-conversion.
- VSA has been employed to demodulate the RF signal and extract baseband components. To this end, the VSA has been synchronized to the signal generator; they have shared the same 10 MHz reference clock. I and Q components, made

available by the VSA, have been transferred to the control and processing unit, via the IEEE-488 bus.

- The proposed measurement algorithm, running on the processing and control unit, has provided the estimates of the detected I/Q impairments.

**B. Results**

Table III.6 and Table III.7 summarize the results obtained for each sub-carrier modulation pattern taken into account. They also gives the range of values within which amounts of imposed impairments have been chosen. Results are given in terms of minimum and maximum values of difference between imposed and measured impairment amount,  $\Delta$  (Table III.6), and experimental standard deviation,  $\sigma$  (Table III.7). Both  $\Delta$  and  $\sigma$  are expressed in percentage relative terms. Gain imbalance,  $\beta$ , is normalized to the value of Q branch gain,  $G_Q$ , and voltage offsets,  $c_I$  and  $c_Q$ , are normalized to the nominal peak value of the baseband component. From the analysis of the values accounted for in Table III.6 and Table III.7, the following considerations can be drawn.

**Table III.6 - Measurement results: difference between imposed and estimated values.**

Range of values of imposed I/Q impairments		$\Delta$ %					
		QPSK		16-QAM		64-QAM	
		min	max	min	max	min	max
$\beta$	0.05–0.30	0.10%	6.2%	0.53%	6.0%	0.78%	5.2%
$\phi$	0.021–0.131 rad	0.13%	6.5%	0.88%	6.5%	1.0%	5.9%
$c_I$	0.05–0.30	0.18%	4.8%	0.93%	5.3%	0.77%	5.0%
$c_Q$	0.05–0.30	0.10%	2.9%	0.55%	4.1%	0.30%	3.6%

**Table III.7 - Measurement results: experimental standard deviation.**

Range of values of imposed I/Q impairments		$\sigma$ %					
		QPSK		16-QAM		64-QAM	
		min	max	min	max	min	max
$\beta$	0.05–0.30	1.3%	5.9%	1.3%	5.0%	1.0%	5.7%
$\phi$	0.021–0.131 rad	1.4%	7.2%	1.3%	6.6%	1.4%	6.8%
$c_I$	0.05–0.30	1.5%	4.5%	1.0%	4.9%	1.3%	4.9%
$c_Q$	0.05–0.30	1.0%	3.5%	0.99%	3.8%	1.1%	4.0%

- The proposed method provides good results in terms of difference between imposed and measured impairment amounts;  $\Delta\%$  is, in fact, mostly inferior to 6%, except for some rare cases, enlisted in the table, in which the simultaneous presence of all impairments can result in a slightly higher value.
- The method performs well also with respect to repeatability; the experienced values of  $\sigma\%$  are, in fact, mostly inferior to 6-7%.
- Measurement of voltage offset on the Q branch,  $c_Q$ , is characterized by the lowest values of  $\Delta\%$  and  $\sigma\%$ . This is probably due to the fact that the other impairments do not appear in relation (III.57) utilized to estimate  $c_Q$ , and therefore do not have any influence on its estimation.
- The performance of the method seems to be independent of sub-carrier modulation pattern. Maximum values of  $\Delta\%$  and  $\sigma\%$  experienced for the three considered patterns concur.

Fig.III.19 allows a more detailed analysis of the performance of the method. It refers to experiments conducted in the presence of gain imbalance and quadrature error, for QPSK sub-carrier modulation pattern. In particular, Fig.III.19a and Fig.III.19b show the values respectively of  $\Delta\%$  and  $\sigma\%$  experienced with regard to gain imbalance measurements, for several impairment amount combinations. Similarly, Fig.III.19c and Fig.III.19d refer to quadrature error measurements and account for, respectively,  $\Delta\%$  and  $\sigma\%$  achieved with the same combinations of imposed impairment amounts. The following considerations arise.

- The lower the impairment amount, the higher the values of  $\Delta\%$  and  $\sigma\%$ . The existence of a sensitivity limit for the method can be inferred.
- When different impairments are simultaneously present, measurement results for one of them are influenced, but not compromised, by the amounts of the others. It is generally true, and evident from Fig.III.19, that the higher the amount of quadrature error, the higher the values of  $\Delta\%$  and  $\sigma\%$  experienced with regard to gain imbalance measurements. The dual case is equally true and evident from the same figure.

### III.4.5 - Conclusion

A new method for the evaluation of I/Q impairments in OFDM transmitters has been presented. The method is based on a suitable analytical model that properly accounts for the way I/Q impairments affect the RF output signal, taking into account the effect of mirror sub-

carrier interference. The analytical model exploited and with the original measurement procedure implemented allow overcoming key limitations of other solutions, mainly designed for traditional transmitter testing and troubleshooting. Moreover, the method does not require particular test input sequences, thus allowing non-intrusive measurements.

Results of a wide experimental activity carried out on laboratory OFDM signals have given evidence of the good performance of the method; differences between imposed and measured impairment amounts and experimental standard deviations generally lower than 6% have been experienced. Moreover, no dependence on the particular modulation pattern adopted on sub-carriers to characterize measurement results.

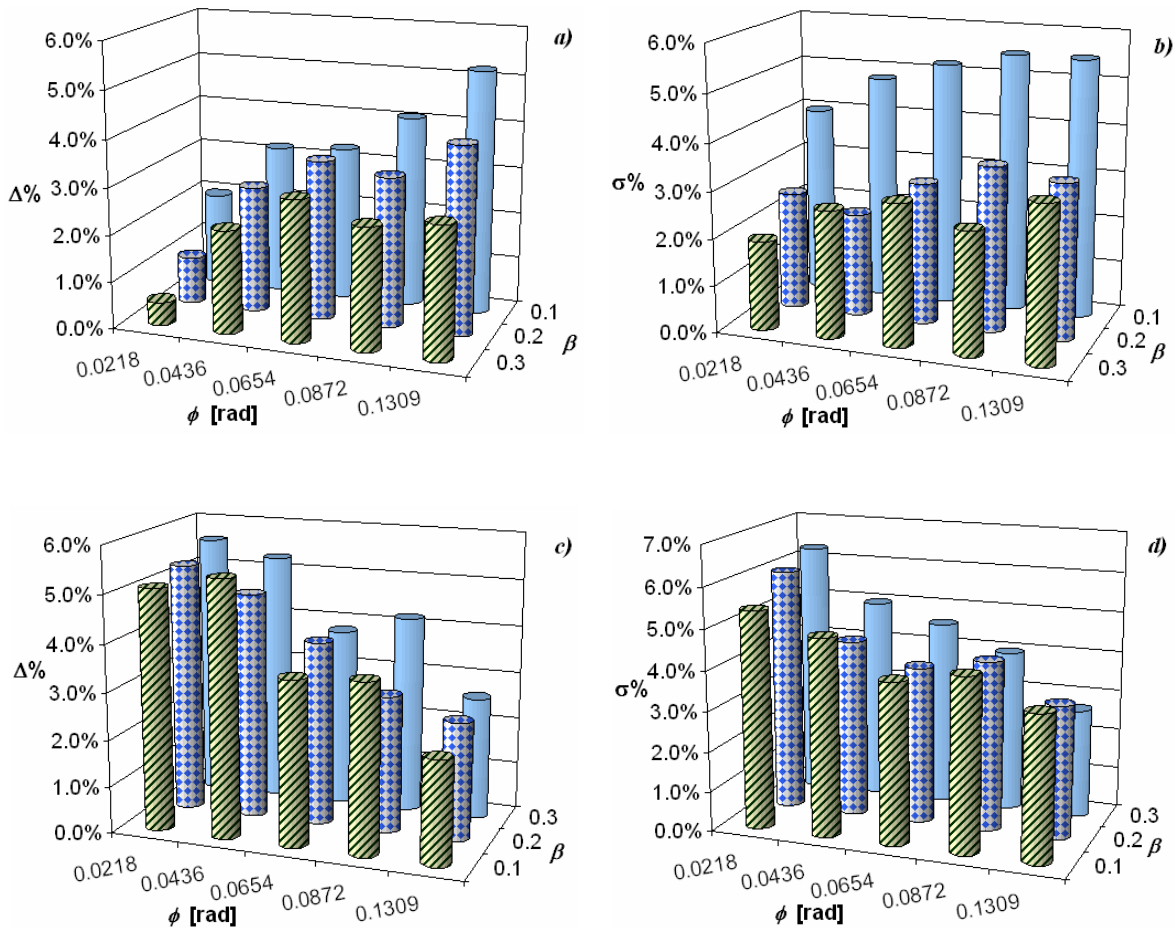


**Fig.III.19 – Measurement results for QPSK sub-carrier modulation, in the presence of gain imbalance and quadrature error: a) difference from imposed and measured amounts and b) experimental standard deviation concerning gain imbalance measurements; c) difference from imposed and measured amounts and d) experimental standard deviation concerning quadrature error measurements. All differences and experimental standard deviations are expressed in percentage relative terms.**

## **CHAPTER IV**

### **CONCLUSION**

This Ph.D. thesis has dealt with performance evaluation and troubleshooting of radiofrequency digital communication transmitters. The original contribution has consisted in the proposal of innovative measurement methods, based on digital signal processing, and addressed to power measurement, CCDF curve evaluation, transient measurement, and I/Q impairment detection and evaluation. Suitable measurement stations have been set up to experimentally test all the proposed methods and assess their performance. Experimental outcomes, including comparison with other proposals and results provided by instrumentation available on the market, have shown the effectiveness and accuracy of the methods.

Possible future developments concern new methods for power measurement in the presence of in-channel interference based on advanced signal processing techniques, such as cyclostationary analysis, optimization and/or extension of methods for I/Q impairment measurement to new communication standards, and the implementation of some of the proposed algorithms on suitable digital signal processors, or as add-on software modules on DSOs.



## **REFERENCES**

- [1] “Digital cellular telecommunications system (Phase 2+); Radio transmission and reception,” ETSI Tech. Spec.100 910, Ver.8.19.0, 2005.
- [2] 3rd Generation Partnership Project, Technical Specification Group Radio Access Networks, “Base Station (BS) conformance testing (FDD),” Release 6, 3GPP TS 25.141, V.6.11.0, Sept.2005.
- [3] “Specification of the Bluetooth System,” Bluetooth SIG, Core Package v.1.2, 2003.
- [4] “IEEE Standard 802.11 - Information Technology - Telecommunication and information exchange between systems – Local and Metropolitan area networks – Specific Requirements. Part 11: Wireless LAN Medium Access Control (MAC) and Physical Layer (PHY) specifications”, Reaffirmed 2003.
- [5] “IEEE Standard 802.11a- Information Technology- Telecommunication and information exchange between systems – Local and Metropolitan area networks - Specific Requirements. Part 11: Wireless LAN Medium Access Control (MAC) and Physical Layer (PHY) specifications - Amendment 1: High-speed Physical Layer in the 5 GHz band”, Reaffirmed 2003.
- [6] “IEEE Standard 802.11b- Information Technology- Telecommunication and information exchange between systems – Local and Metropolitan area networks – Specific Requirements. Part 11: Wireless LAN Medium Access Control (MAC) and Physical Layer (PHY) specifications: Higher-Speed Physical Layer Extension in the 2.4 GHz band”, Reaffirmed 2003.
- [7] “IEEE Standard 802.11g- Information Technology- Telecommunication and information exchange between systems – Local and Metropolitan area networks – Specific Requirements. Part 11: Wireless LAN Medium Access Control (MAC) and Physical

Layer (PHY) specifications - Amendment 4: Further Higher Data Rate Extension in the 2.4 GHz band”, Reaffirmed 2003.

- [8] “802.16 IEEE Standard for Local and Metropolitan Area Networks. Part 16: Air Interface for Fixed Broadband Wireless Access Systems” 2004.
- [9] “Radio Broadcasting Systems; Digital Audio Broadcasting (DAB) to mobile, portable and fixed receivers”, ETSI European Standard EN 300 401 v.1.3.3, 2001.
- [10] “Digital Video Broadcasting (DVB); Framing structure, channel coding and modulation for 11/12 GHz satellite services”, ETSI European Standard EN 300 421 v.1.1.2, 1997.
- [11] “Digital Video Broadcasting (DVB): Framing Structure, Channel Coding and Modulation for Cable Systems,” ETSI EN 300 744 Ver 1.3.1, 1998.
- [12] “Digital Video Broadcasting (DVB); Framing structure, channel coding and modulation for digital terrestrial television”, ETSI European Standard EN 300 744 v.1.5.1, 2004.
- [13] J. G. Proakis, *Digital Communications*, 3rd ed. New York: McGraw-Hill, 1995.
- [14] C. E. Shannon, “A Mathematical Theory of Communication,” *Bell Syst. Tech. J.*, vol.27, pp.379-423, July 1948.
- [15] C. E. Shannon, “A Mathematical Theory of Communication,” *Bell Syst. Tech. J.*, vol.27, pp.623-656, October 1978.
- [16] D. A. Huffman, “A Method for the Construction of Minimum Redundancy Codes,” *Proc. IRE*, vol.40, pp.1098-1101, September 1952.
- [17] C. E. Shannon, “Communication in the Presence of Noise,” *Proc. IRE*, vol.37, pp.10-21, January 1949.
- [18] D. Slepian, *Key Papers in the Development of Information Theory*, IEEE Press, New York, 1974.
- [19] H. Nyquist, “Certain Topics in Telegraph Transmission Theory,” *AIEE Trans.*, vol.47, pp.617-644, 1928.
- [20] I. Gerst, J. Diamond, “The Elimination of Intersymbol Interference by Input Pulse Shaping,” *Proc. IRE*, vol.53, July 1961.
- [21] D. W. Tufts, “Nyquist’s Problem-The Joint Optimization of Transmitter and Receiver in Pulse Amplitude Modulation,” *Proc. IEEE*, vol.53, pp.248-259, March 1965.
- [22] J. W. Smith, “The Joint Optimization of Transmitted Signal and Receiving Filters for Data Transmission Systems,” *Bell Syst. Tech. J.*, vol.44, pp.1921-1942, December 1965.
- [23] F. Hlawatsch, F. Boudreaux-Bartels, “Linear and quadratic time-frequency signal representations,” *IEEE Signal Processing Magazine*, vol.9, No.2, pp. 21-67, Apr 1992.

- 
- [24] B. Barkat, B. Boashash, "Instantaneous frequency estimation of polynomial FM signals using the peak of the PWVD: Statistical performance in the presence of additive Gaussian noise," *IEEE Trans. Signal Processing*, vol.47, pp.2480–2490, Sept. 1999.
- [25] L. Cohen, *Time–Frequency Analysis*, Prentice Hall, 2000.
- [26] B. Boashash, "Estimating and interpreting the instantaneous frequency of a signal," *Proc. IEEE*, vol. 80, No.4, pp. 520–568, Apr. 1992.
- [27] S. Mann and S. Haykin, "'Chirplets' and 'Warblets': Novel Time-Frequency Methods," *Electronics Letters*, vol. 28, no. 2, pp. 114-116, January 1992.
- [28] L. Angrisani, P. Daponte, and M. D'Apuzzo, "A measurement method based on time-frequency representations for testing GSM equipment," *IEEE Trans. Instrum. Meas.*, vol. 49, pp. 1050–1056, Oct. 2000.
- [29] "Testing and troubleshooting digital RF communications transmitter designs", Application Note 1313, Agilent Technologies Literature No.5968-3578E, 2002.
- [30] "Understanding CDMA measurements for base stations and their components," Application Note 1311, Agilent Technologies Literature no.5968-0953E, 2000.
- [31] "Understanding GSM/EDGE Transmitter and Receiver Measurements for Base Transceiver Stations and Their Components," Application Note 1312, Agilent Technologies Literature No.5968-2320E, 2002.
- [32] "Understanding PDC and NADC Transmitter Measurements for Base Transceiver Stations and Mobile Stations," Application Note 1324, Agilent Technologies Literature No.5968-5537E, 2000.
- [33] "Characterizing Digitally Modulated Signals with CCDF Curves", Application Note, Agilent Technologies Literature No.5968-6875E, 2000.
- [34] "Digital Video Broadcasting (DVB): Measurement Guidelines for DVB Systems," ETSI Tech. Report 101 290, Ver 1.2.1, 2001.
- [35] "Using Error Vector Magnitude Measurements to Analyze and Troubleshoot Vector-Modulate Signals", Product Note 89400-14, Agilent Technologies Literature No.5965-2898E, 2000.
- [36] L. Angrisani, M. D'Apuzzo, M. D'Arco, "New digital signal-Processing approach for transmitter measurements in third generation Telecommunications systems," *IEEE Trans. Instrum. Meas.*, vol. 53, No.3, pp. 622-629, June 2004.

- [37] “Comparing power measurements on digitally modulated signals,” Product Note Agilent 8560E/8590E Spectrum Analyzers, Agilent Technologies Literature no. 5968-2602E, 2000.
- [38] “4 steps for making better power measurements,” Applicat. Note 64-4C, Agilent Technologies Literature no. 5965-8167E, 2000.
- [39] “Real-time spectrum analysis tools aid transition to third-generation wireless technology,” Tektronix Literature No. 2EW-13 227-0, 1999.
- [40] “WCDMA measurement guide-Agilent Technologies E4406A VSA series transmitter tester,” Agilent Technologies Literature no. E4406-90132, 2000.
- [41] Wolf and B. Buxton, “Measure adjacent channel power with a spectrum analyzer,” *Microwaves RF*, pp. 55–63, Jan. 1997.
- [42] “ACP measurements on amplifiers designed for digital cellular and PCS systems,” Tektronix Literature no. 2DA-12 149-0, 1998.
- [43] “Agilent EPM-P series single-and dual-channel power meters-Agilent E9320 family of peak and average power sensors,” Product Overview, Agilent Technologies Literature-1471E, 2000.
- [44] L. Angrisani, M.D’Apuzzo, M.D’Arco, “A New Method for Power Measurements in Digital Wireless Communication Systems,” *IEEE Trans. on Instrum. and Measur.*, vol.52, No.4, August 2003, pp.1097-1106.
- [45] D.Percival, A.Walden, *Spectral Analysis for Physical Applications. Multitaper and Conventional Multivariate Techniques*, Cambridge University Press, 1998.
- [46] T.W.Anderson, “Comments on the performance of maximum entropy algorithms,” *Proc. IEEE*, vol.66, pp.1581-1582.
- [47] A.Papoulis, “Levinson’s Algorithm, Wold’s Decomposition, and Spectral Estimation,” *SIAM Review*, N°.27, pp.405-441.
- [48] S.M.Kay, J.Makhoul, “On the Statistics of the Estimated Reflection Coefficients of an Autoregressive Process,” *IEEE Trans. on Acoustic, Speech, and Signal Processing*, vol.31, No.6, 1983, pp.1447-1455.
- [49] <http://www.lecroy.com/tm/products/Scopes/LCSeries/LC684DXL/TecnicalSpecifications.asp>
- [50] [http://www.home.agilent.com/cgi-bin/pub/agilent/Product/cp\\_Product.jsp?NAV\\_ID=-536898379.536881805.00&LANGUAGE\\_CODE=eng&CONTENT\\_KEY=1000002155%3aepsg%3apro&ID=1000002155%3aepsg%3apro&COUNTRY\\_CODE=US](http://www.home.agilent.com/cgi-bin/pub/agilent/Product/cp_Product.jsp?NAV_ID=-536898379.536881805.00&LANGUAGE_CODE=eng&CONTENT_KEY=1000002155%3aepsg%3apro&ID=1000002155%3aepsg%3apro&COUNTRY_CODE=US)

- 
- [51] “MS2687B Spectrum Analyzer Data Sheet,” Anritsu Catalog No. MS2687B-E-A-1-(4.00), 2005.
- [52] “Agilent E4406A Vector Signal Analyzer Data Sheet,” Agilent Technologies Literature no. 5968-3030E, 2005.
- [53] “Agilent PSA Series Spectrum Analyzers Data Sheet,” Agilent Technologies Literature no. 5980-1284E, 2005.
- [54] “Agilent E4416A/E4417A EPM-P Series Power Meters and E-Series E9320 Peak and Average Power Sensors Data Sheet,” Agilent Technologies Literature no. 5980-1469E, 2005.
- [55] “Agilent ESG-A and ESG-D RF Signal Generators Data Sheet,” Agilent Technologies Literature no. 5989-4074EN, 2005.
- [56] <http://www.eutelsat.com>
- [57] “Designing and Testing 3GPP W-CDMA Base Transceiver Stations”, Application Note, Agilent Technologies Literature No.5980-1239E, 2003.
- [58] L. Angrisani, M. D'Arco, R. Schiano Lo Moriello, M. Vadursi, “Optimal sampling strategies for band-pass measurement signals,” *Proc. of XIII IMEKO Intern. Symposium on Measur. for Research and Industry Appl.*, Athens, Greece, 29 Sept.-01 Oct. 2004, pp.343-348.
- [59] L. Angrisani, M. D'Apuzzo, M. D'Arco, “New digital signal-processing approach for transmitter measurements in third generation telecommunication systems,” *IEEE Trans. on Instr. and Meas.*, vol.53, n.3, pp.622-629, June 2004.
- [60] C. Balz, “CCDF determination – a comparison of two measurement methods,” News from Rohde&Schwarz, n.172, pp.52-53, 2001.
- [61] “Electromagnetic compatibility and Radio spectrum Matters (ERM); Land mobile service; Radio equipment intended for the transmission of data (and/or speech) using constant or non-constant envelope modulation and having an antenna connector; Part 1: Technical characteristics and methods of measurement”, ETSI EN 300 113-1 v.1.5.1, September 2003.
- [62] “Measuring Transmitter Transients with the 89400 Series Vector Signal Analyzers”, Product Note 89400-5, Agilent Technologies Literature No.5962-9493E, 2000.
- [63] “Measuring Frequency Settling Time for Synthesizers and Transmitters”, Rohde&Schwarz Literature Application Note No.1MA15\_0E, 1999.

- [64] S.Mann, S.Haykin, "The chirplet transform: Physical considerations," *IEEE Trans. On Signal Processing*, vol.41, pp.2745-2761, Nov.1993.
- [65] L.Angrisani, M.D'Arco, "A Measurement Method Based on a Modified Version of the Chirplet Transform for Instantaneous Frequency Estimation," *IEEE Trans. on Instr. and Meas.*, vol.51, No.4, pp.704-712, August 2002.
- [66] A.D. Poularikas, *The transforms and applications handbook*, CRC Press, 2000.
- [67] L.Angrisani, R.Colella, "Detection and Evaluation of I/Q Impairments in RF Digital Transmitters," *IEE Proceedings – Science, Measurement and Technology*, Vol.151, No.1, January 2004, pp.39-45.
- [68] J. Hartigan, *Clustering Algorithms*, Wiley, New York, 1975.
- [69] V. Faber, "Clustering and the Continuous k-Means Algorithm," *Los Alamos Science*, N.22, 1994, pp. 138-144.
- [70] "Digital cellular telecommunications system (Phase 2 & Phase 2+); Base Station System (BSS) equipment specification; Radio aspects," ETSI EN 301 087, Ver. 8.2.1, 2000.
- [71] "Designing and testing WCDMA User Equipment", Application Note 1356, Agilent Technologies Literature No.5980-1238E, 2003.
- [72] "EDGE Wireless Networks: Challenges in Maintenance and Testing," Tektronix Literature No. 2EW-17611-O, 2004.
- [73] "W-CDMA/UMTS Wireless Networks: Challenges in Maintenance and Testing – 2<sup>nd</sup> edition," Tektronix Literature No. 2EW-12789-O, 2004.
- [74] A. Mashhour, A. Borjak, "A Method for Computing Error Vector Magnitude in GSM EDGE Systems –Simulation Results," *IEEE Communications Letter*, vol.5, No.3, March 2001, pp.88-91.
- [75] K.Voelker, "Apply Error Vector Measurements in Communications Design," *Microwaves & RF*, Dec. 1995.
- [76] J. K. Cavers and M. W. Liao, "Adaptive compensation for imbalance and offset losses in direct conversion transceivers," *IEEE Trans. Veh. Technol.*, vol. 42, pp. 581–588, Nov. 1993.
- [77] R. Hassun, M. Flaherty, R. Matreci, and M. Taylor, "Effective evaluation of link quality using error vector magnitude techniques," *Proc. IEEE Wireless Commun. Conf.*, 1997, pp. 89–94.
- [78] M. Heutmaker, "The error vector and power amplifier distortion," *Proc. of IEEE Wireless Communications Conf.*, 1997.

- 
- [79] T. Nakagawa and K. Araki, "Effect of phase noise on RF communication signals," in *Proc. of IEEE Veh. Tech. Conf. 2000*, vol. 2, 2000, pp. 588–591.
- [80] H. Ku and J. S. Kenney, "Estimation of error vector magnitude using two-tone intermodulation distortion measurements," *Proc. IEEE/MTT Microwave Symp. Dig.*, vol. 1, 2001, pp. 17–20.
- [81] J. L. Pinto and I. Darwazeh, "Phase distortion and error vector magnitude for 8-psk systems," *Electronic Letters*, vol. 37, pp. 437–438, 2001.
- [82] A. Georgiadis, "Gain, Phase Imbalance, and Phase Noise Effects on Error Vector Magnitude," *IEEE Transactions on Vehicular Technology*, vol.53, No.2, March 2004, pp.443-449.
- [83] S. Hori, T. Kumagai, T. Sakata, M. Morikura, "A New Vector Error Measurement Scheme for Transmit Modulation Accuracy of OFDM Systems," *Proc. of IEEE Veh. Tech. Conf. 2000*, pp.1240-1244.
- [84] S. Rapuano G. Truglia, "An improved image processing-based method for disturbance classification in telecommunication networks," *IEEE Transactions on Instrumentation and Measurement*, Vol.54, No.5, Oct. 2005, pp.2068- 2074.
- [85] R. Van Nee, R. Prasad, *OFDM for Wireless Multimedia Communications*, Artech House Publishers, 2000.
- [86] S. B. Weinstein and P. M. Ebert, "Data Transmission by Frequency-Division Multiplexing Using the Discrete Fourier Transform," *IEEE Trans. Commun. Techn.*, vol. COM-19, no. 5, pp. 628–634, Oct. 1971.
- [87] A. R. S. Bahai, B. R. Saltzberg, *Multi-Carrier Digital Communications: Theory and Applications of OFDM*, Kluwer Academic/Plenum Publishers, New York, 1999.
- [88] "Broadband Radio Access Networks (BRAN); HIPERLAN Type 2; Physical layer", ETSI Technical Specification TS 101 475 v.1.3.1, 2001.
- [89] J.Tubbax, B.Come, L.Van der Perre, L.Deneire, S.Donnay, M.Engels, "Compensation of IQ imbalance in OFDM systems," *Proc. of ICC '03, IEEE Intern. Conf. on Communications 2003*, vol.5, pp.3403-3407.



## LIST OF FIGURES

Fig.I.1 – Block diagram of a radiofrequency digital transmitter.....	6
Fig.I.2 – CCDF curve of a CDMA signal.....	9
Fig.I.3 – Error vector definition.....	10
Fig.I.4 – I/Q section of a digital transmitter.....	13
Fig.I.5 – Effect of the presence of gain imbalance for a 64-QAM signal constellation with unitary maximum I/Q component value.....	13
Fig.I.6 – Effect of the presence of quadrature error for a 64-QAM signal constellation with unitary maximum I/Q component value.....	14
Fig.I.7 – Effect of the presence of positive offsets on the in-phase and quadrature components for a 64-QAM signal constellation with unitary maximum I/Q component value.....	14
Fig.I.8 – Incorrect symbol rate and evolution versus time of EVM.....	15
Fig.I.9 – Evolution versus time of EVM in the presence of wrong filter coefficients and/or incorrect windowing.....	16
Fig.I.10 – Magnitude spectrum of EV in the presence of an interfering tone inside signal bandwidth.....	17
Fig.II.1 – Flow chart diagram of the PSD estimation routine.....	26
Fig.II.2 – Measurement station.....	28

Fig.II.3 – PSD of a WCDMA signal estimated through the proposed approach.....	30
Fig.II.4 – PSD of <i>Rai International 4</i> signal attained through the spectrum analyzer <i>Anritsu MS2687B<sup>TM</sup></i> ; very critical measurement conditions are highlighted.....	31
Fig.II.5 – Envelope power of a W-CDMA signal; its high variability is due to the noise-like nature of the signal.....	33
Fig.II.6 – Power CCDF curve of the signal referred to in Fig.II.5.....	34
Fig.II.7 – Evaluation of the CCDF from the instantaneous power trajectory: the bold line is the mean power level, while the thin dotted line is 1 dB above. The value of $CCDF(x)$ , with $x=1$ dB, is computed as the ratio between the duration of all the time intervals indicated by the arrows and the overall duration of the signal.....	36
Fig.II.8 – Measurement station.....	37
Fig.II.9 – Comparison between the CCDF provided by the VSA and those provided by a) the time-domain approach, and b) the time-frequency approach, when different values of the sampling frequency, $f_s$ , and therefore of the ratio $p$ , are taken into account. Details of low and high power levels are given in a1), a2), b1), b2).....	39
Fig.II.10 – Standard measurement setup.....	41
Fig.II.11 – Instantaneous frequency trajectory of the test signal.....	44
Fig.II.12 – Instantaneous power trajectory of the test signal.....	44
Fig.II.13 – Evolution versus time of the test signal.....	45
Fig.II.14 – Instantaneous frequency trajectory gained when optimal values of STFT parameters are used. Measured (solid line) and nominal (dotted line) trajectories are compared.....	47
Fig.II.15 – Instantaneous power trajectory gained when optimal values of STFT parameters are used. Measured (solid line) and nominal (dotted line) trajectories are compared.....	47
Fig.II.16 – Evolution versus time of the signal acquired from the bug transmitter.....	48
Fig.II.17 – Instantaneous frequency trajectory, obtained through the use of CT, of the signal at the output of the bug transmitter.....	49
Fig.II.18 – Instantaneous power trajectory, obtained through the use of CT, of the signal at the output of the bug transmitter.....	49
Fig.II.19 – Evolution versus time of the signal acquired from the walkie-talkie.....	50
Fig.III.1 – I/Q diagram for QPSK signal.....	54
Fig.III.2 – I/Q diagram for 16-QAM signal.....	54

Fig.III.3 – I/Q impairment model.....	55
Fig.III.4 – Ideal 64-QAM constellation with amplitude imbalance ( $\beta=0.1$ ), quadrature error ( $\phi= \pi/64$ ), and voltage offsets ( $c_I=-0.05$ , $c_Q=0.075$ ). Red crosses and blue dots represent nominal and actual symbol positions, respectively. I and Q components are normalized to their maximum value.....	56
Fig.III.5 – Measurement station.....	60
Fig.III.6 – Difference $\Delta\%$ , in percentage relative terms, between measured and imposed a) amplitude imbalance ( $A\equiv\beta$ ) and b) quadrature error; experimental standard deviation $\sigma\%$ , in percentage relative terms, related to c) amplitude imbalance and d) quadrature error.....	61
Fig.III.7 – Effect of joint gain imbalance and quadrature error on the constellation diagram of a QPSK signal; $g$ and $\phi$ are, respectively, equal to 0.1710 and $\pi/32$ rad.....	65
Fig.III.8 – EV components due to a gain imbalance, $g$ , equal to 0.1146.....	67
Fig.III.9 – EV components due to a quadrature error, $\phi$ , equal to $\pi/16$ rad.....	67
Fig.III.10 – EV components due to a voltage offset on component I, $c_I$ , equal to 0.15.....	68
Fig.III.11 – Measurement station.....	72
Fig.III.12 – I/Q polar diagram of a DVB signal in the presence of gain imbalance.....	73
Fig.III.13 – I and Q waveforms related to the signal in Fig.III.12.....	73
Fig.III.14 – Symbol-by-symbol estimation of gain imbalance.....	75
Fig.III.15 – Basic OFDM modulation scheme.....	77
Fig.III.16 – I/Q diagram of an OFDM signal.....	78
Fig.III.17 – I/Q diagram of an OFDM sub-carrier (QPSK).....	79
Fig.III.18 – I/Q diagram of an OFDM sub-carrier (16-QAM).....	80
Fig.III.19 – Measurement results for QPSK sub-carrier modulation, in the presence of gain imbalance and quadrature error: a) difference from imposed and measured amounts and b) experimental standard deviation concerning gain imbalance measurements; c) difference from imposed and measured amounts and d) experimental standard deviation concerning quadrature error measurements. All differences and experimental standard deviations are expressed in percentage relative terms.....	86



## LIST OF TABLES

Table II.1 – Comparison of measurement results obtained in the experiments on uplink WCDMA signals.....	29
Table II.2 – Comparison of measurement results obtained in the experiments on downlink WCDMA signals.....	30
Table II.3 – Comparison of channel power measurement results obtained in the experiments on DVB S signals.....	31
Table II.4 – Average values of rmse between measured and reference CCDF curves.....	38
Table II.5 – Results achieved with optimal windows.....	46
Table II.6 – Measurement results related to the bug transmitter.....	49
Table II.7 – Measurement results related to the walkie-talkie.....	50
Table III.1 – Results of experimental tests on signals affected by different combinations of impairments.....	62
Table III.2 – Impairment amounts for WCDMA signals.....	72
Table III.3 – Impairment amounts for DVB signals.....	73
Table III.4 – Measurement results for WCDMA signals.....	74
Table III.5 – Measurement results for DVB signals.....	75
Table III.6 – Measurement results: difference between imposed and estimated values.....	84
Table III.7 – Measurement results: experimental standard deviation.....	84